

STUDIES ON THE PROPERTIES OF PMMA-BASED  
POLYMER ELECTROLYTE FOR LITHIUM  
RECHARGEABLE BATTERY

TAN KIA WUI

MASTER OF ENGINEERING SCIENCE

FALCULTY OF ENGINEERING AND SCIENCE  
UNIVERSITI TUNKU ABDUL RAHMAN  
JANUARY 2013



**STUDIES ON THE PROPERTIES OF PMMA-BASED POLYMER  
ELECTROLYTE FOR LITHIUM RECHARGEABLE BATTERY**

By

**TAN KIA WUI**

**A thesis submitted to the Department of Electrical and Electronic  
Engineering,  
Universiti Tunku Abdul Rahman,  
In partial fulfillment of the requirement for the degree of  
Master of Engineering Science  
January 2013**

## ABSTRACT

### STUDIES ON THE PROPERTIES OF PMMA-BASED POLYMER ELECTROLYTE FOR LITHIUM RECHARGEABLE BATTERY

Tan Kia Wui

In this study, four poly(methyl methacrylate) (PMMA) hosted solid polymer electrolyte systems were prepared by a solution cast technique. A fixed amount of ethylene carbonate and propylene carbonate (EC/PC) (70/30) mixture was set as plasticiser; aluminum oxide ( $\text{Al}_2\text{O}_3$ ) and fumed silica ( $\text{SiO}_2$ ) were implemented as ceramic filler and lithium perchlorate ( $\text{LiClO}_4$ ) as dopant salt. The study was carried out using Electrochemical Impedance Spectroscopy (EIS), Fourier Transform Infrared Spectroscopy (FTIR), X-ray Diffraction (XRD) and Scanning Electron Microscope (SEM). The integrating 30 wt% of EC/PC into PMMA enhanced the ionic conductivity from  $3.19 \times 10^{-11} \text{ Scm}^{-1}$  to  $7.57 \times 10^{-10} \text{ Scm}^{-1}$ . With another addition of 25 wt% of  $\text{LiClO}_4$ , the ionic conductivity is increased to  $3.95 \times 10^{-5} \text{ Scm}^{-1}$ . This has inferred the enhancement of charge carrier density in the polymer electrolyte. A further addition of ceramic fillers with 12 wt% of  $\text{Al}_2\text{O}_3$  and  $\text{SiO}_2$ , boosted the ionic conductivity to  $1.02 \times 10^{-4} \text{ Scm}^{-1}$  and  $2.48 \times 10^{-4} \text{ Scm}^{-1}$ , respectively. This enhancement is attributed to the Lewis acid-base interaction and the formation of three dimensional networks for ionic conduction. In the temperature vs conductivity studies, the entire polymer electrolytes showed the Arrhenius behaviour. Through the XRD studies the enhancement of amorphous region is

confirmed. The result is further proven by FTIR studies indicating the occurrence of complexation between host polymer and the additives. The SEM images showed the formation of three dimensional networks with dispersion of ceramic fillers. It can be concluded that appropriate amount of lithium salt (25 wt% of  $\text{LiClO}_4$ ) and ceramic filler (12 wt% of  $\text{Al}_2\text{O}_3$  and 12 wt% of  $\text{SiO}_2$ ) enhances the ionic conductivity of the PMMA-based solid polymer electrolyte.

## ACKNOWLEDGEMENTS

Firstly, I would like to take this opportunity to express my deepest appreciation and gratitude to my supervisor, Dr. Chew KuewWai and co-supervisor, Dr. Yong ThianKhok for their assistance and guidance throughout this project stint. The supervision and support that they gave truly help the progression and smoothness of this research. I really appreciate all their effort and guidance during this research period.

My grateful thanks also go to UTAR as this work was supported by UTAR Research Fund (UTARRF). It also provides the venue for education and research instruments, apparatus and facilities. In addition, it provides a good working environment for the completion of this research. I also wish to express my appreciation to all the laboratory officers for their assistance and patience throughout this lab work.

Finally, I would like to thank my family members and course mates for their support, encouragement and suggestions in this research.

## APPROVAL SHEET

This dissertation/ thesis entitled “**STUDIES ON THE PROPERTIES OF PMMA-BASED POLYMER ELECTROLYTE FOR LITHIUM RECHARGEABLE BATTERY**” was prepared by TAN KIA WUI and submitted as partial fulfillment of the requirements for the degree of Master of Engineering Science at UniversitiTunku Abdul Rahman.

Approved by:

\_\_\_\_\_  
(Dr. Chew KuewWai  
Supervisor  
Department of Electrical and Electronic Engineering  
Faculty of Engineering and Science  
UniversitiTunku Abdul Rahman

Date:\_\_\_\_\_

\_\_\_\_\_  
(Dr. Yong ThianKhok)  
Co-supervisor  
Department of Electrical and Electronic Engineering  
Faculty of Engineering and Science  
UniversitiTunku Abdul Rahman

Date:\_\_\_\_\_

**FACULTY OF ENGINEERING AND SCIENCE**

**UNIVERSITI TUNKU ABDUL RAHMAN**

Date: 28/1/2013

**SUBMISSION OF THESIS**

It is hereby certified that TAN KIA WUI (ID No: 10UEM07420) has completed this thesis entitled **STUDIES ON THE PROPERTIES OF PMMA-BASED POLYMER ELECTROLYTE FOR LITHIUM RECHARGEABLE BATTERY** under the supervision of **Dr. CHEW KUEW WAI** (Supervisor) from the Department of Electrical and Electronic Engineering, Faculty of Engineering and Science, and **Dr. YONG THIAN KHOK** (Co-Supervisor) from the Department of Electrical and Electronic Engineering, Faculty of Engineering and Science.

I understand that University will upload softcopy of my thesis in pdf format into UTAR Institutional Repository, which may be made accessible to UTAR community and public.

Yours truly,

\_\_\_\_\_

(TAN KIA WUI)

## DECLARATION

I hereby declare that this dissertation is based on my original work except for quotations and citations which have been duly acknowledged. I also declare that it has not been previously or concurrently submitted for any other degree at UTAR or other institutions.

Name : TAN KIA WUI

Date : 28/1/2013

## TABLE OF CONTENTS

	Page
<b>ABSTRACT</b>	ii
<b>ACKNOWLEDGEMENTS</b>	iv
<b>APPROVAL SHEET</b>	v
<b>SUBMISSION OF THESIS</b>	vi
<b>DECLARATION</b>	vii
<b>TABLE OF CONTENT</b>	viii
<b>LIST OF TABLES</b>	xi
<b>LIST OF FIGURES</b>	xii
<b>LIST OF ABBREVIATIONS</b>	xvi
<b>CHAPTERS</b>	
<b>1.0 INTRODUCTION</b>	<b>1</b>
1.1 Background of Studies	1
1.2 Justification of Studies	3
1.3 Aim and Objectives of Research	4
1.5 Organisation of Thesis	5
<b>2.0 LITERATURE REVIEW</b>	<b>7</b>
2.1 Types of Battery	7
2.2 The Development of Lithium ion Polymer Battery	9
2.2.1 Main Components of a Rechargeable Battery	11
2.2.2 Discharging and Recharging Mechanism of Lithium ion Rechargeable Battery	12
2.2.3 Lithium Ion Polymer Battery	14
2.3 The Development of Polymer Electrolyte	17
2.4 Development of PMMA-Based Polymer Electrolyte	19
2.5 Electrolytes for Li-Ion Battery	21
2.5.1 Solid Polymer Electrolyte (SPE)	22
2.5.2 Gelled Polymer Electrolyte (GPE)	24
2.5.3 Composite Solid Polymer Electrolyte (CSPE)	26
2.6 Ionic Conductivity of Polymer Electrolyte	28
2.6.1 The Effect of Plasticizer to the Ionic Conductivity in Polymer Electrolyte	30
2.6.2 The Effect of Lithium Salt to the Ionic Conductivity in Polymer Electrolyte	32
2.6.3 The Effect of Inorganic Filler to the Ionic Conductivity in Polymer Electrolyte	33
2.6.4 The Effect of Temperature towards the Ionic Conductivity	35

<b>3.0</b>	<b>RESEARCH METHODOLOGY</b>	<b>37</b>
3.1	Materials	37
3.1.1	Poly(methylmethacrylate) (PMMA)	37
3.1.2	Lithium Perchlorate (LiClO <sub>4</sub> )	40
3.1.3	Ethylene Carbonate (EC)	42
3.1.4	Propylene Carbonate (PC)	44
3.1.5	Aluminum Oxide (Al <sub>2</sub> O <sub>3</sub> )	46
3.1.6	Silicon Dioxide (SiO <sub>2</sub> )	48
3.1.7	Tetrahydrofuran THF	50
3.2	Solution-Cast Technique	51
3.3	Characterisations	53
3.3.1	Electrochemical Impedance Spectroscopy (EIS)	54
3.3.2	Fourier Transform Infrared Spectroscopy (FTIR)	58
3.3.3	X-Ray Diffraction (XRD)	60
3.3.4	Scanning Electron Microscope (SEM)	64
<b>4.0</b>	<b>RESULT AND DISCUSSION</b>	<b>68</b>
4.1	Electrochemical Impedance Spectroscopy (EIS) Studies	68
4.1.1	Ionic Conductivity at ambient temperature	70
4.1.1.1	Ionic Conductivity for determining the optimum EC and PC mixture ratio	70
4.1.1.2	Ionic Conductivity Results for PMMA-EC/PC system	71
4.1.1.3	Ionic Conductivity Results for PMMA-EC/PC-LiClO <sub>4</sub> system	73
4.1.1.4	Ionic Conductivity Results for PMMA-EC/PC-LiClO <sub>4</sub> -Al <sub>2</sub> O <sub>3</sub> system	76
4.1.1.5	Ionic Conductivity Results for PMMA-EC/PC-LiClO <sub>4</sub> -SiO <sub>2</sub> system	79
4.1.1.6	Summary of Ionic Conductivity Result at ambient Temperature	82
4.1.2	Temperature Dependence of Ionic Conductivity of Polymer Electrolytes	84
4.1.3	Dielectric Relaxation Studies	87
4.1.3.1	Dielectric Relaxation Studies on Polymer Electrolytes at Room Temperature	88
4.1.3.2	Dielectric Relaxation Studies on Polymer Electrolytes in the Temperature Range of 298 K to 373	95
4.2	X-ray Diffraction (XRD) Studies	100
4.2.1	PMMA-EC/PC samples XRD Result	101
4.2.2	PMMA-EC/PC-LiClO <sub>4</sub> samples XRD Result	104
4.2.3	PMMA-EC/PC-LiClO <sub>4</sub> -Al <sub>2</sub> O <sub>3</sub> samples XRD Result	108
4.2.4	PMMA-EC/PC-LiClO <sub>4</sub> -SiO <sub>2</sub> samples XRD Result	111
4.2.5	Summary of XRD characterization	113
4.3	Fourier Transform Infrared (FTIR) Studies	116
4.3.1	FTIR for PMMA-EC/PC samples	116
4.3.2	FTIR for PMMA-EC/PC-LiClO <sub>4</sub> samples	124
4.3.3	FTIR for PMMA-EC/PC-LiClO <sub>4</sub> -Al <sub>2</sub> O <sub>3</sub> samples	131

4.3.4	FTIR for PMMA-EC/PC-LiClO <sub>4</sub> 6SiO <sub>2</sub> samples	135
4.3.5	Summary of FTIR Spectroscopy	140
4.4	Scanning Electron Microscopy (SEM) Studies	144
4.4.1	PMMA-EC/PC SEM	144
4.4.2	PMMA-EC/PC-LiClO <sub>4</sub> SEM	147
4.4.3	PMMA-EC/PC-LiClO <sub>4</sub> -Al <sub>2</sub> O <sub>3</sub> SEM	150
4.4.4	PMMA-EC/PC-LiClO <sub>4</sub> -SiO <sub>2</sub> SEM	154
4.4.5	SEM images for Highest Ionic Conductivity Samples in each system	157
4.5	Mechanical Properties	159
<b>5.0</b>	<b>CONCLUSION</b>	<b>167</b>
5.1	Summary	167
5.2	Suggestion for Future Work	170
	<b>LIST OF REFERENCES</b>	<b>172</b>

## LIST OF TABLES

Table		Page
2.1	Examples of primary and secondary batteries	8
2.2	Anode material, cathode materials and type of polymer electrolyte used in lithium ion rechargeable battery	12
3.1	Physical Properties of the Poly(methylmethacrylate) (PMMA)	39
3.2	Physical Properties of Lithium Perchlorate (LiClO <sub>4</sub> )	42
3.3	Physical Properties of Ethylene Carbonate	43
3.4	Physical Properties of Propylene Carbonate	45
3.5	Physical Properties of Aluminum Oxide (Al <sub>2</sub> O <sub>3</sub> )	47
3.6	Physical properties of SiO <sub>2</sub>	49
3.7	Physical properties of Tetrahydrofuran (THF)	51
4.1	Ionic conductivity of the best sample in each system	81
4.2	Intensity obtained at diffraction peaks for samples (1-x) PMMA ó (x) EC/PC	102
4.3	Intensity peak obtained at diffraction peaks for (1-x)PMMA-EC/PC- (x) LiClO <sub>4</sub> system	106
4.4	Intensity peak obtained at diffraction peaks for (1-x)PMMA-EC/PC-LiClO <sub>4</sub> - (x)Al <sub>2</sub> O <sub>3</sub> system	109
4.5	Intensity obtained at diffraction peaks for (1-x)PMMA-EC/PC-LiClO <sub>4</sub> - (x)SiO <sub>2</sub> system	112
4.6	Vibration modes and wavenumber of pure PMMA	118
4.7	Vibration modes and wavenumber of pure EC	119
4.8	Vibration modes and wavenumber of pure PC	120
4.9	Vibration modes and wavenumber of pure LiClO <sub>4</sub>	125
4.10	Vibration modes and wavenumber of pure Al <sub>2</sub> O <sub>3</sub>	132
4.11	Vibration modes and wavenumber of pure SiO <sub>2</sub>	136
4.12	Overall tensile strength and tensile strain for the best ionic conductivity sample	166
5.1	Work done by other researchers in solid polymer electrolyte system	169

## LIST OF FIGURES

Figure		Page
2.1	Discharge and recharge mechanism for a lithium ion rechargeable battery	14
2.2	Solid polymer electrolyte battery (Linden and Reddy, 2002)	15
3.1	Chemical structure of MMA	39
3.2	Chemical structure of LiClO <sub>4</sub>	41
3.3	Chemical structure of Ethylene Carbonate	43
3.4	Chemical structure of Propylene Carbonate	44
3.5	Chemical structure of Alumina Oxide (Al <sub>2</sub> O <sub>3</sub> )	46
3.6	Chemical structure of SiO <sub>2</sub>	48
3.7	Chemical structure of Tetrahydrofuran (THF)	50
3.8	Polymer Electrolyte Samples	52
3.9	Cole-Cole plot of AC impedance spectroscopy	55
3.10	Equivalent circuit of the AC impedance spectroscopy	56
3.11	Experimental setup of Solartron SI 1260 Impedance/ Gain-Phase Analyzer	57
3.12	Operation of the FTIR spectroscopy	59
3.13	Experimental setup of Perkin Elmer Spectrum RX1 FTIR spectroscopy	60
3.14	Diffraction in the crystalline material	62
3.15	Experimental setup of the Shimadzu XRD-6000 diffractometer	63
3.16	Experimental setup of the Hitachi S-3400N Scanning Electron Microscope	67
4.1	Cole-Cole plot of a.c. impedance spectroscopy for 12 wt % Al <sub>2</sub> O <sub>3</sub> , 12 wt% SiO <sub>2</sub> and sample without filler	68
4.2	Ionic Conductivity of EC in (EC + PC)	70
4.3	Ionic Conductivity versus wt% of EC/PC mixture added into PMMA	72
4.4	Ionic Conductivity versus wt% of LiClO <sub>4</sub> added into PMMA-EC/PC	74
4.5	Ionic Conductivity versus wt% of nano-sized Al <sub>2</sub> O <sub>3</sub> added into PMMA-EC/PC- LiClO <sub>4</sub>	77
4.6	Ionic Conductivity versus wt% of nano-sized SiO <sub>2</sub> added into PMMA-EC/PC-LiClO <sub>4</sub>	80
4.7	Ionic conductivity of the best sample in each system	82
4.8	Temperature dependence of polymer electrolytes with 12 wt% of SiO <sub>2</sub> , 12 wt% of Al <sub>2</sub> O <sub>3</sub> and without filler	85
4.9	Real part of complex permittivity ( $\epsilon'$ ) for PMMA-EC/PC-(x wt%) LiClO <sub>4</sub> corresponding to frequency	89
4.10	Real part of complex permittivity ( $\epsilon'$ ) for PMMA-EC/PC-LiClO <sub>4</sub> -(x wt%) Al <sub>2</sub> O <sub>3</sub> corresponding to frequency	90
4.11	Real part of complex permittivity ( $\epsilon'$ ) for PMMA-EC/PC-LiClO <sub>4</sub> -(x wt%) SiO <sub>2</sub> corresponding to frequency	90

4.12	Imaginary part of complex permittivity ( $\epsilon''$ ) for PMMA-EC/PC-(x wt%) LiClO <sub>4</sub> corresponding to frequency	92
4.13	Imaginary part of complex permittivity ( $\epsilon''$ ) for PMMA-EC/PC-LiClO <sub>4</sub> -(x wt%) Al <sub>2</sub> O <sub>3</sub> corresponding to frequency	93
4.14	Imaginary part of complex permittivity ( $\epsilon''$ ) for PMMA-EC/PC-LiClO <sub>4</sub> -(x wt%) SiO <sub>2</sub> corresponding to frequency	93
4.15	Real part of complex permittivity ( $\epsilon'$ ) for PMMA-EC/PC- 25 wt% of LiClO <sub>4</sub> corresponding to frequency in the temperature range of 298-373K	96
4.16	Real part of complex permittivity ( $\epsilon'$ ) for PMMA-EC/PC-LiClO <sub>4</sub> - 12 wt% of Al <sub>2</sub> O <sub>3</sub> corresponding to frequency in the temperature range of 298-373K	97
4.17	Real part of complex permittivity ( $\epsilon'$ ) for PMMA-EC/PC-LiClO <sub>4</sub> - 12 wt% of SiO <sub>2</sub> corresponding to frequency in the temperature range of 298-373K	97
4.18	Imaginary part of complex permittivity ( $\epsilon''$ ) for PMMA-EC/PC- 25 wt% of LiClO <sub>4</sub> corresponding to frequency in the temperature range of 298-373K	99
4.19	Imaginary part of complex permittivity ( $\epsilon''$ ) for PMMA-EC/PC-LiClO <sub>4</sub> - 12 wt% of Al <sub>2</sub> O <sub>3</sub> corresponding to frequency in the temperature range of 298-373K	99
4.20	Imaginary part of complex permittivity ( $\epsilon''$ ) for PMMA-EC/PC-LiClO <sub>4</sub> - 12 wt% of SiO <sub>2</sub> corresponding to frequency in the temperature range of 298-373K	100
4.21	XRD patterns of (a) pure PMMA, (b) 5 wt% EC/PC, (c) 10 wt% EC/PC, (d) 15 wt% EC/PC, (e) 20 wt% EC/PC, (f) 25 wt% EC/PC, (g) 30 wt% EC/PC, (h) 35 wt% EC/PC added into PMMA	102
4.22	XRD patterns of (a) pure PMMA, (b) pure LiClO <sub>4</sub> , (c) 0 wt% LiClO <sub>4</sub> , (d) 5 wt% LiClO <sub>4</sub> , (e) 15 wt% LiClO <sub>4</sub> , (f) 25 wt% LiClO <sub>4</sub> , (g) 35 wt% LiClO <sub>4</sub> , (h) 50 wt% LiClO <sub>4</sub> doped into PMMA-EC/PC system	105
4.23	XRD patterns of (a) pure PMMA, (b) pure Al <sub>2</sub> O <sub>3</sub> , (c) 0 wt% Al <sub>2</sub> O <sub>3</sub> , (d) 4 wt% Al <sub>2</sub> O <sub>3</sub> , (e) 8 wt% Al <sub>2</sub> O <sub>3</sub> , (f) 12 wt% Al <sub>2</sub> O <sub>3</sub> , (g) 16 wt% Al <sub>2</sub> O <sub>3</sub> , (h) 20 wt% Al <sub>2</sub> O <sub>3</sub> , dispersed into PMMA-EC/PC-LiClO <sub>4</sub> system	109
4.24	XRD patterns of (a) pure PMMA, (b) pure SiO <sub>2</sub> , (c) 0 wt% SiO <sub>2</sub> , (d) 4 wt% SiO <sub>2</sub> , (e) 8 wt% SiO <sub>2</sub> , (f) 12 wt% SiO <sub>2</sub> , (g) 16 wt% SiO <sub>2</sub> , (h) 20 wt% SiO <sub>2</sub> dispersed into PMMA-EC/PC-LiClO <sub>4</sub> system	112
4.25	XRD patterns of (a) pure PMMA, (b) pure LiClO <sub>4</sub> , (c) pure Al <sub>2</sub> O <sub>3</sub> , (d) pure SiO <sub>2</sub> , (e) PMMA (70):EC/PC (30), (f) PMMA-EC/PC (75): LiClO <sub>4</sub> (25), (g) PMMA-EC/PC-LiClO <sub>4</sub> (88): Al <sub>2</sub> O <sub>3</sub> (12), (h) PMMA-EC/PC- LiClO <sub>4</sub> (88): SiO <sub>2</sub> (12)	114
4.26	FTIR spectrum for pure PMMA	118
4.27	FTIR spectrum for pure EC	119
4.28	FTIR spectrum for pure PC	120

4.29	FTIR spectrum for a) pure PMMA, b) pure EC, c) pure PC, d) 5wt%, e) 10 wt%, f) 15 wt%, g) 20wt%, h) 25 wt%, i) 30 wt%, j) 35 wt%, of EC/PC added into PMMA	121
4.30	FTIR spectrum for pure PMMA and PMMA- 30wt% EC/PC in the range of 1000-1550cm <sup>-1</sup>	122
4.31	FTIR spectrum for pure PMMA and PMMA- 30wt% EC/PC in the range of 700-930 cm <sup>-1</sup>	123
4.32	FTIR spectrum for pure PMMA and PMMA- 30wt% EC/PC in the range of 1550-1900 cm <sup>-1</sup>	123
4.33	FTIR spectrum for pure LiClO <sub>4</sub>	125
4.34	FTIR spectrum for a) pure PMMA, b) pure LiClO <sub>4</sub> , c) 0wt%, d) 5wt%, e) 10 wt%. f) 15 wt%. g) 20wt%,h) 25 wt%. i) 30 wt%. j) 35 wt%. k) 40wt%. l) 45wt%. m) 50 wt% of LiClO <sub>4</sub> doped into PMMA- EC/PC system	126
4.35	Formation of doublet peak for PMMA-EC/PC-25 wt% LiClO <sub>4</sub> in the range of 740-790 cm <sup>-1</sup>	128
4.36	PMMA-30 wt% EC/PC and PMMA-EC/PC-25 wt% LiClO <sub>4</sub> in the range of 2860-3050 cm <sup>-1</sup>	129
4.37	FTIR spectrum for pure Al <sub>2</sub> O <sub>3</sub>	131
4.38	FTIR spectrum for a) pure PMMA, b) pure Al <sub>2</sub> O <sub>3</sub> , c) 0wt%, d)2wt%, e) 4 wt%, f) 6 wt%, g) 8wt%, h) 10 wt%, i) 12 wt%, j)14 wt%, k) 16wt%, l) 18wt%, m) 20 wt%, of Al <sub>2</sub> O <sub>3</sub> dispersed into PMMA-EC/PC-LiClO <sub>4</sub> system	133
4.39	PMMA-EC/PC-LiClO <sub>4</sub> with 12 wt% and without Al <sub>2</sub> O <sub>3</sub> in the range of 550-900cm <sup>-1</sup>	134
4.40	FTIR spectrum for pure SiO <sub>2</sub>	135
4.41	FTIR spectrum for a) Pure PMMA, b) SiO <sub>2</sub> , c)0wt%, d)2wt%, e) 4 wt%, f) 6 wt%, g) 8wt%, h) 10 wt%, i) 12 wt%, j) 14 wt%, k) 16wt%, l) 18wt%, m) 20 wt%, of SiO <sub>2</sub> dispersed into PMMA-EC/PC-LiClO <sub>4</sub> system	138
4.42	Comparison of shifting in vibration peak of CH <sub>2</sub> rocking mode of PMMA in without SiO <sub>2</sub> and 12 wt% of SiO <sub>2</sub>	139
4.43	Comparison of change in shape of vibrational peak in the range of 610-650cm <sup>-1</sup>	139
4.44	FTIR spectrum for a) pure PMMA, b) pure EC c) pure PC d) pure LiClO <sub>4</sub> e) pure Al <sub>2</sub> O <sub>3</sub> f) pure SiO <sub>2</sub> g)PMMA-30wt% EC/PC h) PMMA-EC/PC-25wt% LiClO <sub>4</sub> i) PMMA-EC/PC-LiClO <sub>4</sub> -12wt% Al <sub>2</sub> O <sub>3</sub> , j) PMMA-EC/PC-LiClO <sub>4</sub> -12wt% SiO <sub>2</sub>	141
4.45	SEM image of pure PMMA	145
4.46	SEM image of PMMA- 10wt% EC/PC	145
4.47	SEM image of PMMA- 30wt% EC/PC	146
4.48	SEM image of PMMA-EC/PC- 5 wt% LiClO <sub>4</sub>	148
4.49	SEM image of PMMA-EC/PC- 25 wt% LiClO <sub>4</sub>	148
4.50	SEM image of PMMA-EC/PC- 50 wt% LiClO <sub>4</sub>	149
4.51	SEM image of PMMA-EC/PC-LiClO <sub>4</sub> -4 wt% Al <sub>2</sub> O <sub>3</sub>	151
4.52	SEM image of PMMA-EC/PC-LiClO <sub>4</sub> -12 wt% Al <sub>2</sub> O <sub>3</sub>	152
4.53	SEM image of PMMA-EC/PC-LiClO <sub>4</sub> -20 wt% Al <sub>2</sub> O <sub>3</sub>	152

4.54	SEM image of PMMA-EC/PC-LiClO <sub>4</sub> -4 wt% SiO <sub>2</sub>	154
4.55	SEM image of PMMA-EC/PC-LiClO <sub>4</sub> -12 wt% SiO <sub>2</sub>	155
4.56	SEM image of PMMA-EC/PC-LiClO <sub>4</sub> -20 wt% SiO <sub>2</sub>	155
4.57	SEM images for highest ionic conductivity sample of each system	157
4.58	Tensile stress and strain result of pure PMMA	162
4.59	Tensile stress and strain result of PMMA- 30 wt% of EC/PC	162
4.60	Tensile stress and strain result of PMMA-EC/PC- 25 wt% LiClO <sub>4</sub>	163
4.61	Tensile stress and strain result of PMMA-EC/PC- LiClO <sub>4</sub> - Al <sub>2</sub> O <sub>3</sub>	164
4.62	Tensile stress and strain result of PMMA-EC/PC- LiClO <sub>4</sub> - SiO <sub>2</sub>	165
4.63	Overall tensile stress of the best ionic conductivity sample	166
4.64	Overall tensile strain of the best ionic conductivity sample	166

## LIST OF ABBREVIATIONS

PEO	Poly(ethylene oxide)
PAN	Poly(acrylonirile)
PMMA	Poly(methyl methacrylate)
PVC	Poly(vinyl chloride)
PVDF	Poly(vinylidene fluoride)
SPE	Solid polymer electrolyte
GPE	Gelled polymer electrolyte
CSPE	Composite solid polymer electrolyte
EC	Ethylene carbonate
PC	Propylene carbonate
LiClO <sub>4</sub>	Lithium perchlorate
SiO <sub>2</sub>	Fumed Silica
TiO <sub>2</sub>	Titanium oxide
Al <sub>2</sub> O <sub>3</sub>	Aluminum oxide
THF	Tetrahydrofuran
EIS	Electrochemical impedance spectroscopy
FTIR	Fourier transform infrared spectroscopy
XRD	X-ray diffraction
SEM	Scanning electron microscope
n	Charge carrier concentration,
q	Charge on the mobile species
μ	Mobility of ions
T <sub>g</sub>	Glass transition temperature

$\text{Li}^+$	Lithium ions
	Ionic conductivity in $\text{Scm}^{-1}$
$R_b$	Bulk impedance in Ohm
A	Surface Area in $\text{cm}^2$
t	Thickness
$\lambda$	Wavelength in m
$\theta$	Incident Angle
d	d- spacing
	Tensile Stress
F	Applied Force
A	Area
$\varepsilon$	Tensile Strain
$l_i$	Elongated Length
$l_o$	Original Length

# CHAPTER 1

## INTRODUCTION

### 1.1 Background of Study

In view of the demand for energy and environment, the research on electrochemical energy has undergone rapid development as an alternative energy source. The lithium ion rechargeable battery, with a significantly higher energy density and lighter weight has replaced the conventional rechargeable battery such as NiMh, NiCd, NiZn, AgNi, etc as a primary choice for portable electronics devices (Ahmad, 2009). Recently, different types of lithium-ion rechargeable battery with different capacity, shape and size are commercially available. However, the most common type of lithium-ion rechargeable battery is still uses the liquid electrolyte in the battery system. This type of battery is not completely safe because it is suffering from leakage and is flammable. In order to eliminate the internal short-circuiting in the cell, a separator must be placed in between the cathode and the anode (Osaka et al., 1997). Furthermore, the formation of lithium dendrites during the charging period will lower the cycling efficiency and will lead to internal short circuiting in the battery (Song et al., 1999).

In the current progress, researchers are looking for an alternative to replace the liquid electrolyte. It has been discovered that polymer electrolyte may be a good candidate to replace the liquid electrolyte as it does not suffer from leakage and have no flammable problem (Tan et al., 2007). Besides that, the intrinsic advantages of polymer electrolyte make it favourable to replace the conventional liquid electrolyte. By using solid polymer electrolyte as the battery electrolyte, a separator is not required. Hence, a possible explosion can be avoided. Furthermore, polymer electrolytes offer better flexibility and shape versatility which allow for the fabrication of thin and flexible shape of lithium ion batteries with good mechanical integrity (Deka and Kumar, 2010).

The initial work on polymer electrolytes were mainly focused on the complexes of poly(ethylene oxide) PEO with the incorporation of various inorganic lithium salts. Unfortunately, these systems failed to exhibit any desirable ionic conductivity due to its high degree of crystallisation and low solubility of salt in amorphous region (Berthier et al., 1983). In order to attain a high ambient-temperature conductivity, a polymer that is amorphous in nature and has a flexible backbone is preferred (Ahmad, 2009). Due to this reason, PMMA-based electrolyte is preferred due to its amorphous nature, flexible backbone, solvent retention ability and less reactive towards lithium electrode (Ahmad et al., 2006; Appetecchi et al., 1995).

## 1.2 Justification of Studies

PEO-based solid polymer electrolyte have received much attention over the past few decades for many applications such as batteries, fuel cells, super capacitors, display devices, sensors, etc (Scrosati, 2000). Due to its high degree of crystalline, PEO-based polymer electrolyte faced an inherent problem of low ionic conductivity that limits the application of this type of polymer electrolyte (Pradhan et al.,2008). To attain a high room temperature ionic conductivity, several types of polymer electrolyte based on poly(acrylonirile) (PAN) (Huang et al., 1996; Wang et al.,1997), poly(methyl methacrylate) (PMMA) (Bohnkeet al., 1993;Stallworth et al., 1995), poly(vinyl chloride) (PVC) (Pistoia et al., 1996; Sung et al., 1998) and poly(vinylidene fluoride) (PVDF) (Tsuchida et al., 1993; Jiang et al., 1998) are developed and characterised. In order to enhance the ionic conductivity in SPEs, several modifications are reported such as an addition of excessive plasticiser to generate gelled polymer electrolyte (GPE) or nano-composite filler to generate composite solid polymer electrolyte (CSPE).

As reported by Rajendran and Sivakumar (2008), ethylene carbonate (EC) ( $\epsilon = 89$ ) and propylene carbonate (PC) ( $\epsilon = 64.4$ ) exhibit a high dielectric constant which may be a good candidate to dissolve lithium salt and forming complexation with polymer. In fact, most of the studies based on EC/PC plasticiser mixture are to generate GPE. In the present study, the EC/PC

mixture is used to generate plasticised SPE with controlled EC/PC mixture to avoid the formation of gel. A study by Deka and Kumar (2010) showed that the dispersion of ceramic filler in the polymeric complexes could prevent the polymer chain reorganisation. In addition, the ionic conductivity and interfacial properties when come into contact with lithium electrode could be improved with the addition of ceramic filler (Saikia et al., 2009). In this current project, SiO<sub>2</sub> and Al<sub>2</sub>O<sub>3</sub> are used as ceramic filler.

### **1.3 Aim and Objectives of Research**

#### Aim:

- To develop a high ionic conductivity PMMA-based solid type of polymer electrolyte.

#### Objectives:

- To enhance the ionic conductivity of polymer electrolyte with plasticiser upon addition of lithium salt and nano-sized fillers.
- To examine the mechanisms of the conducting ions in the polymer electrolytes through dielectric analysis.
- To study the complexation within the polymer electrolytes systems by Fourier Transform Infrared Spectroscopy (FTIR).
- To study the structural behaviour of the polymer electrolytes by X-Ray Diffraction (XRD) and Scanning Electron Microscope (SEM).

## 1.4 Organisation of Thesis

Basically, this thesis emphasises on the development of solid polymer electrolyte based on PMMA as a host polymer. The preparation of the electrolyte thin film and the behaviour of the polymer electrolyte are determined and discussed.

The literature review of this study is reported in Chapter 2. Different types of battery and the development of lithium-ion polymer battery are discussed. The discussion on the polymer electrolyte is focused on PMMA-based electrolyte which can be further classified into solid polymer electrolyte (SPE), gelled polymer electrolyte (GPE) and composite solid polymer electrolyte (CSPE). The effects of additives such as plasticiser, lithium salts and ceramic filler toward electrical and mechanical properties are reported.

In Chapter 3, the research methodology of this study is discussed. The raw materials (PMMA, LiClO<sub>4</sub>, EC, PC, Al<sub>2</sub>O<sub>3</sub>, SiO<sub>2</sub> and THF) used in this study are explained. This is followed by an explanation of the solution cast technique. Later, the characterisation methods used in this study such as Electrochemical Impedance Spectroscopy (EIS), Fourier Transform Infrared Spectroscopy (FTIR), X-Ray Diffraction (XRD) and the Scanning Electron Microscope (SEM) are explained.

The results obtained from the experiments are shown and discussed in Chapter 4. The ionic conductivity behaviour at ambient temperature and higher temperature are discussed. This is followed by the characterisation of XRD where the chemical composition and crystalline structure of the materials are reported. Later, the results obtained from FTIR are discussed where the spectrums are plotted and the bonding of materials are explained. Lastly, the micro-structures of polymer electrolytes obtained from SEM are examined.

Finally, the conclusions of this study are reported in Chapter 5. In addition, the suggestions and recommendations for future research in this area of study are discussed.

## CHAPTER 2

### LITERATURE REVIEW

#### 2.1 Types of Battery

Normally, a battery is made up of one or more electrochemical cells which convert the stored chemical energy into electrical energy. There are two general types of battery, which are non-rechargeable battery (so-called primary battery) and rechargeable battery (so-called secondary battery). Non-rechargeable battery is a kind of battery in which the electrochemical reaction is not reversible and must be disposed of after used. The advantages of using primary battery are convenient and inexpensive. Comparatively, the rechargeable battery can be recharged electrically back to the initial condition after discharging i.e. the electrochemical reaction is reversible. The different shapes and sizes of rechargeable battery make it usable for a wide range of applications. As compared to primary batteries, the rechargeable batteries have a lower total usage cost and are more environmental friendly than the disposable primary batteries. Table 2.1 shows the examples of primary and secondary batteries.

**Table 2.1: Examples of primary and secondary batteries**

<b>Primary Batteries</b>	<b>Secondary Batteries</b>
cadmium/mercury oxide	nickel-zinc
lithium/manganese dioxide	nickel-iron
lithium/sulfur dioxide	nickel-hydrogen
magnesium	lithium ion
zinc/carbon	Lithium ion polymer
zinc/mercury oxide	silver-cadmium
zinc/silver oxide	sodium/nickel chloride
	zinc/chlorine

Since the first industrial implementation by Sony Corporation in 1991, lithium ion (Li-ion) battery has achieved tremendous technological and commercial success (Osinska et al., 2009). The contributions such as high energy density, high working voltage, long cycle and low weight make this type of electrochemical energy storage devices an ideal power source for many applications such as electrical vehicles, portable power sources and space exploration.

The development of a solid-state battery based on solid electrolytes have been most active in the area of portable rechargeable batteries due to the advantages over conventional lithium-ion battery such as improved safety and easy of fabrication (Li et al., 2003). Therefore, researchers dedicated most interest in the development of rechargeable batteries in order to exploit its advantages and market needs.

## 2.2 The Development of Lithium ion Polymer Battery

Pioneer work with the lithium battery began in 1912 under G.N. Lewis. However, until the early 1970s the first non-rechargeable lithium battery became commercially available. Lithium is the lightest weight, highest voltage, and greatest energy density of all metals. The first published interest in lithium batteries began in the works of Harris in 1958. The work eventually led to the development and commercialisation of a variety of primary lithium cells during 1970s.

The original design of the Li-ion polymer battery is invented in 1970s; the researcher uses a dry solid polymer electrolyte only in the battery system. This electrolyte resembles a plastic-like film and act as a separator that does not conduct electricity but allows an exchange of ions between anode to cathode. The polymer electrolyte offers simplifications with respect to fabrication, safety, light weight and flexibility. There is no leaking problem and any danger of flammability because no liquid or gelled electrolyte is used. With the provision of a thin film of electrolyte system, the form, shape and size of the battery can be fabricated easily at lower production cost (Mahendran and Rajendran, 2003).

Although using the solid polymer electrolyte in a lithium ion polymer battery has several advantages, but it still suffers from poor conductivity. Due to its high internal resistance, the battery cannot deliver the current to modern communication devices or spinning up the hard drives of mobile computing equipment. Even though heating the cell to 60°C or higher temperature will eventually increase the conductivity to acceptable levels but this requirement is unsuitable for practical applications.

Therefore, research continues to develop a solid Li-ion polymer battery that performs at room temperature. A solid Li-ion polymer is commercially available in 2005. It is expected to be very stable and would run 1000 full cycles with higher energy densities. In order to build up a small Li-ion polymer battery system, gelled electrolyte has been invented. Most of the commercial Li-polymer batteries used today for mobile phones are a hybrid and contain gelled electrolyte. With the implementation of gelled electrolyte, the characteristics and performance are similar to the solid type where these polymer electrolytes are used to replace the porous separator and to enhance ion conductivity.

### **2.2.1 Main Components of a Rechargeable Battery**

A battery is a device that converts the chemical energy contained in its active materials directly into electrical energy by an electrochemical reaction. For a rechargeable system, the battery is discharged and recharged by a reversal of process by transferring the electrons from anode to cathode or vice versa.

A battery consists of three main components, which are anode, cathode and electrolyte. The anode or negative electrode which gives up electrons to the external circuit and are oxidised during the electrochemical reaction. Besides, the cathode or positive electrode which accepts electron from the external circuit is reduced during the electrochemical reaction. Whereby, the electrolyte is an ionic conductor which is sandwiched between anode and cathode to provide the medium for transfer of ions between anode and cathode. All these parts are connected properly in order to ensure the safety when discharging and recharging of the battery.

A polymer electrolyte plays an important role due to the safety and environmental issues. A polymer electrolyte acts as a separator between anode and cathode to prevent internal short circuit and at the same time, provide good ionic conductivity. The polymer electrolytes have more advantages compared

to the conventional liquid electrolyte such as; it is not flammable and has no leakage problem. The common usage of anode materials, cathode materials and types of polymer electrolyte are shown in Table 2.1.

**Table 2.2: Anode material, cathode materials and type of polymer electrolyte used in lithium ion rechargeable battery**

Anode Material	Cathode Material	Type of Polymer Electrolyte
Graphite ( $\text{LiC}_6$ )	$\text{LiCoO}_2$	Liquid electrolyte
Hard Carbon ( $\text{LiC}_6$ )	$\text{LiMn}_2\text{O}_4$	Solid polymer electrolyte
Titanate ( $\text{Li}_4\text{Ti}_5\text{O}_{12}$ )	$\text{LiNiO}_2$	Gel polymer electrolyte
Si ( $\text{Li}_{4.4}\text{Si}$ )	$\text{LiFePO}_4$	Composite polymer electrolyte
Ge ( $\text{Li}_{4.4}\text{Ge}$ )	$\text{Li}_2\text{FePO}_4\text{F}$	
	$\text{LiCo}_{1/3}\text{Ni}_{1/3}\text{Mn}_{1/3}\text{O}_2$	
	$\text{Li}(\text{Li}_d\text{Ni}_x\text{Mn}_y\text{Co}_z)\text{O}_2$	

### 2.2.2 Discharging and Recharging Mechanism of Lithium Ion Rechargeable Battery

A lithium-ion battery belongs to a family of rechargeable battery (secondary battery) types in which lithium ions move from the negative electrode to the positive electrode during discharge, and back again when charging. The common lithium ion rechargeable battery uses liquid electrolyte as a medium to promote ionic conductivity. Normally, a porous separator is placed in between the anode and cathode to isolate both electrodes in order to prevent internal short-circuit while allowing the ions to transfer through the electrolyte.

Generally, a battery converts the chemical energy stored in the electrodes into electric energy through an electrochemical oxidation-reduction process. As shown in Figure 2.1, the positive electrode is made of Lithium cobalt oxide, or  $\text{LiCoO}_2$ . The negative electrode is made of carbon. The battery is recharged when an external DC power supply is connected. The lithium ions move through the electrolyte from the positive electrode to the negative electrode and is attached to the carbon. During the discharging process where an external load is connected to the battery therefore the lithium ions which is attached to the carbon (cathode) move back to the  $\text{LiCoO}_2$  electrode. The chemical reaction in the anode and cathode is shown in the following process.

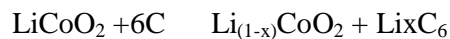
The cathode half-reaction (with charging being forward) is:



The anode half-reaction is:



Overall reaction is:



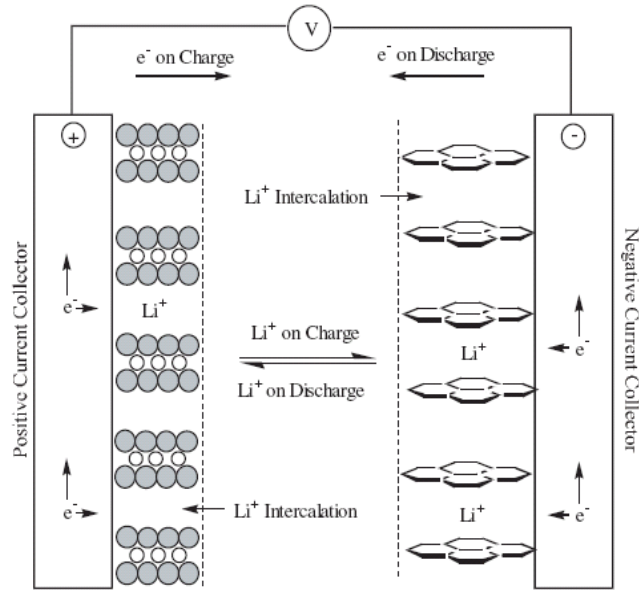


**Figure 2.1: Discharge and recharge mechanism for a lithium ion rechargeable battery (Linden and Reddy, 2002)**

### 2.2.3 Lithium Ion Polymer Battery

The main objective for the development of the rechargeable lithium batteries is to produce batteries that have high energy density, high power density, and good cycle life and charge retention. The following characteristics are critical when choosing a proper electrolyte for rechargeable lithium battery (Linden and Reddy, 2002):

1. Good ionic conductivity ( $>10^{-3}$  S/cm from -40 to 90 degree C) to minimise internal resistance.
2. Lithium ion transference number approaching unity (to limit concentration polarisation)
3. Wide electrochemical voltage window (0 to 5V)
4. Thermal stability (up to 70 degree C)
5. Compatibility with other cell components

Figure 2.2 illustrates the components of the lithium polymer battery, the polymer electrolyte acts as electrolyte and separator, a thin lithium metal foil as the anode material and transition metal oxide blend backed by a metal-foil current collector as the positive electrode. As the polymer electrolyte act as a separator, therefore no extra separator material is needed.

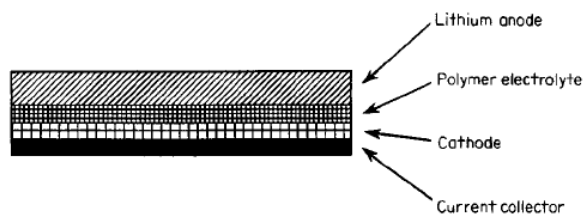


**Figure 2.2: Solid polymer electrolyte battery (Linden and Reddy, 2002)**

The rechargeable lithium ion battery which uses a solid type of polymer electrolyte (SPE) is considered to have a safety advantage over the organic liquid electrolyte because of their lower reactivity with lithium and the absence of a volatile, flammable organic solvent. Another potential advantage of the

solid polymer battery is its capability to be easily fabricated in a variety of shapes and forms. Very thin batteries for cell phones, PDAs and similar application can be manufactured at the other extreme. Moreover, large thin plates can be manufactured and assembled in multiplate prismatic to produce very high energy density batteries. The advancement of high capacity battery has lead to the development of automotives to allow the development of high performances EV and the mobile industries.

The mechanism of discharging and recharging is almost similar to the conventional lithium ion battery as shown in Figure 2.1 except for the intercalation process where lithium ions are reversibly removed and placed into electrodes without significantly changing the electrodes structure. During the charging process the positive electrode material is oxidised while its negative electrode material is reduced. Lithium ions are de-intercalated from the positive electrode material and then intercalated into negative electrode material. As for the discharging operation, the opposite processes takes place when the negative electrode material is oxidised and the positive electrode material is reduced.

### 2.3 The Development of Polymer Electrolyte

Polymer electrolytes have gained wide attention due to its potential application in rechargeable lithium-ion batteries during the last two decades. For the promising application of polymer electrolyte, lithium-ion polymer rechargeable batteries are applicable in automotive industries, portable devices, aerospace applications, etc.

The term "Solid State Ionics" was given by Prof Takehiko Takahashi in 1960, who did pioneering work investigating ionic motion in solid polymer electrolytes. Solid state Ionics is not only limited to ionic conductors but also includes conductors and mixed conductors, in which the electric conduction is affected by migration not only of ions but also electrons or positive holes. Initially, the conventional liquid electrolytes were replaced by gel polymer electrolyte and later by composite solid polymer electrolytes leading to all solid state electrochemical devices (Gray, 1997a).

With the use of polymer electrolyte in lithium batteries, high specific energy and specific power, safe operation, flexibility in packaging and low cost of fabrication can be expected (Gray, 1991; MacArthur and Powers, 1996). The poor ionic conductivity of solid polymer electrolyte can be enhanced by adding plasticiser to form gel polymer electrolyte where the plasticiser effect might

make the lithium salt favourably dissociated and enhance the amorphous region in polymeric matrix (Sekhon et al., 2006; Singh et al. 2009). Further enhancement can be achieved by dispersing a nano-sized filler to form a composite solid polymer electrolyte where the ion pairs and ion aggregates can be dissociated due to the Lewis acid-base interaction to build up a new ionic pathway for ionic transportation (Scrosati et al., 2000).

Polymer electrolytes can be divided into four types, which are:-

- Solid polymer electrolyte (SPE)
- Gelled polymer electrolyte (GPE)
- Composite solid polymer electrolyte (CSPE)
- Composite polymer electrolyte (CPE)

Generally, a solid polymer electrolyte (SPE) is based on neat (is it neat or heat) high polymers, which serve as both solvent to dissolve lithium salts and mechanical matrix to support the processability. A gelled polymer electrolyte (GPE) is formed based on the engagement of polymer in a liquid electrolyte solution. Coheres, the Composite solid polymer electrolyte (CSPE) is formed based on the dispersion of composite or ceramic filler into SPE when the composite or ceramic filler is dispersed into the GPE.

## 2.4 Development of PMMA-Based Polymer Electrolyte

PMMA has been chosen as a host polymer because of its advanced physical properties like good film forming, thermal and chemical stability. PMMA itself is an amorphous (random arrangement of the asymmetrical carbon atom) by nature and it is colourless, transparent, has an excellent life period, and good mechanical properties (Rajendran et al., 2002). The common name for PMMA is acrylic glass which is a member of the acrylates family which is often used as an alternative to glass. In the current trend, PMMA is commonly used as a host polymer in polymer electrolyte due to the amorphous nature, excellent physical properties and higher ionic conductivity as compared to other polymer. The ionic conductivity is only conducted in amorphous region. It is believed that PMMA may be a good candidate to use as a host polymer in order to develop polymer electrolyte.

As reported by Tan et al. (2007), the ionic conductivity value of pure PMMA solid polymer electrolyte is  $10^{-10} \text{ Scm}^{-1}$ . Although the ionic conductivity of pure PMMA exhibits slightly higher than other polymer, but the low ionic conductivity makes it unfavourable to use as a polymer electrolyte. In fact, the ionic conductivity of the solid polymer electrolyte could be elevated to a higher level ( $10^{-7}$ - $10^{-5} \text{ Scm}^{-1}$ ) by integrating different plasticiser and lithium salt into the polymeric matrices. With the addition of 25 wt% of EC and 25 wt% of  $\text{LiCF}_3\text{SO}_3$ , the ionic conductivity is enhanced to ~

$1.36 \times 10^{-5} \text{ Scm}^{-1}$  (Tan et al., 2007). Othman et al. (2007) revealed that the ionic conductivity is varied according to different lithium salt and plasticiser added into the polymer electrolyte system. The conductivity of [PMMA-EC]- $\text{LiCF}_3\text{SO}_3$  system is  $3.40 \times 10^{-5} \text{ Scm}^{-1}$  and [PMMA-EC]- $\text{LiBF}_4$  system is about  $4.07 \times 10^{-7} \text{ Scm}^{-1}$  (Othman et al., 2007). It is revealed that the dielectric parameters and solubility of additives are strongly influenced by the nature of electrolyte materials.

Another approach to further enhance the ionic conductivity is dispersing the inorganic ceramic filler into the solid polymer electrolyte and developing the composite solid polymer electrolyte. Adebahr et al. (2003) and Ahmad et al. (2003) reported that the dispersion of nanosized ceramic filler particles not only increases its mechanical properties, but also enhances its ionic conductivity. The conductivity of a filler added polymer electrolyte system can be achieved by the conductivity at the order of  $10^{-3} \text{ Scm}^{-1}$  (Ahmad et al., 2003). Studies showed that composite filler with high dielectric constant helps to dissolve the electrolyte salt and increase ion conduction through the solvent domain surrounding the polymer matrix (Deka and Kumar, 2010). Besides, Adebahr et al. (2003) claimed that dispersing of filler to the PMMA based electrolyte decreases the polymer/cation interaction and introduces a new pathway for lithium ions transportation.

In the current research, many strategies have been accomplished to enhance the ionic conductivity of polymer electrolytes. These include the incorporating of solvent (plasticisers) to form plasticised or gel polymer electrolytes, dispersing with inorganic fillers to make composite polymer electrolytes and synthesising new polymer electrolyte.

## **2.5 Electrolytes for Li-Ion Battery**

There are several types of electrolyte including liquid electrolyte, solid polymer electrolyte (SPE), gelled polymer electrolyte (GPE) and composite solid polymer electrolyte (CSPE). Electrolyte is one of the main components sandwiched between anode and cathode to complete the circuitry in the battery. A polymer electrolyte functions as a separator to anode and cathode and at the same time, provides a medium for the transferring of ions between anode and cathode during the redox processes.

In order to improve the safety and ionic conductivity of the polymer electrolytes, many researchers have been carried out to overcome these problems. Current research in lithium-ion battery technology replaces the liquid electrolyte with a polymer membrane which is capable to function as a separator and as the electrolyte (Fenton et al., 1973). Xu et al. (1998) revealed that polymer electrolytes are good compatibility with lithium metal which

exhibits no leakage, low self-discharge, elastic relaxation under stress, easy processing, continued production, and good electrical conductivity.

On the other hand, the polymer electrolyte formed from polymer, salts and plasticiser should have high chemical stability in order to prevent any chemical reaction between the electrolytes and electrodes. Linden and Reddy (2002) summarised that electrolytes should have good ionic conductivity to minimise internal resistance, lithium ion transference number approaching unity to limit concentration polarisation, wide electrochemical voltage window ranging from 0 to 5V, good thermal stability and good compatibility with other components in the batteries.

### **2.5.1 Solid Polymer Electrolyte (SPE)**

Solid polymer electrolyte or SPE is defined as a solid solution of the conducted ions. The ions can be transported inside and through the host under the effect of an electric field. The fundamental of ionic conduction in the polymer electrolytes is the covalent bonding between the polymer backbones with the ionising group. The electron donor group in the polymer forms solvation to the cation component in the dopant salt and then facilitates ion separation, leading to ionic hopping mechanism. In recent years, polymer electrolyte has been used as an electrolyte in lithium batteries. The polymer

electrolyte plays three important roles in the solid polymer electrolyte (SPE) battery.

- 1) It is a lithium ion carrier and it can be formed into thin films to improve the energy density.
- 2) It acts as an electrode separator, which eliminates the need to incorporate an inert porous separator.
- 3) It is a binder which ensures good electrical contact with the electrodes. The flexibility and mechanical resilience allowed SPEs to have a major advantage over all other -solid-state cells.

According to Ahmad (2009) the advantages of using these SPE over liquid electrolyte in a battery system are:

- a) Excellent processability and flexibility that could enable the fabrication of ultrathin lithium cells of various geometric shapes so that high energy and power density could be achieved for versatile application.
- b) Higher safety due to the absence of flammable organic solvents and the much lower reactivity of macro-molecules toward lithium.

- c) The possible prevention of the growth of lithium dendrite crystals upon cycling.
- d) The high dimensional stability, which will lead to the elimination of a separator, so that further improvement in both energy density and manufacturing cost could be achieved due to the simplified cell configuration and enhanced packing efficiency.

The SPEs are good compatibility with lithium metal, no leakage, and low self-discharge, elastic relaxation under stress, easy processing, continued production, and good electrical conductivity (Rajendran et al., 2003).

### **2.5.2 Gelled Polymer Electrolyte (GPE)**

Due to the low conductivity, a concept of gelled polymer electrolyte (GPE) was introduced. The ionic conductivity could be increased by incorporating a liquid plasticiser into host polymer. Song et al. (1999) reported that the gel-type membranes may benefit in ionic transport mechanism, which is similar to that of their liquid components. Ionic conductivity of these membranes is closely related to the diffusive motion of low molecular weight solvent mixture within the gel. The ionic conductivity of gelled type polymer electrolyte is reported to exhibit ionic conductivity as high as  $10^{-3} \text{ S cm}^{-1}$  (Deka and Kumar, 2010)

Compare to liquid electrolyte, gelled polymer electrolyte exhibits a higher ionic conductivity due to an increase in carrier concentration. Besides that, the gel electrolytes shows more advantages than Liquid electrolytes due to the fact that the liquid phase still provides the channels for ion conduction in the gel medium whereas the polymer provides the mechanical support and mainly acts as a stiffener. This effect might increase the number of carrier concentration (n). According to the formula of ionic conductivity in Liquid electrolyte or GPE,

$$\text{Conductivity } (\sigma) = nq\mu$$

where n is the charge carrier concentration,

q is the charge on the mobile species

$\mu$  is the mobility of ions

The ionic conductivity in GPE depends upon two factors which are carrier concentration and mobility. The conductivity of charge carrier (n) depends upon the concentration of salt containing the mobile species. If the salt is completely dissociated, the formation of ion aggregation takes place which shall lower the conductivity. However, large numbers of charge concentration may also lead to ion association resulting in the formation of ion aggregates which blocked the ionic motion between anode and cathode.

Although the GPEs provide many advantages to battery system, however the ionic conductivity and mechanical integrity of GPEs are mutually exclusive (Ahmad et al., 2006). The approach to overcome the dimensional stability and mechanical properties of the gelled polymer electrolyte (GPE) is attributed to the addition of nanosized inorganic composite fillers to yield composite polymer electrolyte (CPE). The toughness of the polymer electrolyte can be increased through the addition of fillers such as silica particle whereas the presence of fillers can give rise to flaws, which can reduce both the fracture strength of the polymer and the elongation to failure (Quartarone et al., 1998). Besides that, the ionic conductivity of the composite polymer electrolyte is increased accordingly to the dispersion of inorganic fillers.

### **2.5.3 Composite Solid Polymer Electrolyte (CSPE)**

Composite solid polymer electrolyte is a class of reinforced polymers with low quantities of micro- or nano-metric sized fillers particles, to improve mechanical integrity, enhanced film processability, as well as the strength. This electrolyte is obtained by doping ceramic particles such as  $\text{Al}_2\text{O}_3$ ,  $\text{SiO}_2$  and  $\text{TiO}_2$  in the polymer matrix (Liu et al., 2003; Adebahr et al., 2003; Dissanayake et al., 2003). According to Adebahr et al. (2003), the addition of filler particle to polymer effectively controls the growth of the passivation layer on the Li electrode, as well as increases its stability during long-term storage.

Besides, the usage of ceramic fillers tends to reduce the glass transition temperature ( $T_g$ ) and crystallinity of the polymer, and therefore allow amorphous polymer to maintain liquid-like characteristics and increase their conductivity (Weston and Steele, 1982). The increase in conductivity is mainly attributed to the decrease in the level of crystallinity in polymers due to the presence of fillers. Other than that, due to the Lewis acid-base interactions between the polar surface groups of the inorganic solid oxide fillers and the electrolyte ionic species which yield a greater degree of salt dissociation through the formation of ionic-ceramic complex (Xiong et al., 2003; Croce et al., 2006).

The particle size of the fillers may affect the properties of the composite solid polymer electrolyte. The mechanical strength and the electrochemical performance of the electrolytes are expected to increase with the decreasing of the filler size (Kim et al., 2003; Srun Jung et al. 2009; MadhuryyaDeka and Ashok Kumar, 2010). Krawiec et al. (1995) reported the relationship between the particle size and conductivity. The composite of PEO,  $\text{LiBF}_4$  system showed an increase in conductivity in going over from  $10^{-5}$  (micrometer) to  $10^{-4}$  (nanosized)  $\text{Scm}^{-1}$  for  $\text{Al}_2\text{O}_3$  fillers dispersed into the polymeric complex. This effect is related to a new transport mechanism which develops due to interaction between the polymer and the ceramic phase. This interaction serves as a path for the conduction of lithium ions. Furthermore, addition of ceramic filler can also prevent the polymer chain reorganisation, which promotes the

ion transportation and improves the interfacial, electrochemical stability and mechanical properties of the polymer electrolyte (Kim et al., 2003).

## **2.6 Ionic Conductivity of Polymer Electrolyte**

Ionic conductivity is certainly the most important concern for polymer electrolytes. Ionic conductivity or ionic transport occurs mainly through a coupling between the ions and polymer segmental motion. The early work using PEO as the host polymer which shows that ionic conduction only takes place mainly in the amorphous region (Haris et al., 1986; Selvasekarapandian et al., 2006). As the ionic transportation mechanism are concerned in PEO-based polymer electrolyte, the PEO segment assisted motion in the amorphous region and the ion hopping along coordination sites in the crystalline phase are suggested independently (Xiong et al., 2003).

The ionic conductivity of polymer electrolytes has been attained through the incorporation of substantial amounts of plasticisers. The purpose of plasticiser is served to reduce the crystalline content and increase the polymer segmental mobility. At the same time plasticisers can result in greater ion dissociation which allows greater numbers of charge carriers for ionic transport (Song et al., 1999). Ito et al. (1987) revealed that the contribution of PEG plasticizer enhanced the conductivity of the PEO-LiCF<sub>3</sub>SO<sub>3</sub> at room

temperature. The PEG aids in ionic transport mainly by reducing crystallinity and increasing the free volume of the system.

Many researchers reported that the ionic conductivity of polymer electrolytes has a specific dependence on the amorphous nature of the sample. The ionic conductivity is increased with the suitable incorporation of plasticisers into the polymer electrolyte (Ragavendran et al., 2004). Besides that, dielectric constant and viscosity of the plasticiser are important parameters to be considered. High value of dielectric constant ensures better salt dissociation that increases the number of free mobile charge carriers and lower viscosity which increases ionic mobility. Therefore, with the addition of plasticiser which tends to decouple the ionic motion from the polymer chain leading to the increase of the ionic mobility by lowering the viscosity of ionic environment (Forsyth et al., 1997).

Generally, the ionic conductivity in a polymer electrolyte is determined by the amorphous nature of the polymer, the high conductivity can be observed from the polymer electrolyte with enhanced amorphous character and a reduced energy barrier to the segmental motion of lithium ions in the matrix. Polymer electrolyte is strongly dependent on the glass transition temperature  $T_g$ , where low  $T_g$  is necessary for high ionic conductivity (Gray, 1997b). From these approaches, the improvements have been achieved either by reducing the crystallinity of the polymers or by lowering the glass transition temperature.

### **2.6.1 The Effect of Plasticiser to the Ionic Conductivity in Polymer Electrolyte**

As mentioned earlier, plasticiser is used to enhance the ionic conductivity by lowering the glass transition temperature ( $T_g$ ). The plasticiser aids in the ionic transport mainly by reducing crystallinity (induce amorphous region), increasing the free volume and addition of the transit site available in the system.

Ionic conductivity is certainly the most important concern for the polymer electrolytes. The effect of plasticiser on the polymer segmental and ionic mobility and conductivity depends on the specific nature of the plasticiser, including viscosity, dielectric constant, polymer-plasticiser interaction and ion-plasticiser interaction. The research done shows that all plasticised electrolyte films exhibit an enhancement in conductivity as compared to the unplasticised electrolytes. It is showing that ionic mobility plays the pivotal role in the improvement of the conductivity of polymer electrolytes.

Mahendran et al. (2005) reported that plasticiser molecules being relatively small in size compared with polymer molecules penetrate into the polymer matrix and establish attractive force between the plasticiser molecule and chain segments. The addition of plasticiser introduces more free volume to

the polymer, which lowers the glass transition temperature. The effect is due to the reduction in cohesive force between the polymer chains which increase the segmental mobility thus enhancing the conductivity. The increase in conductivity by the addition of plasticisers may be due to the existence of separate ionic path ways for the migration of the free lithium ions through the plasticiser. This path provides a less viscous medium to allow  $\text{Li}^+$  ions to pass through (Rajendran and Mahendran, 2001).

Ionic conductivity of polymer electrolytes has been attained through the incorporation of substantial amounts of plasticisers. Plasticiser such as PC and EC are preferred because of its high dielectric constant 64.4 for PC and 89.6 for EC (Tobishima and Yamaji, 1984). With the low molecular weight of plasticisers, it helps to dissociate lithium salt which provides more mobile charge carriers and reduces the viscosity of the polymer matrix leading to higher ionic conductivity. Some researchers reported that EC is a better solvent than PC due to its higher dielectric constant and lower viscosity. These properties enhance ionic conductivity because they favour salt dissociation and high ionic diffusion rates. However, EC is a solid at room temperature where its melting point is  $36.2\text{ }^\circ\text{C}$ . Therefore, a mixture with PC is required for practical applications (Li and Balbuena, 1999).

## **2.6.2 The Effect of Lithium Salt to the Ionic Conductivity in Polymer Electrolyte**

For a solid type of polymer electrolyte, doping the lithium salt into the polymeric complex tends to increase the charge carriers in the polymer electrolyte system. An ideal electrolyte solute for ambient-temperature electrochemical devices should be able to completely dissolve and dissociate in the non-aqueous media, and the solvated ions (especially  $\text{Li}^+$ ) should be able to travel in the medium with high mobility (Ahmad, 2009).

The increase in conductivity is due to the increase in the number of free mobile ions as more salt is dissolved into the solution. When the salt content is increased, the number of free ions also increases, hence increases the conductivity (Othman et al., 2007). However, as the salt concentration increases beyond its saturation level, the number of carrier ions also increase which in turn cause the retarding effects such as ion pairs or ion triplets, charge cloud effects, and restriction to chain mobility (Rajendran et al., 2010). The segmental motions and the charge carriers are reduced hence the ionic conductivity is decreased. The effect of decrease in ionic conductivity agrees well with the literature when at high salt concentrated polymer electrolytes indicates the formation of ion pairs, ion aggregates and ionic cluster, which reduces the ionic mobility (Selvasekarapandian et al., 2006; Osman et al., 2005).

The lithium salts with low lattice energy and large anions are generally expected to dissociate better with lithium salt, thereby providing a higher concentration of ions (Mahendran and Rajendran, 2003; Kang X., 2004). As reported by Rajendran and Sivakumar (2008), the lithium perchlorate has smaller ionic radius and smaller dissociation energy which is highly soluble in most of the organic solvents. Therefore, the lithium perchlorate ( $\text{LiClO}_4$ ) is selected as a doping salt for this research.

### **2.6.3 The Effect of Inorganic Filler to the Ionic Conductivity in Polymer Electrolyte**

The dispersion of filler into the polymer electrolyte has brought several advantages to the particular electrolyte system such as improvement of the mechanical strength, enhancing the ionic conductivity and also the electrochemical stability. The conductivity in this composite is not likely to be contributed directly from the movement of ion-ceramic complex due to a heavy mass. The major conduction path is originated from the local diffusion within the amorphous polymer matrix. According to Ahmad (2009), the increase in conductivity is mainly attributed to the decrease in the level of crystallinity in polymers due to the presence of fillers.

By using the SiO<sub>2</sub> as ceramic filler in the polymer electrolyte, SiO<sub>2</sub> reduces the glass transition temperature and crystallinity of the polymer, and allows the amorphous polymer to provide specific liquid-like characteristics. The addition of ceramic fillers into a polymer improved the ionic conductivity by reducing the crystallisation tendency (Scrosati et al., 2000).

Besides that, the addition of inorganic fillers may prevent the polymer chain reorganisation, which promotes the ion transportation. The Lewis acid-base interactions between the polar surface groups of the inorganic solid oxide fillers and the electrolyte ionic species yield a greater degree of salt dissociation through the formation of ionic-ceramic complex (Croce et al., 2006). The enhancement of ionic conductivity might be due to the Lewis acid-base type oxygen and OH surface groups on filler grains which interact with the cations and anions and therefore providing additional sites creating favourably high conducting pathway in the vicinity of grains for the migration of ions (Dissanayake et al., 2003).

Although the dispersion of fillers helps to increase the ionic conductivity of the polymer electrolyte, a high concentration of filler tends to reduce the ionic conductivity of the polymer electrolyte due to the blocking effect. As reported, the blocking effect is imposed by the more abundant filler grains which could make the long polymer chains more immobilised and make

the grains get close to one another, leading to the decreasing of the conductivity (Dissanayake et al., 2003).

#### **2.6.4 The Effect of Temperature towards the Ionic Conductivity**

In a conventional solid type of polymer electrolyte, the relaxation and segmental motion of the solvent chains are regarded as the key factors in enabling ion transport. It is suggested that a sufficient conductivity can be obtained only when the energy of ions are over its energy level (Jung et al., 2009). Further increase of ionic conductivity for an amorphous polymer electrolyte is possible. From the established theory, when the temperature increases, the conductivity also increases for all complexes, this can be recognised by the free volume model (Miyamoto and Shibayama, 1973).

The increment of temperature causes an increase in conductivity due to an increase of free volume in the electrolyte in respect of the ionic and segmental mobility. Therefore, the free volume around the polymer chain causes the increment of mobility for ions and polymer segmental mobility. According to Mahendran et al. (2005), the conductivity increases when the temperatures increase. As the temperature increases, the polymer can expand easily and produce free volume. Thus, ions and solvated molecules as well as polymer segments can move into the free volume. Besides that, the overall

mobility of ion and polymer segment which are determined by the free volume leads to an increase in ionic and segmental mobility that will assist ion transport and practically compensate for the retarding effect of the ion clouds (Mahendran et al., 2005).

When the temperature is increased, the vibrational energy of segment is sufficient to push against the hydrostatic pressure imposed by its neighbouring atoms and creates a small amount of space surrounding its own volume that generate extra transit site for ionic movement (Rajendran and Prabhu, 2010). Moreover, the conduction mechanism is not entirely attributable to the segmental motions of the polymer and is more likely to involve ion hopping between static sites or limited motions of parts of the polymer chain (Rajendran and Mahendran, 2001).

## CHAPTER 3

### RESEARCH METHODOLOGY

#### 3.1 Materials

A series of solid polymer electrolyte thin films are developed through solution-cast technique. PMMA (poly (methyl methacrylate) is used as the host polymer, EC (ethylene carbonate) and PC (propylene carbonate) mixture is applied as a plasticiser, LiClO<sub>4</sub> (lithium perchlorate) is used as a carrier source and the dispersion of Al<sub>2</sub>O<sub>3</sub> (aluminium oxide) and SiO<sub>2</sub> (silicon dioxide) as ceramic fillers.

##### 3.1.1 Poly(methylmethacrylate) (PMMA)

PMMA is a hard, clear, colourless and transparent amorphous polymer with good resistance to acid. PMMA has good insulating properties ( $1\text{E}-19 \text{ }^{-1}$ ) with high dielectric strength (2.6 at 1MHz). Combining the stiffness, density and moderate toughness behaviours allowed this material to be applied in a

wide range of applications. In addition, PMMA has good thermal properties with good resistance to temperature changes, moderate transition temperature ( $T_g$ ) of 105• C, a heat deflection temperature in the range of 74 to 100• C and service temperature about 93• C.

The reasons for choosing PMMA is mainly because the amorphous phase and flexible backbone in nature which leads to high ionic conductivity. Ahmad (2009) mentioned that to attain a high ambient-temperature conductivity, a polymer that is amorphous in nature and has a flexible backbone is more preferred. Polymer material of high molecular weight is usually used to provide good mechanical strength and filming processability. Besides, PMMA is selected because of its higher surface resistance, good interfacial stability towards lithium electrodes and high ability to solvate inorganic salts to form a complexation between polymer and salt (Stephan et al., 2002).

As mentioned in Chapter 2, ions are transported in the polymeric host material which is amorphous. The chain motions or rearrangements of the polymer host virtually contribute to the ion transport. Hence, an amorphous polymeric host is one of the importance factors to enhance the ambient temperature ionic conductivity. Besides that, the amorphous properties and a high molecular weight of PMMA would enhance the ionic conductivity and

mechanical integrity of the polymer electrolyte. The structure of PMMA is illustrated in Figure 3.1.

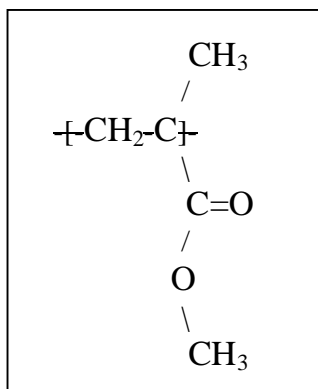


**Figure 3.1: Chemical structure of MMA**

**Table 3.1: Physical Properties of the Poly(methylmethacrylate) (PMMA)**

Linear Formula	$[\text{CH}_2\text{C}(\text{CH}_3)(\text{CO}_2\text{CH}_3)]_n$
Molecular Weight (average)	996,000 by GPC
Density	1180 kg/m <sup>3</sup>
Transition Temperature	105 °C
Flash Point	>250 °C
Water Absorption	0.1 - 0.5 % (50% rh)
Tensile Strength	55 - 80 MN/m <sup>2</sup>
Flexural Strength	100 - 150 MN/m <sup>2</sup>
Specific Heat	1.25 - 1.7 kJ/kg/oC
Appearance (Form)	Crystals or Powder
Transmission for visible light (wave length)	92 %

The advantages of PMMA are:-

-Broad softening range attribute to thermal agitation of the molecules breaks down the weak secondary bonds. The rate at which this occurs throughout the formless structure varies; producing a broad temperature range for softening.

-Usually transparent-the looser structure transmits light so the material appears transparent

-Low shrinkage on solidification, the random arrangement of molecules produces little volume change and hence low shrinkage.

-Low chemical resistance where the more open random structure enables chemicals to penetrate deep into the material and to destroy many of the secondary bonds, thus it can be dissolved easily in solvent

### 3.1.2 Lithium Perchlorate (LiClO<sub>4</sub>)

Lithium perchlorate is the chemical compound with the formula LiClO<sub>4</sub>. It is a white crystalline lithium salt with high solubility in many solvents. It decomposes at about 400 °C, yielding lithium chloride and oxygen, the latter being over 60% of its mass. It has both the highest oxygen to weight and oxygen to volume ratio of all perchlorates, which makes it especially advantageous for aerospace applications. Lithium perchlorate is also

extensively used as an electrolyte in lithium batteries, as it does not undergo oxidation on the anode. The chemical structure of  $\text{LiClO}_4$  is shown in Figure 3.2.

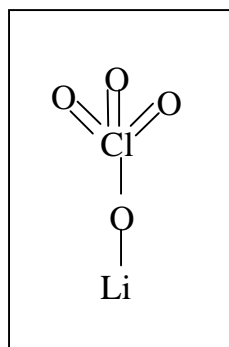


**Figure 3.2: Chemical structure of  $\text{LiClO}_4$**

Lithium perchlorate has been accepted for developing electrolyte in the battery system due to its solubility and high conductivity and high anodic stability. As compared with other lithium salts,  $\text{LiClO}_4$  has the advantage of being relatively less hygroscopic and is relatively stable to ambient moisture in comparison with their counterparts. It is being used frequently as a salt in various laboratory tests because of its ease of handling and cost-effectiveness (Ahmad, 2009).

Rajendran and Sivakumar (2008) reported that  $\text{LiClO}_4$  has a smaller ionic radius, smaller dissociation energy and is highly soluble in most of the organic solvents. Mahendran and Rajendran (2005) also mentioned that the salt

has low lattice energy and large anions which are generally expected to promote greater dissociation of salts, thereby more salts will be dissociated to provide a higher concentration of ions.

**Table 3.2: Physical Properties of Lithium Perchlorate (LiClO<sub>4</sub>)**

Molecular formula	LiClO <sub>4</sub>
Molecular weight	106.39 g/mol
Density	2.42 g/cm <sup>3</sup> , solid
Melting point	236 °C
Boiling point	430 °C
Solubility in water	60 g/100 mL
Solubility in organic solvents	Soluble
Appearance	white crystals
Odor	odourless

### 3.1.3 Ethylene Carbonate (EC)

Ethylene carbonate (EC) is an ester of ethylene glycol and carbonic acid. This is an organic chemical also named 1,3-Dioxolane-2-one. Ethylene Carbonate is a transparent crystalline solid in room temperature and it is odourless, colourless and soluble in water. The chemical structure can be seen in Figure 3.3 below.

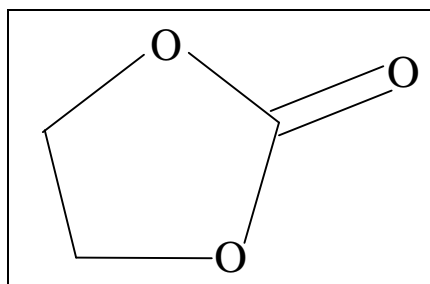


**Figure 3.3: Chemical Structure of Ethylene Carbonate**

EC is used as a plasticiser due to its high dielectric constant about 89.6 at 40°C and lower viscosity (Rajendran et al., 2003). Low viscosity and high dielectric constant as a plasticiser in the polymer host helps to enhance the conductivity of polymer electrolytes (Rajendran and Prabhu, 2010).

**Table 3.3: Physical Properties of Ethylene Carbonate**

Linear Formula	$C_3H_4O_3$
Molar Mass	88.06 g/mol
Density	1.34 g/cm <sup>3</sup> (20 °C)
Melting point	36 °C
Boiling point	248 °C
Flash point	150 °C
Solubility	214 g/l (20 °C)
dielectric constant	89.6 (40°C)

### 3.1.4 Propylene Carbonate (PC)

Propylene carbonate (PC) also known as 4-Methyl-1, 3-dioxolan-2-one. It is an organic compound and also a colourless and odourless liquid. Propylene carbonate is used as a polar solvent that, unlike water, does not donate protons to the dissolved substances. Due to its high dielectric constant, it is frequently used as a high-permittivity component of electrolytes in lithium batteries, usually together with a low-viscosity solvent. Its high polarity allows it to create an effective solvation shell around lithium ions, thereby creating a conductive electrolyte. The chemical structure is shown in the Figure 3.4 and the physical properties are shown in Table 3.4.

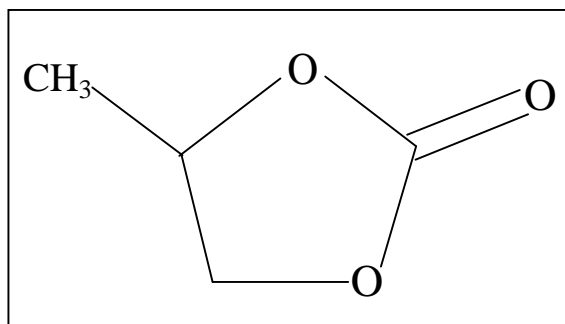


**Figure 3.4:** Chemical Structure of Propylene Carbonate

**Table 3.4: Physical Properties of Propylene Carbonate**

Molecular formula	C <sub>4</sub> H <sub>6</sub> O <sub>3</sub>
Molar mass	102.09 g/mol
Density	1.205 g/mL
Boiling point	241.7°C
Flash point	275°F (135°C) by closed cup
Solubility of propylene carbonate	17.5% at 25°C
Dielectric constant	64.9 at 20°C

Propylene carbonate is preferred because of its high dielectric constant and low molecular weight which will enhance the dissociation of ion pairs of the salt (Rajendran et al., 2010). Ahmad (2009) also reported that a high dielectric constant and inert stability of propylene carbonate toward lithium made it attractive for maximum research attention in the polymer electrolyte field.

Li and Balbuena (1999) reported that EC is a better plasticiser than PC due to its higher dielectric constant and lower viscosity. These properties enhance the ionic conductivity because they favour salt dissociation and high ionic diffusion rates. However, EC is a solid at room temperature where its melting point is 36.2 °C. Li and Balbuena (1999) studied the EC/PC mixture which shows that EC tends to substitute PC in the first shell of the cation. Consequently, the effective radius of the complex ion solvent is smaller lead to higher ionic conductivities.

Deepa et al. (2002) revealed that the synergistic effect of both EC and PC providing desired characteristics such as a high degree of dissociation and fast ion migration. The synergistic effect also affects the physico-chemical properties of individual plasticiser like high dielectric and low viscosity of EC and the low freezing point of PC along with its good plasticising characteristics which are contributed towards improving conductivity performance.

### 3.1.5 Aluminium Oxide ( $\text{Al}_2\text{O}_3$ )

Aluminium oxide belongs to the family of inorganic compounds with the chemical formula  $\text{Al}_2\text{O}_3$  commonly referred as alumina. Aluminium oxide is an electrical insulator but has an excellent thermal conductivity and also insulator for a ceramic material and it usually occurs in crystalline form. The chemical structure and physical properties are shown in Figure 3.5 and Table 3.5, respectively.

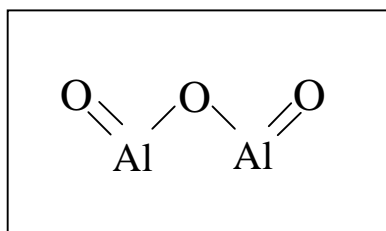


**Figure 3.5:** Chemical Structure of Aluminium Oxide ( $\text{Al}_2\text{O}_3$ )

**Table 3.5: Physical Properties of Aluminium Oxide (Al<sub>2</sub>O<sub>3</sub>)**

Molecular formula	Al <sub>2</sub> O <sub>3</sub>
Molar mass	101.96 g mol <sup>-1</sup>
Density	3.95-4.1 g/cm <sup>3</sup>
Appearance	white solid crystal
Melting point	2072 °C
Boiling point	2977 °C
Odor	Odorless
Solubility in water	Insoluble

According to Croce et al.(1999), Al<sub>2</sub>O<sub>3</sub> is dispersed in PEO-LiClO<sub>4</sub> to form complexes with the basic oxygen atoms in the PEO chains and acts as cross-linking centers for PEO segments, thereby reducing the reorganisation tendency of the polymer chain and promoting preferred Li<sup>+</sup> transport at the boundaries of the filler particles. Thus, the ionic conductivity of the particular polymer electrolyte will be increased.

Krawiec et al. (1995) also agreed that the dispersing of Al<sub>2</sub>O<sub>3</sub> tends to increase the ionic conductivity of polymer electrolyte. They also mentioned that decreasing the size of the Al<sub>2</sub>O<sub>3</sub> from micrometer to nanometer, the ionic conductivity is enhanced significantly. Dispersion of this filler to the polymer electrolyte, the cell or battery performance of the system is maintained at 95% of the initial capacity after 100 cycles (Jung et al., 2009).

### 3.1.6 Silicon Dioxide (SiO<sub>2</sub>)

Silicon dioxide is also known as silica. It is an oxide of silicon with a chemical formula of SiO<sub>2</sub>. It has been known for its hardness since antiquity. Silica is used primarily in the production of glass for windows, drinking glasses, beverage bottles, and many other uses. The majority of optical fibres for telecommunications are also made from silica. Thin films of silica grown on silicon wafers via thermal oxidation methods can be quite beneficial in microelectronics, where they act as electric insulators with high chemical stability. In electrical applications, it can protect the silicon, store charge, block current, and even act as a controlled pathway to limit current flow. The Chemical Structure is shown in Figure 3.6 and the physical properties are shown in Table 3.6.

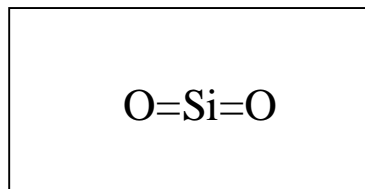


**Figure 3.6:** Chemical Structure of SiO<sub>2</sub>

**Table 3.6: Physical properties of SiO<sub>2</sub>**

Molecular formula	SiO <sub>2</sub>
Molar mass	60.0843 g/mol
Density	2.634 g/ cm <sup>3</sup>
Melting point	1650(±75) °C
Boiling point	2230 °C
Solubility in water	0.012 g/100 mL
Appearance	white powder

Generally, SiO<sub>2</sub> is found to act as a passive filler and played a predominant role in controlling the rheological properties while ions transport properties (Ahmad et al., 2006). The dispersion of SiO<sub>2</sub> in the polymer electrolyte system is to reduce the glass transition temperature (T<sub>g</sub>) and crystallinity of the polymer which allows amorphous polymer to provide specific liquid-like characteristics for the transportation of ions (Kim et al., 2003).

Jung et al.(2009) reported that Silica has been expected to enhance the ionic conductivity of polymer electrolytes due to the surface hydroxyl groups which can be easily modified for a specific need. The nanosized SiO<sub>2</sub> was found to contribute to the rapid formation of compact and stable passive films, which stabilise the interface between the electrolyte and lithium electrode. Besides that, the dispersion of the nano-sized SiO<sub>2</sub> powder is also capable to enhance the mechanical strength, conductivity, and electrochemical properties of the SPEs.

### 3.1.7 Tetrahydrofuran THF

Tetrahydrofuran (THF) is a colourless liquid with ether-like smell. It is an aprotic solvent with a dielectric constant of 7.6 and is usually applied as a polar solvent and it is used to dissolve a wide range of nonpolar and polar chemical compounds. THF is particularly capable of dissolving many ionic species which is commonly used in specialty syntheses. In many cases, THF makes higher yields and faster reaction rates possible. In addition, THF's high volatility and very high purity facilitate solvent removal and recovery without leaving residues in the desired polymer electrolyte thin films. The chemical structure is shown in Figure 3.7 and the physical properties are shown in Table 3.7.

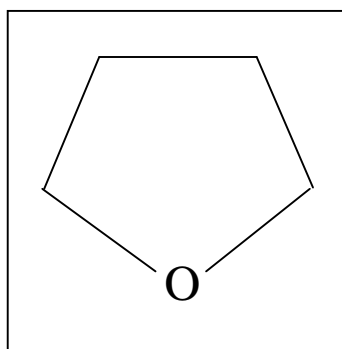


**Figure 3.7:** Chemical structure of Tetrahydrofuran (THF)

**Table 3.7: Physical properties of Tetrahydrofuran (THF)**

Chemical formula	C <sub>4</sub> H <sub>8</sub> O
Molar mass	72.11 g/mol
Density	0.89 g/ cm <sup>3</sup>
Solubility	soluble
Melting point	-108.5 °C
Boiling point	65 - 66 °C
Flash point	-21.5 °C
Evaporation number	2.3

### 3.2 Solution-Cast Technique

Four systems of polymer electrolyte samples (PMMA-EC/PC, PMMA-EC/PC-LiClO<sub>4</sub>, PMMA-EC/PC-LiClO<sub>4</sub>-Al<sub>2</sub>O<sub>3</sub> and PMMA-EC/PC-LiClO<sub>4</sub>-SiO<sub>2</sub>) were prepared using the solution-cast technique. Prior to the preparation of the polymer electrolytes, LiClO<sub>4</sub> was dried at 60 °C for overnight to eliminate any trace water in the material. The quantity of materials integrated was expressed in weight percentage (wt%). Appropriate amounts of materials were dissolved in THF. The solution was then stirred continuously for 24 hours on a hot plate stirrer at room temperature to obtain homogeneous solution. After that, the solution was poured into Petri dishes and the Petri dishes are covered with aluminium foil with a few holes to avoid direct exposure to atmosphere. However, the samples are allowed to evaporate slowly inside the fume hood for 24 hours to form a polymer electrolyte thin film. The films were

then transferred into a desiccator for further drying. The polymer sample is depicted in Figure 3.8.

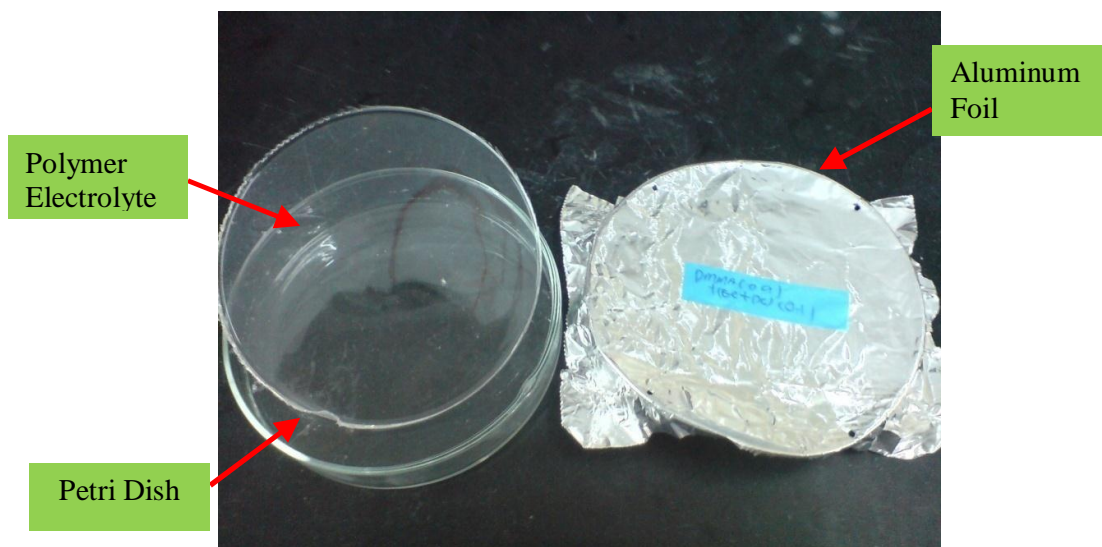


**Figure 3.8: Polymer Electrolyte Samples**

In the initial stage, the pre-determined EC: PC ratio is obtained at 70:30. The weight of PMMA was fixed as 1 gram, while the EC/PC weight percentage was from 0 wt% until 50 wt%, with an increment of 5 wt%. After the PMMA-EC/PC samples with the best ionic conductivity was determined, the sample with 70 wt% of PMMA and 30 wt% of EC/PC achieved the highest ionic conductivity. Therefore, this ratio is being fixed in this system and the sample preparation process was then repeated with an addition of  $\text{LiClO}_4$  (5wt% to 50 wt%).

In the last stage of the sample preparation,  $\text{Al}_2\text{O}_3$  (grain size of 40-47 nm) inorganic fillers and  $\text{SiO}_2$  (grain size of 7nm) inorganic fillers are dispersed separately into the best ionic conductivity sample in the PMMA-EC/PC-LiClO<sub>4</sub>. PMMA-EC/PC (75 wt%) and LiClO<sub>4</sub> (25wt%) were employed as it achieved the maximum ionic conductivity in the PMMA-EC/PC-LiClO<sub>4</sub> system. In this work, dispersion of 2 to 20 wt% of  $\text{Al}_2\text{O}_3$  and  $\text{SiO}_2$  inorganic fillers with an increment of 2 wt% is dispersed in order to obtain two different systems of samples. All of these samples generated from the solution-cast technique will then be characterised by EIS, FTIR, XRD and SEM.

### **3.3 Characterisations**

The polymer electrolyte thin films generated from the solution cast technique are characterised by electrochemical impedance spectroscopy (EIS) to determine the ionic conductivity ( ), fourier transform infrared spectroscopy (FTIR) to identify the interaction between molecules and the structural changes, x-ray diffraction (XRD) to reveal the information about crystallographic structure and chemical composition and scanning electron spectroscopy (SEM) to investigate the micro-structure of the particularly thin films.

### 3.3.1 Electrochemical Impedance Spectroscopy (EIS)

Electrochemical Impedance Spectroscopy (EIS) is a characterisation technique used to determine the bulk resistance ( $R_b$ ) of the solid polymer electrolytes. A conductivity study on the polymer electrolytes was carried out using the Solartron SI 1260 Impedance/Gain-Phase Analyser with the frequency ranging from 1Hz to 1MHz. The thickness of the polymer electrolytes was measured by using a micrometer screw gauge. As the ionic conductivity varies corresponding to the thickness of the sample, therefore, the measurement of thickness was repeated onto the polymer electrolyte sample in order to obtain an average thickness. The prepared electrolyte samples were placed between two stainless steel plates that acted as the electrodes for the conductivity studies and an AC voltage at 10 mV was applied with varied frequency. The  $R_b$  of the samples was then determined through the Cole-Cole plot as shown in Figure 3.9, which cause the intercept on the real axis of the spectrum.

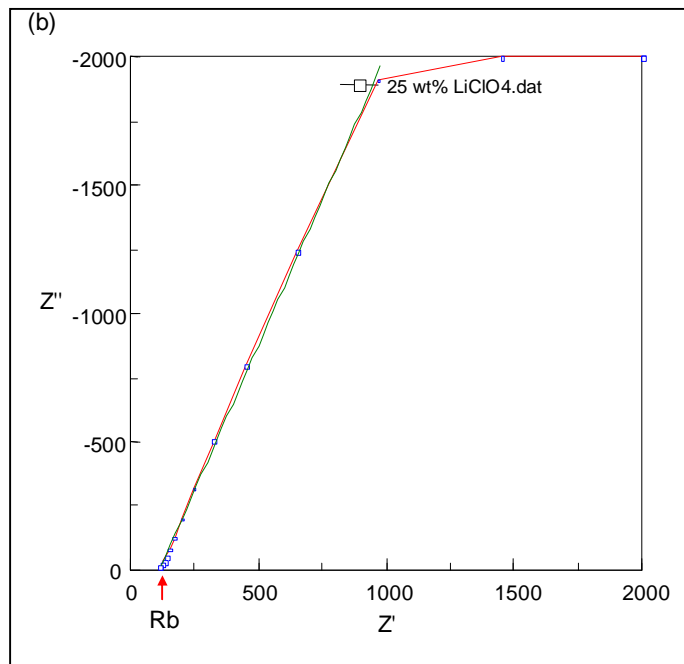
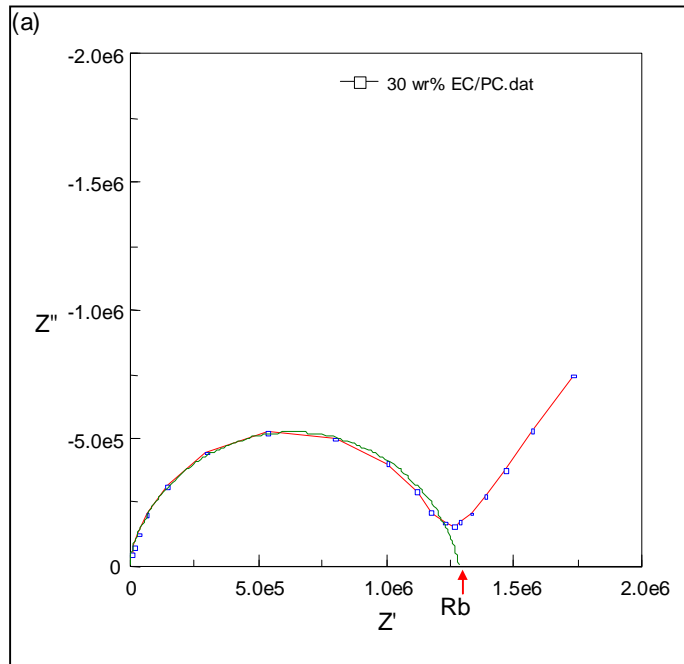


**Figure 3.9: Cole-Cole plot of AC impedance spectroscopy**

The plot in Figure 3.9 (a) shows a slight depressed semicircle which corresponds to the bulk resistance ( $R_b$ ) and a spur corresponding to the

interfacial resistance ( $R_s$ ). The non vertical spikes at low frequency might attribute to the surface roughness in electrolyte and electrodes interface (Rajendran et al., 2010). Besides that, the high frequency semi-circle yields information about the properties of the electrolyte such as bulk resistance ( $R_b$ ) and bulk capacitance ( $C_b$ ). This effect is attributed to the migration of ions and the dielectric polarisation in the polymer electrolyte film (Ragavendran et al., 2004). For the cole-cole plot in Figure 3.9 (b), this response is typically for the electrolyte with a major contribution towards total resistance from bulk resistance ( $R_b$ ) and contributeminorly to the interfacial resistance ( $R_s$ ). This straight line is inclined towards the real axis representing the electrode/electrolyte double layer capacitance behaviour (Raghavan et al., 2010). The attribute to the current carriers are ions and the total conductivity is mainly contributed by ion conduction (Rajendran and Sivakumar, 2008).

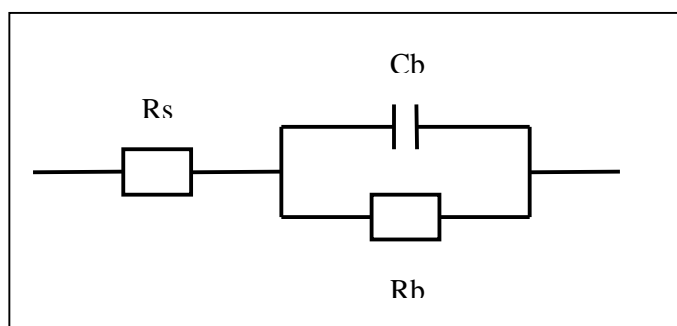


**Figure 3.10: Equivalent circuit of the AC impedance spectroscopy**

The equivalent circuit representing the AC response of the polymer electrolyte with the electrodes is shown in Figure 3.10. The electrodes became alternatively positively and negatively charged and the alternating field across

the electrolyte caused the lithium ions to migrate back and forth in phase with the voltage. Resistor  $R_b$  is used to represent the movement of the lithium ions in the electrolyte in the equivalent circuit. On the other hand, the immobile polymer chains became polarised in the alternating field as they were devoid of mobile charges. This dielectric polarisation is represented by a capacitor  $C_b$  in the circuit (Stephan et al., 1999). As the lithium ions moved around in the alternating field, they were alternatively accumulated and depleted at each of the electrodes. The bulk polarisation and ionic migration are physically parallel; therefore  $C_b$  and  $R_b$  that are representing them are connected in parallel, while both of them are connected in series with the interfacial resistor ( $R_s$ ) to represent the grain boundary resistance in the polymer electrolyte. Figure 3.11 shows the experimental setup of the EIS.

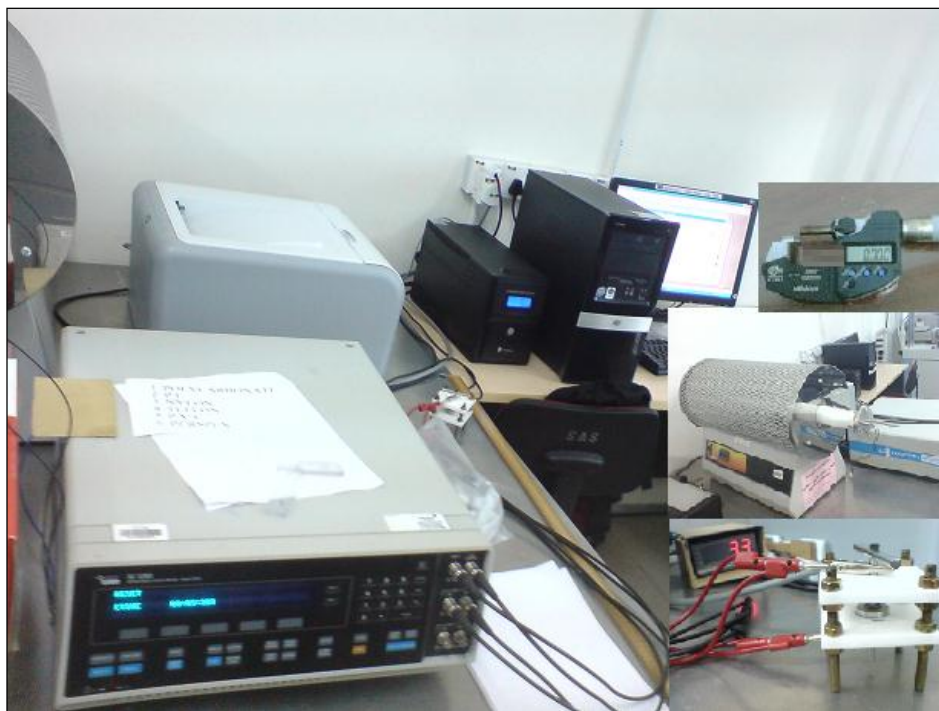


**Figure 3.11: Experimental setup of Solartron SI 1260 Impedance/Gain-Phase Analyzer**

### 3.3.2 Fourier Transform Infrared Spectroscopy (FTIR)

Fourier transform infrared spectroscopy (FTIR) is a technique to obtain an infrared spectrum of emission and absorption of a solid such as metal, powder and thin film. An FTIR spectrometer simultaneously collects spectral data in a wide spectral range.

S. Rajendran et al. (2009) revealed that FTIR is an efficient tool to study the local structural changes in polymers. The IR spectra of these materials vary according to their composition and may be able to show the occurrence of the complexation and interaction between various constituents. IR spectroscopy has been used to enumerate the inter- and intra-molecular interactions of the components of the polymer-salt complexes. Such interaction could induce changes in vibrational modes of the atoms or molecules in the material, which in turn changes the physical and chemical properties of the constituents of the complex.

The operation of the FTIR is shown in Figure 3.12. The IR spectrometer consists of two mirrors located at a right angle to each other and oriented perpendicularly, with a beam splitter placed at the vertex of the right angle and oriented at a 45° angle relative to the two mirrors. The beam splitter split the light from the source ideally 50 % of the light is reflected towards the

fixed mirror and 50 % is transmitted towards the moving mirror. Light is reflected from the two mirrors back to the beam splitter and 50 % of the original light passes into the sample. Once the infrared beam is passed through the sample, the molecules absorbed the infrared radiation and is then excited to a higher energy state. Therefore, the energies associated with these vibrations are quantized within a molecule. The amount of energy absorbed at each wavelength was recorded. The frequencies which have been absorbed by the sample are determined by a detector and the signal is amplified.

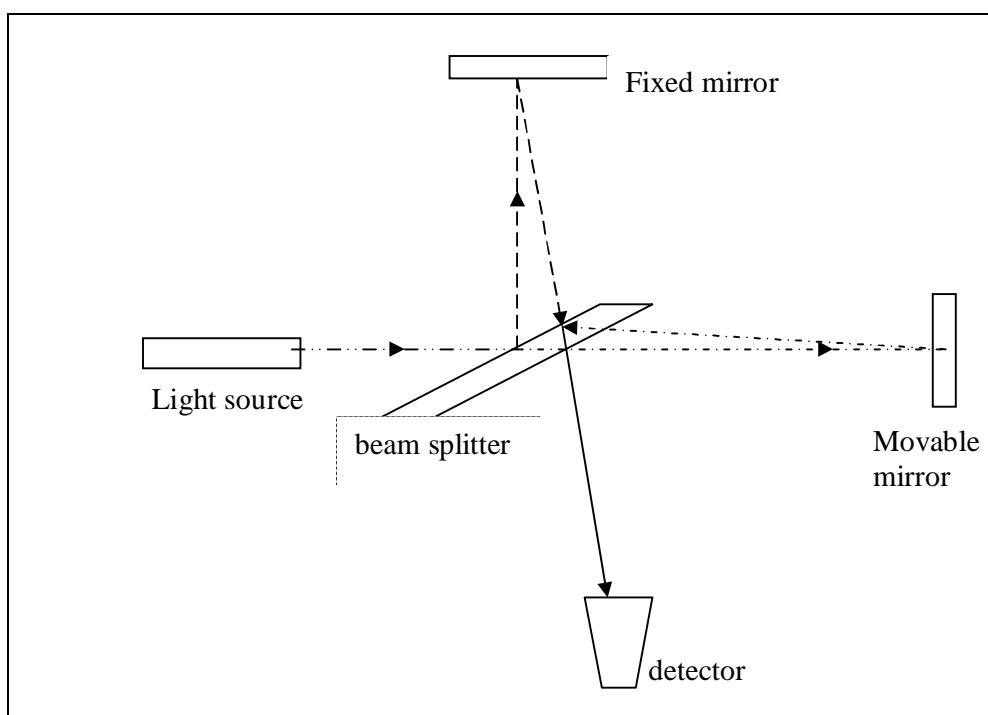


**Figure 3.12: Operation of the FTIR spectroscopy**

The FTIR characterisation was done on the polymer electrolytes using the Perkin Elmer Spectrum RX1 within the range of  $400\text{-}4000\text{ cm}^{-1}$  and the resolution of the spectra obtained at room temperature was 4 and recorded in

the transmittance mode in order to identify the existence of ion-ion pairs and also to confirm the occurrence of complexation in the samples.



**Figure 3.13: Experimental setup of Perkin Elmer Spectrum RX1 FTIR spectroscopy**

### 3.3.3 X-Ray Diffraction (XRD)

X-ray diffraction (XRD) is a useful characterisation tool to reveal information about the crystallographic structure and chemical composition of materials and thin films. This technique is based on observing the scattered intensity of an X-ray beam hitting a sample as a function of incident and scattered angle, polarisation, and wavelength or energy. In general, X-ray is an electromagnetic radiation of wavelength  $\sim (10^{-10}\text{m})$ . Usually, a filament (tungsten) is electrically heated and thus a beam of electron is emitted with a

high potential difference in between 20 to 50 kV which strikes to a metal target (Cu).

Using the Bragg's approach of diffraction, crystals can be regarded as built up in layers or planes such that each acts as a semi-transparent mirror. This is known as the angle of incidence other than the Bragg's angle when the reflected beams are out of phase, has a destructive interference or when cancellation occurs. The derivation of Bragg's law is shown in Figure 3.14, where the two X-ray beams, 1 and 2, are reflected from adjacent planes i.e. A and B within the crystal. As an X-ray that reflects from a plane of atom inside, the crystal travelled more distance than an X-ray that reflects from a crystal's surface. The perpendicular distance between pairs of adjacent planes, d-spacing (d) and the angle of incidence, or Bragg angle ( $\theta$ ) are related to the distance xy by

$$xy = yz = d \sin \theta \quad (3.1)$$

Thus

$$xy + yz = 2d \sin \theta \quad (3.2)$$

But

$$xy + yz = n \lambda \quad (3.3)$$

Therefore

$$2d \sin \theta = n \lambda \quad (3.4)$$

where  $\lambda$  = wavelength of X-ray ( $10^{-10}$ m)  
 $d$  = spacing between layers of atoms  
 $\theta$  = incident angle between the X-ray and the surface

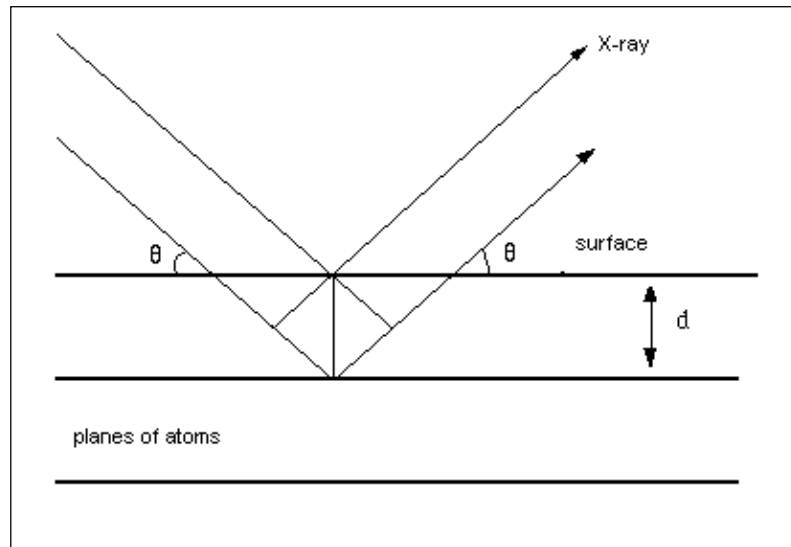


**Figure 3.14: Diffraction in the crystalline material**

The Crystal structures with their regularly repeating patterns may be referred to as a 3D grid thus the repeating unit of the grid, the unit cell, can be found. The grid may be divided up into sets of planes in various orientations and it is these planes which are considered in derivation of Bragg's law. Each set of plane has a characteristic d-spacing and the Bragg angle can be evaluated for a given wavelength. For instance, diffraction occurs as a result of interaction between X-rays and atoms but the atoms do not reflect X-rays but scatter or diffract them in all directions.

In the current research, the XRD characterisation study is done by using the Shimadzu XRD-6000 diffractometer with a range which varies from  $5^\circ$  to  $80^\circ$ . Besides that, the scan speed was  $2.5^\circ / 2$  per minute and step size was  $0.02^\circ / 2$ . After that, the polymer electrolyte sample is placed in the path of a monochromatic X-ray beam, the planes in the crystallites will orient at the correct angle to fulfill the Bragg condition and hence form the diffraction. The diffraction beam makes an angle of  $2\theta$  with the incident beam and the diffraction pattern is performed by automatic diffractometers. Figure 3.15 shows the experimental setup of the Shimadzu XRD-6000 diffractometer.



**Figure 3.15: Experimental setup of the Shimadzu XRD-6000 diffractometer**

### 3.3.4 Scanning Electron Microscope (SEM)

The scanning electron microscope (SEM) is a type of electron microscope that images the sample surface by scanning it with a high-energy beam of electrons in a raster scan pattern. The structure and surface morphology study on polymer electrolyte was carried out using the Hitachi S-3400N scanning electron microscope operated at 20 kV with a magnification about 1000X. The polymer electrolyte is placed on a multi-holder and then engages the multi-holder in the Hitachi S-3400N Scanning electron microscope. Before that, the polymer electrolyte samples were initially coated with a thin layer of gold to prevent electrostatic charging. Once the scanning is ready, the chamber is vacuumed to prevent the interaction of the beam with any extraneous particles in the atmosphere. Figure 3.16 shows the Experimental setup of the Hitachi S-3400N Scanning Electron Microscope.

Scanning electron microscopy is extremely versatile for providing structural information over a wide range of magnification. At one extreme, Scanning electron microscopy complements the optical microscopy for studying the texture, topography and surface features of solid pieces. Because of the depth focus of SEM instruments, the resulting pictures have a definite three-dimension quality. The types of signals produced by an SEM include secondary electrons and back-scattered electrons, specimen current and transmitted electrons. Secondary electron detectors are common in all SEMs,

the signals result from interactions of the electron beam with atoms at or near the surface of the sample. In the most common or standard detection mode, the secondary electron imaging in SEM can produce very high-resolution images of a sample surface, revealing details about less than 1 to 5 nm in size.

In the operation of SEM, an electron beam emitted from an electron gun fitted with a tungsten filament cathode. The electron beam has an energy ranging from few hundred eV to 50eV and is focused by one or two condenser lenses to a spot about 1 nm to 5 nm in diameter. The beam passes through pairs of scanning coils or pairs of deflector plates in the electron column which deflect the beam so that it scans in a raster fashion over a rectangular area of the sample surface. When the primary electron beam interacts with the sample, the electrons lose energy by repeated random scattering and absorption within a teardrop-shaped volume of the specimen named interaction volume, which extends from less than 100 nm to around 5  $\mu\text{m}$  into the surface. These electrons are reflected by the surface of the sample with no loss of energy (backscatter electron). They may be absorbed and emit secondary electrons of low energy. They may also be absorbed and give rise to the emission of visible light, and also give rise to electric currents within the specimen. All these effects can be detected and hence given a map of the surface topography of samples. For backscattered electrons, it consists of high-energy electrons originating in the electron beam, which are reflected or back-scattered out of the specimen interactions with specimen atoms. The atomic number of the elements in the sample is used to determine the contrast in the produced image.

The image will show the distribution of different chemical phases in the sample.

The spatial resolution of the SEM depends on the size of the electron spot which in turn depends on both the wavelength of the electrons and the electron-optical system (magnetic electron-optical system) which produces the scanning beam. The resolution is also limited by the size of the interaction volume which is very large as compared to the distances between atoms, so the resolution of the SEM is not high enough to image down to the atomic scale. However, SEM has compensating advantages such as the ability to image a comparatively large area of the specimen, to image bulk materials and the variety of analytical modes available for measuring the composition and nature of the specimen.



**Figure 3.16: Experimental setup of the Hitachi S-3400N Scanning Electron Microscope**

## CHAPTER 4

### RESULT AND DISCUSSION

#### 4.1 Electrochemical Impedance Spectroscopy (EIS) Studies

The bulk resistance ( $R_b$ ) for a particular polymer electrolyte sample is obtained from the Cole-Cole plot as shown in Figure 4.1. The ionic conductivity of the sample can be determined using the Equation 4.1.

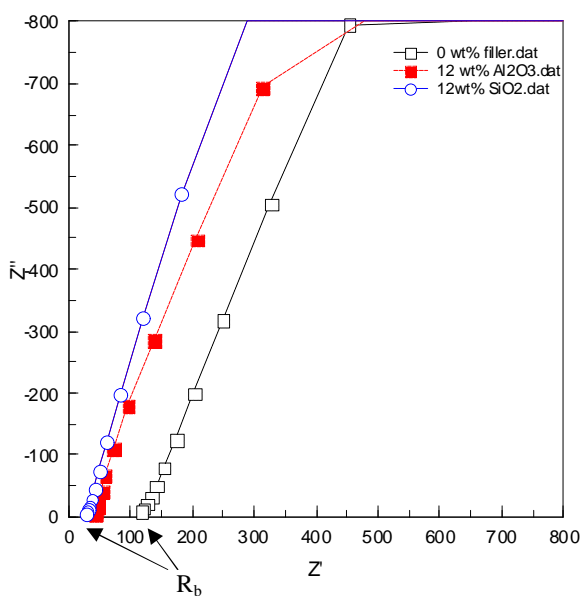


Figure 4.1: Cole-Cole plot of a.c. impedance spectroscopy

Figure 4.1 shows the Cole-Cole plot of a.c impedance spectroscopy for  $\text{LiClO}_4$ ,  $\text{Al}_2\text{O}_3$  and  $\text{SiO}_2$ . The straight lines inclined towards the real axis in the samples when Lithium Perchlorate ( $\text{LiClO}_4$ ) is added. This behaviour is caused by a major contribution towards bulk resistance ( $R_b$ ). Therefore, the  $R_b$  can be obtained by the interception on the real axis for the polymer electrolyte (Raghavan et al., 2010) as:

$$\sigma = \frac{t}{R_b A} \quad (4.1)$$

where  $\sigma$  = ionic conductivity

$t$  = thickness of the sample

$A$  = surface area of the sample

$R_b$  = bulk resistance

In the Cole-Cole plot, the disappearance of the high frequency semi-circular portion which revealed that the current ionic conduction is conducted by ions. The low ion diffusion resistance results in higher ionic conductivity (Osaka et al., 1997).

## 4.1.1 Ionic Conductivity at Ambient Temperature

### 4.1.1.1 Ionic Conductivity for determining the optimum EC and PC mixture ratio

Figure 4.2 shows the ionic conductivity behavior of EC/PC which was mixed at different weight ratio.

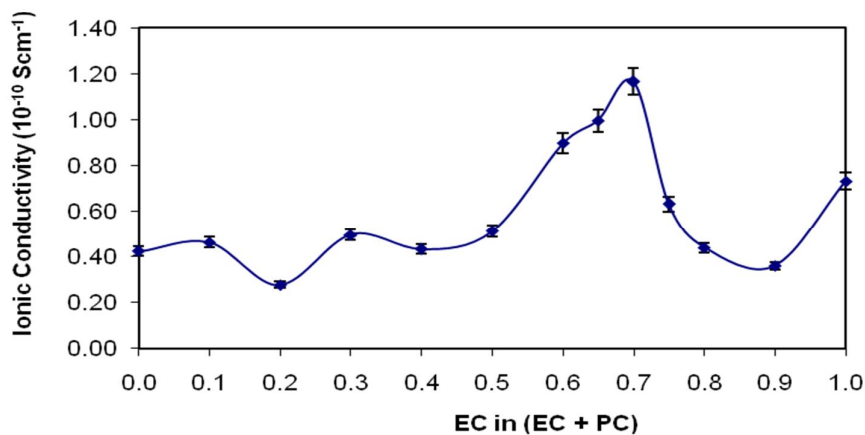


**Figure 4.2** Ionic Conductivity of EC in (EC + PC)

From the observation, 70% of EC and 30% of PC mixture exhibit the highest conductivity in all the system with good mechanical properties. The synergist effect of binary plasticiser plays an important role to softening or improving the mechanical properties of polymer host. The proper formulation of EC/PC ratio may help to optimise the synergist effects to the host polymer. Thus, pre-determining the ratio of EC/PC mixture is important to enhance the flexibility and performance of polymer electrolyte.

In general, the EC/PC mixture is used as a binary solvent for solvating the lithium salt neither to generate liquid electrolyte nor integrate a host polymer into the liquid electrolyte to generate gelled type polymer electrolyte. In the present studies, EC/PC mixture is used as plasticiser.

#### **4.1.1.2 Ionic Conductivity Results for PMMA-EC/PC system**

Pure PMMA polymer film is rigid, fragile, and transparent with a smooth film surface. The mechanical property of PMMA is altered by an addition of plasticiser (EC/PC mixture with 70:30). With the increment of EC/PC mixture, polymer thin films are getting more softened. For PMMA sample to be added with more than 30 wt% of EC/PC mixtures, the mechanical polymer systems will become gel like and will lose the mechanical integrity. As the primary objective of the research is to develop a solid type of polymer electrolytes, the result of EC/PC mixture into PMMA polymer are limited to 30 wt % of EC/PC mixture before the polymer film turns into gel.

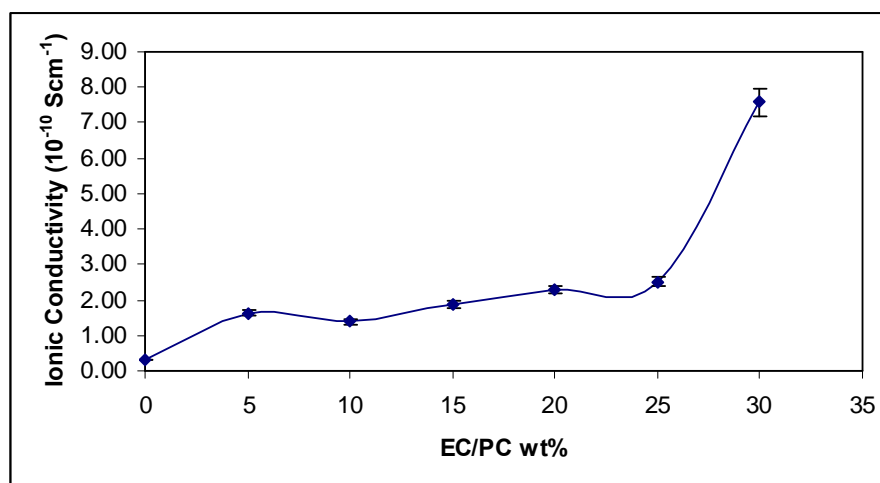


**Figure 4.3: Ionic Conductivity versus wt% of EC/PC mixture added into PMMA**

Figure 4.3 shows that it can be seen that a pure PMMA solid polymer exhibits a very low ionic conductivity about  $3.19 \times 10^{-11} \text{ S cm}^{-1}$ . However, with the addition of 30 wt% of EC/PC mixture plasticiser, the ionic conductivity is enhanced to  $7.57 \times 10^{-10} \text{ S cm}^{-1}$ . As expected, the conductivity is increased with the addition of EC/PC mixture. This is due to the formation of a plasticiser-rich phase which provides a path for the ionic transport and polymer segmental motion which will enhance the polymer segmental motion and ionic transport. Besides, the addition of EC/PC mixture helps to increase the free volume in the polymer matrices, and thus enhanced the polymer segmental motion where the rotation of polymer segment and polymer chain can occur more readily and the ion transport in the polymer electrolyte is faster (Rajendran et al., 2002).

Furthermore, the addition of high dielectric and low viscosity plasticiser into the host polymer helps to enhance the ion and polymer segmental motion as well as solvation ability. At the same time, the addition of plasticiser can lower the degree of crystallinity in particular polymer system, this result can be observed from the XRD studies (Mahendran et al., 2005). As mentioned in the literature, the conductivity behaviour of polymer electrolytes is strongly dependent on the glass transition temperature ( $T_g$ ). Relatively, this sample exhibits a very low conductivity value which is due to no lithium salts being added into the system yet.

#### **4.1.1.3 Ionic Conductivity Results for PMMA-EC/PC-LiClO<sub>4</sub> system**

From the predetermined 70/30 of EC/PC mixture into PMMA host, LiClO<sub>4</sub> lithium salt was added accordingly ranging from 5 wt% to 50 wt%. With the addition of LiClO<sub>4</sub> up to 25 wt%, the SPEs thin film appears transparent. The localised white spot is observed when the addition of LiClO<sub>4</sub> salt is beyond 25 wt%. This is due to the formation of crystalline surface of the insoluble LiClO<sub>4</sub> salt. These crystalline phases are observed by SEM, which will be presented in section 4.6.2.

The addition of LiClO<sub>4</sub> salt to the plasticised polymer caused the ionic conductivity to increase dramatically even with a small amount of LiClO<sub>4</sub> salt

(5 wt%). It can be observed in Figure 4.4 that with the addition of 5 wt% of  $\text{LiClO}_4$  into the plasticised polymer (PMMA-EC/PC) system, the ionic conductivity is elevated from  $7.57 \times 10^{-10} \text{ S cm}^{-1}$  to  $4.17 \times 10^{-8} \text{ S cm}^{-1}$ . As the plasticised polymer provided separate ionic path ways for migration of free  $\text{Li}^+$  ions in the plasticiser-rich phase, the free  $\text{Li}^+$  ions may penetrate through these new paths because of less viscous medium that enhanced the mobility of ions and polymer segmental motion (Mahendran et al., 2005). Doping of the lithium salt into polymer complex involved some structural changes, such as the polar group of plasticiser and polymer backbone favourably to interact with  $\text{LiClO}_4$ . Due to the plasticisation effect, the inter-columbic interaction between  $\text{Li}^+$  and  $\text{ClO}_4^-$  is overcome whereby providing more  $\text{Li}^+$  anions and  $\text{ClO}_4^-$  cations, this result is further confirmed by FTIR studies, as presented in section 4.5.2.

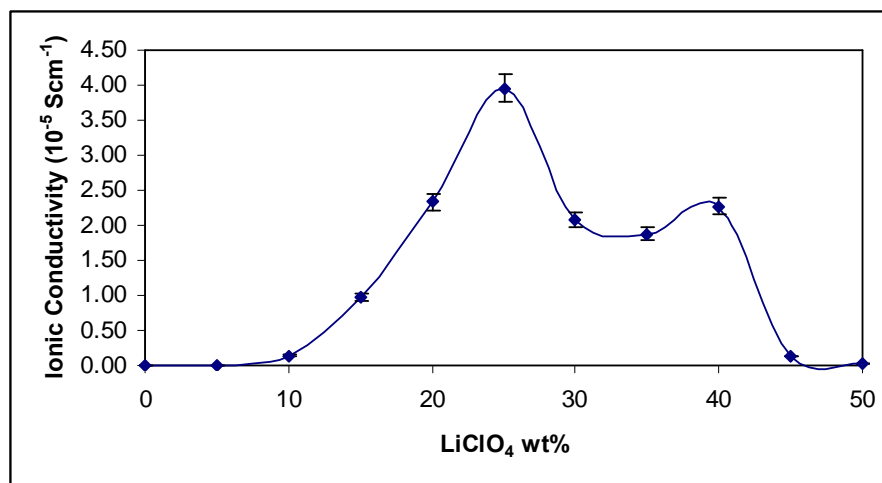


**Figure 4.4: Ionic Conductivity versus wt% of  $\text{LiClO}_4$  added into PMMA-EC/PC**

The highest ionic conductivity obtained was  $3.95 \times 10^{-5} \text{ S cm}^{-1}$  at 25 wt% of  $\text{LiClO}_4$  added into PMMA-EC/PC system. The overall conductivity is elevated about 5 orders of magnitudes at 25 wt% of  $\text{LiClO}_4$  compared to 0% of  $\text{LiClO}_4$ . As the  $\text{LiClO}_4$  concentration increases, the number of carrier ions also increases the ionic conductivity. Besides, the effect of the high dielectric constant of EC/PC mixture helps to dissociate more lithium salt and provides more charge carrier in the polymer matrix. At the same time, the plasticisation effect of the EC/PC mixture with interaction at an appropriate concentration of  $\text{LiClO}_4$  generated an additional transit site available in polymer electrolyte matrices. Therefore, the increase in capacity for  $\text{Li}^+$  motion with lesser energy losses can be achieved.

A further increase of salt concentration causes the ionic conductivity to drop which may be due to the restricted ionic and polymer segmental mobility in a rigid matrix (Rajendran et al., 2003). As the  $\text{LiClO}_4$  concentration is further increased beyond its optimum level or saturation level, the  $\text{Li}^+$  ions become closer to one another thus reduces the overall mobility mode of ion and polymer segment. At a higher salt concentration, the conductivity decreases due to the influencing of the ion pairs, ion triplets, charge cloud effects and restriction to chain mobility and number of effective charge carriers in the solid polymer electrolytes (MacCallum et al., 1986). The formation of random ionic pairs and the clustering of aggregate which do not assist in the ionic transportation might act as a barrier to ionic conduction. Thus, the blocking effect consequently lowers the ionic and chain mobility and causes the ionic

conductivity to decrease. However, a slight increase of ionic conductivity is observed at 40 wt% of LiClO<sub>4</sub> added into PMMA-EC/PC system. This may attribute to the elimination of inter-coulombic interaction between Li<sup>+</sup> and ClO<sub>4</sub><sup>-</sup>. Whereby, the interactions between ClO<sub>4</sub><sup>-</sup> cations with the PMMA backbone, therefore causing the extra transit sites to be formed for Li<sup>+</sup> ions transportation at this concentration (Tan et al., 2007).

#### **4.1.1.4 Ionic Conductivity Results for PMMA-EC/PC-LiClO<sub>4</sub>-Al<sub>2</sub>O<sub>3</sub> system**

Composite solid polymer electrolytes (CSPEs) are formed with the dispersion of nano-sized Al<sub>2</sub>O<sub>3</sub> (40 ~ 47nm) into Solid polymer electrolyte (PMMA-EC/PC-LiClO<sub>4</sub>) system. The predetermined best ionic conductivity sample with 75 wt% of PMMA-EC/PC and 25 wt% of LiClO<sub>4</sub> is used to generate the Composite solid polymer electrolyte. The appearance of these alumina composite solid polymer electrolytes is less transparent and is whitish in colour due to the nature of Al<sub>2</sub>O<sub>3</sub>. It is revealed that this type of ceramic filler is insoluble but is dispersible into the polymeric matrices. From the visual investigation of these samples, the mechanical properties are improved as compared to SPEs. Mainly because the mechanical integrity of these CSPE is improved by the dispersion of nano-sized Al<sub>2</sub>O<sub>3</sub>.

The conductivity behaviour of these alumina CSPEs is presented in Figure 4.5. From this figure, the best ionic conductivity was achieved at a composition with 12 wt% of  $\text{Al}_2\text{O}_3$  filler with the conductivity value of  $1.02 \times 10^{-4} \text{ S cm}^{-1}$ . The ionic conductivity is increased even when a small amount of  $\text{Al}_2\text{O}_3$  is added into the polymer electrolyte. It can be explained that a high dielectric constant nanocomposite  $\text{Al}_2\text{O}_3$  filler could help to dissociate more  $\text{LiClO}_4$  lithium salt to increase more  $\text{Li}^+$  ions transportation between the adjacent nanocomposite grains (Deka and Kumar, 2010). The dis-orderliness of the structure of polymer complex induces the amorphous region when the alumina filler is integrated into the polymer electrolyte which caused the enhancement of ionic conductivity (Ahmad et al., 2006).

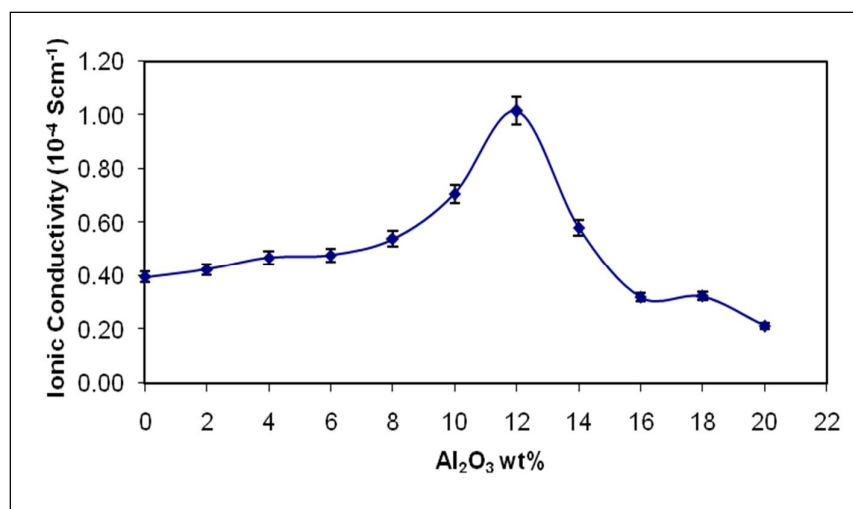


**Figure 4.5: Ionic Conductivity versus wt% of nano-sized  $\text{Al}_2\text{O}_3$  added into PMMA-EC/PC-  $\text{LiClO}_4$**

The increases in the charge carriers as well as in the ionic conductivity are due to the model based on the Lewis acid-base interactions on the surface of fillers. This enhanced the  $\text{Li}^+$  ions mobility under the coexistence of the

ceramic filler. The Lewis acid groups of the added filler such as the  $\text{-OH}$  groups on the  $\text{Al}_2\text{O}_3$  surface may have some interaction with the Lewis acid lithium cations and anions of the  $\text{LiClO}_4$  salt (Low et al., 2010). It can be explained that the  $\text{Al}_2\text{O}_3$  filler may weaken the interaction between polymer chain and  $\text{Li}^+$  ions (possibly to accelerate the dissociation of the lithium salt) and creating a new  $\text{Li}^+$  ions pathway in the polymer complex (Chung et al., 2001). This interaction is further confirmed by FTIR and SEM.

However, a further addition of  $\text{Al}_2\text{O}_3$  beyond 12 wt% causes the conductivity to drop. But an addition of ceramic filler can create a blocking effect, thereby the filler grains can get close to one another which could make the long polymer chains more immobilised leading to the decrease of the conductivity (Dissanayake et al., 2003). It is believed that, excessive of fillers in the polymer electrolyte may create a barrier to block the ionic conduction and reduce the mobility of ionic transportation within the ceramic-rich phase pathway. Another perspective is the presence of ion association that leads to the formation of neutral ion clusters, ion pairs and ion aggregates. The repelling force from the formatted neutral ion clusters, ion pairs and ion aggregates decreases the density of free mobile ions and no contribution on the ionic conduction, decreasing the ionic conductivity (Sharma and Sekhon, 2007).

#### 4.1.1.5 Ionic Conductivity Results for PMMA-EC/PC-LiClO<sub>4</sub>-SiO<sub>2</sub> system

Another Composite solid polymer electrolytes (CSPEs) system is prepared by integrating a nano-sized SiO<sub>2</sub> filler into the Solid polymer electrolyte (PMMA-EC/PC-LiClO<sub>4</sub>) system. From visual observation, the surface of this type of CSPE appears more transparent as compared to the sample added with Al<sub>2</sub>O<sub>3</sub>. It might be due to the nature of SiO<sub>2</sub> and the smaller particle size about 7 nm (Al<sub>2</sub>O<sub>3</sub> = 40~47 nm). However, the appearance of this CSPE is not smooth and becomes brittle at high concentration SiO<sub>2</sub>. The mechanical properties and integrity appears to be better than the one without the addition of SiO<sub>2</sub> filler.

The ionic conductivity is observed to be increased at a low concentration of SiO<sub>2</sub> filler. This effect may be attributed to the surface interactions with lithium cations as mentioned in Section 4.1.1(d). However, for the higher filler concentrations, the blocking effect has led to lower conductivity. From the Figure 4.6, it is shown that the ionic conductivity is increasing at low concentration of filler addition and reached the maximum ionic conductivity of  $2.48 \times 10^{-4} \text{ S cm}^{-1}$  at 12 wt% of fumed silica. The ionic conductivity has increased about one order of magnitude as compared to the best ionic conductivity without filler. This implies that with an addition of 12 wt% of SiO<sub>2</sub> filler it exhibits a higher effect on increasing the ionic

conductivity. A further increase of filler concentration causes the ionic conductivity to decrease drastically.

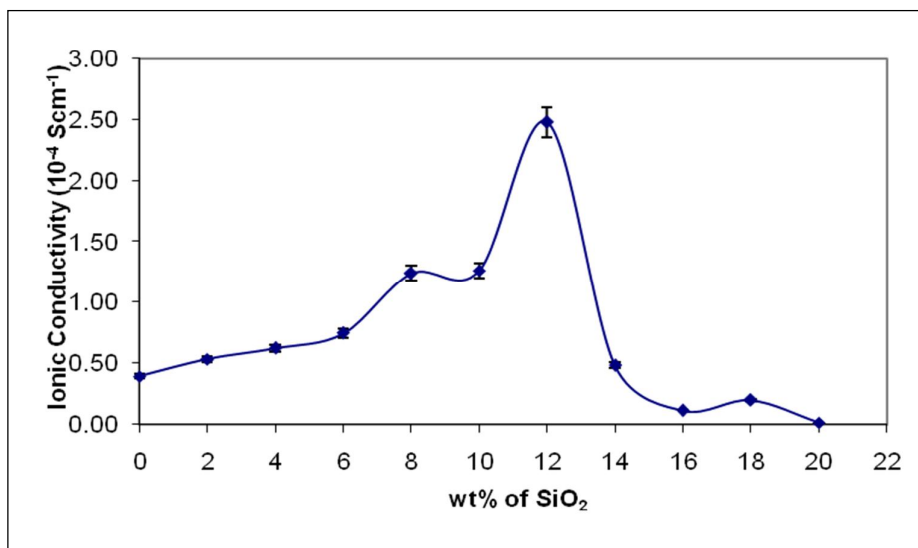


**Figure 4.6: Ionic Conductivity versus wt% of nano-sized  $\text{SiO}_2$  added into PMMA-EC/PC-  $\text{LiClO}_4$**

The enhancement of ionic conductivity is attributed to the mobility of the  $\text{Li}^+$  ions which influence the segmental motion in the free volume. Therefore, the  $\text{Li}^+$  ions can be facilitated with higher speed thus causing a reduction in the total impedance of the polymer electrolyte (Ji et al., 2003). For a certain concentration of  $\text{SiO}_2$  filler, the aggregates of silica can interact through the H-bonding of surface hydroxyl groups, which results in the formation of three-dimensional networks which is confirmed by SEM studies. Through the formation of three-dimensional network, fast  $\text{Li}^+$  ions facilitation could be achieved (Ahmad et al., 2006). For this composite solid polymer electrolyte, the mechanism of Lewis acid-base reaction is similar to the system

dispersed with  $\text{Al}_2\text{O}_3$  filler. The surface groups of  $\text{SiO}_2$  filler (-OH groups) are likely to compete with the Lewis-acid cations for the formation of complexes with the polymer chains. The formation of cross-linking centers prevents the polymer chain reorganisation tendency and promotes a structure modification that produces  $\text{Li}^+$  ions conducting pathway (Scrosati et al., 2000).

The ionic conductivity is decreased when the  $\text{SiO}_2$  fillers is further added into the polymer system beyond its saturated level. This is possibly due to the modification of glass transition temperature ( $T_g$ ) of the polymer composite electrolyte (Pandey et al., 2008). This conductivity profile is similar with the polymer electrolyte systems added with lithium salt and alumina filler. This revealed the blocking of existing conductivity paths by the particles of fumed silica, which hinders the motion of mobile ions (Sharma et al., 2007). The excessive addition of  $\text{SiO}_2$  filler which reduced the number of surface charge layer formed at the PMMA- $\text{SiO}_2$  interface leading to a decrease in the conducting pathway in turn lowered the ionic conductivity (Ramesh and Wen, 2010). Due to the formation of ion aggregates which do not take part in the ionic conduction caused the blocking effect to the ionic transportation. Besides, the reduction in the surface area of  $\text{SiO}_2$  filler and formation of  $\text{SiO}_2$  filler aggregates reduces the charge carrier in the polymer electrolyte (Saikia et al., 2009).

#### 4.1.1.6 Summary of Ionic Conductivity Result at ambient temperature

From the Figure 4.7 and Table 4.1, it is clearly illustrated that the addition of plasticiser and filler enhanced the ionic conductivity performance of polymer electrolyte. The ionic conductivity is increased to 1 order of magnitude when the EC/PC mixture plasticiser is added into pure PMMA.

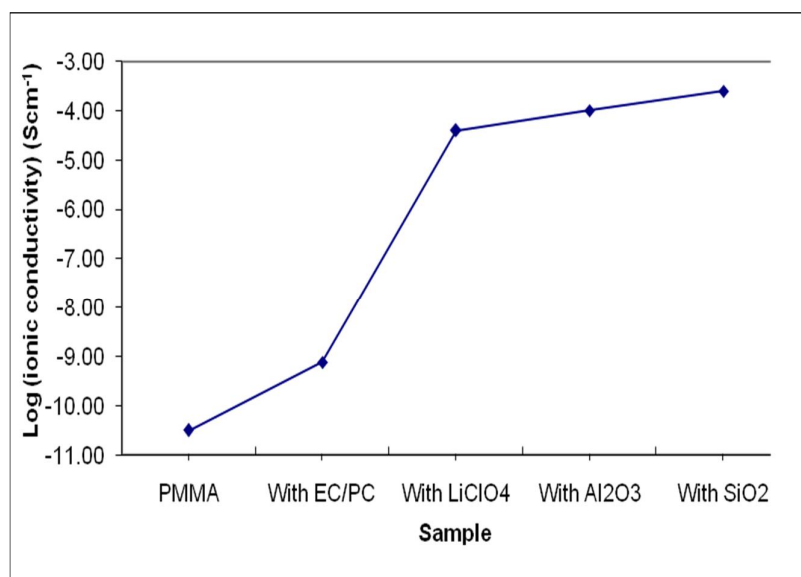


**Figure 4.7: Ionic conductivity of the best sample in each system**

**Table 4.1: Ionic conductivity of the best sample in each system**

Sample	Conductivity at ambient temperature
Pure PMMA	$3.1916 \times 10^{-11} \text{ S cm}^{-1}$
70 wt% PMMA : 30% EC/PC	$7.5708 \times 10^{-10} \text{ S cm}^{-1}$
75 wt% PMMA-EC/PC : 25 wt% LiClO <sub>4</sub>	$3.9519 \times 10^{-5} \text{ S cm}^{-1}$
88 wt% PMMA-EC/PC-LiClO <sub>4</sub> : 12 wt% Al <sub>2</sub> O <sub>3</sub>	$1.0159 \times 10^{-4} \text{ S cm}^{-1}$
88 wt% PMMA-EC/PC-LiClO <sub>4</sub> : 12 wt% SiO <sub>2</sub>	$2.4784 \times 10^{-4} \text{ S cm}^{-1}$

The addition of the LiClO<sub>4</sub> lithium salt into the plasticised host polymer has caused the ionic conductivity to increase by 5 orders of magnitude up to  $10^{05} \text{ Scm}^{-1}$ . The enhancement in the ionic conductivity ascribes the interaction between the host polymer and plasticiser as both of these materials served as a solvent to dissolve the lithium salt.

With the integration of ceramic fillers into the solid polymer electrolyte, the ionic conductivity is further increased to  $10^{-04} \text{ Scm}^{-1}$  in both types of fillers. From these results, it is revealed that the presence of these electrolyte materials have caused favourable conductivity performance in particular polymer electrolyte system and the enhancement in the mechanical properties. The ionic conductivity for SiO<sub>2</sub> is greater than Al<sub>2</sub>O<sub>3</sub>; this may be concluded that the smaller particle size of SiO<sub>2</sub> filler might have a better dispersion phase and provides a better Lewis acid-base interaction with LiClO<sub>4</sub> in the polymer electrolyte.

#### 4.1.2 Temperature Dependence – Ionic Conductivity of Polymer Electrolytes

The polymer electrolytes sample with the highest conductivity (75 wt% PMMA-EC/PC - 25 wt% LiClO<sub>4</sub>) and both samples of composite polymer electrolyte (12 wt% of SiO<sub>2</sub> and 12 wt% Al<sub>2</sub>O<sub>3</sub>) dispersed in PMMA-EC/PC-LiClO<sub>4</sub> system were studied through the impedance measurement for the temperature ranging from 298K to 373K (25°C to 100°C). Through the temperature versus conductivity studies, the activation energy (E<sub>a</sub>) can be calculated from the following equation.

$$\sigma = \sigma_0 \exp \left[ \frac{-E_a}{KT} \right] \quad (4.2)$$

$$\ln \sigma = - \frac{E_a}{KT} + \ln \sigma_0 \quad (4.3)$$

$$\ln \sigma = \frac{-E_a}{1000K} \frac{1000}{T} + \ln \sigma_0 \quad (4.4)$$

$$Y = mX + C \quad (4.5)$$

$$\text{Gradient, } m = \frac{-E_a}{1000K} \quad (4.6)$$

$$E_a = - (1000 K) m \quad (4.7)$$

Where E<sub>a</sub> = the activation energy

T = temperature on Kelvin scale

σ<sub>0</sub> = pre-exponential factor

k = Boltzmann constant (1.3806503 x 10<sup>-23</sup> m<sup>2</sup>kg<sup>s</sup><sup>-2</sup>k<sup>-1</sup>)

Figure 4.8 illustrates the ionic conductivity of the polymer electrolyte against the reciprocal absolute temperature. It can be observed that the polymer electrolytes showed the Arrhenius behaviour as the ionic conductivity enhanced almost linearly with respect to temperature (Jeon et al., 2005).

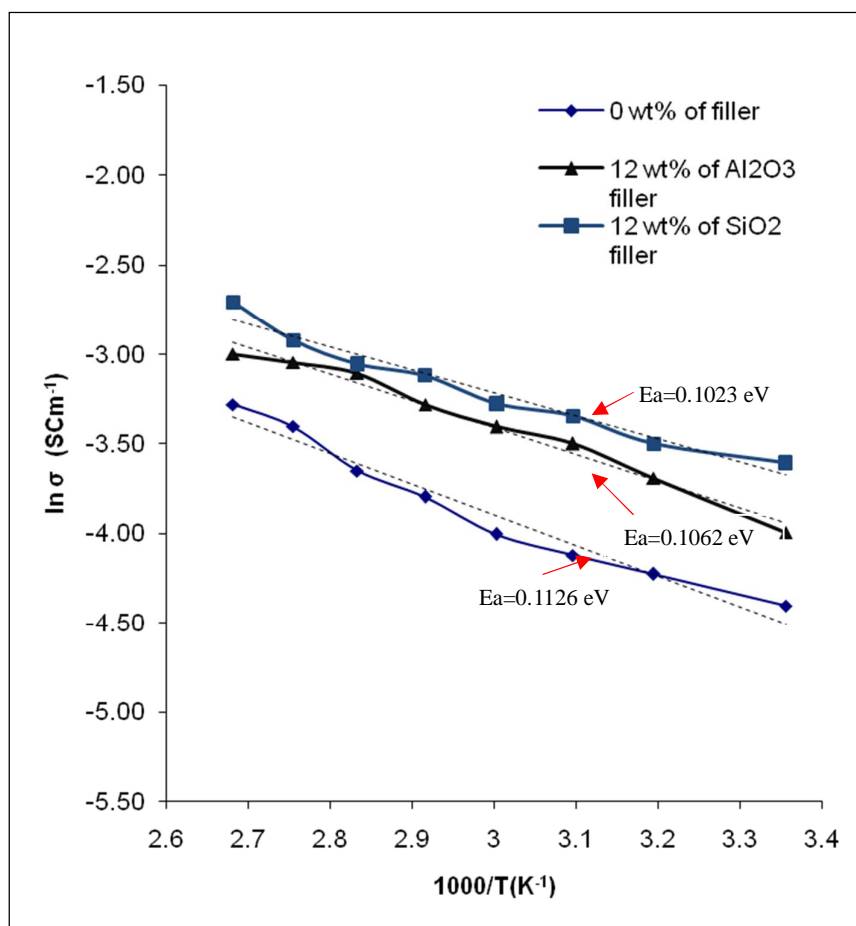


**Figure 4.8:** Temperature dependence of polymer electrolytes with 12 wt% of SiO<sub>2</sub>, 12 wt% of Al<sub>2</sub>O<sub>3</sub> and without filler

From the observation, the ionic conductivity has increased proportionally with the temperature in all polymer electrolytes systems. The similar Arrhenius Plot has been reported by Rajendran et al., 2001; Tan et

al.,2007; Osinska et al., 2009; Raghavan et al., 2010. This is due to the improvement on thermal movement of polymer chain segments and the dissociation of ion aggregates and ion pairs. The enhancement in the mobility of polymer segmental motion and ionic transport with respect to higher temperature has led to a higher ionic conductivity. At low temperature, the polymer segmental motion and ionic mobility is hindered. This is attributed to the increment of cohesive energy which causes from cation-dipole interaction lead to lower conductivity (Rajendran et al., 2009). However at higher temperature, the polymer matrices can expand easily and produce free volume. The overall mobility of ions and polymer segmental motions are increased which compensate the retarding effect of ion clouds (Mahendran et al., 2005 and Rajendran et al., 2010). At higher temperature, the polymer chain absorbed the vibrational energy which is sufficient to push against the hydrostatic pressure imposed by its neighbouring atoms and creates free volume. Thus, the enhancement of mobility for the ions and polymer segment is caused by the free volume movement (Saikia et al., 2008).

Generally, the activation energy ( $E_a$ ) is a combination of the energy of defect formation and the energy of defect migration, and it can be differentiated from the temperature dependence graph slope of the plot (Ramesh and Arof, 2001). As compared with the  $E_a$  obtained from 0 wt% of filler (0.1126eV), 12 wt% of  $Al_2O_3$  (0.1062eV) and 12 wt% of  $SiO_2$  (0.1023eV), the complete amorphous nature of the particular polymer electrolyte will exhibit a low activation energy,  $E_a$  (Ramesh and Arof, 2001).

At higher temperature, the amorphous nature provides a bigger free volume in the polymer matrix which can facilitate fast Li<sup>+</sup> ion motion in the polymer network (Michael et al., 1997). Those results agreed with the conductivity studies where the sample showing the highest conductivity exhibits the lowest activation energy.

### 4.1.3 Dielectric Relaxation Studies

The dielectric relaxation studies are very useful in understanding the behaviour of polymers and the electrolyte materials. The relaxation of dipoles in polymer electrolytes is studied through a broad frequency range (Rajendran and Prabhu, 2010). Initially, when an electric field is applied to a material, the dipoles in the material show the tendency to orient itself in the direction of the applied field. In fact, the mobilisation of the dipole depends on the nature of the materials. The delayed response of the polymer dipoles against the applied electrical field is called dielectric relaxation (Jana and Zhong, 2008).

The complex dielectric behaviour of a polymer electrolyte is expressed as:

$$\epsilon^* = \epsilon' + i \epsilon'' \quad (4.8)$$

$$|\epsilon^*| = [(\epsilon')^2 + (\epsilon'')^2]^{1/2} \quad (4.9)$$

Where  $\epsilon'$  representing the real part of dielectric constant so-called relative permittivity constant or dielectric constant and  $\epsilon''$  representing imaginary part of dielectric constant called relative loss permittivity or dielectric loss in the polymer electrolyte system. These dielectric properties can be expressed as:

$$\epsilon' = \frac{C_p t}{\epsilon_0 A} \quad (4.10)$$

$$\epsilon'' = \frac{\sigma}{\omega \epsilon_0} \quad (4.11)$$

Where  $C_p$ = parallel equivalent static capacitance

$t$  = thickness of sample

$\epsilon_0$  = permittivity of free space ( $8.856 \times 10^{-14} \text{ Fcm}^{-1}$ )

$A$  = surface Area of sample

$\sigma$  = Ionic Conductivity of sample

$\omega$  = angular frequency ( $2\pi \nu$ )

#### 4.1.3.1 Dielectric Relaxation Studies on Polymer Electrolytes at Room Temperature

Figures 4.9 to 4.11 illustrate the dielectric constant corresponding to the frequency for PMMA-EC/PC-LiClO<sub>4</sub>, PMMA-EC/PC-LiClO<sub>4</sub>-Al<sub>2</sub>O<sub>3</sub> and PMMA-EC/PC-LiClO<sub>4</sub>-SiO<sub>2</sub> systems of all samples at room temperature. However, the result for PMMA-EC/PC system is not presented due to the

irregular pattern and low dielectric constant value. There is no distinctive line presented in PMMA-EC/PC system, it might be due to the absence of lithium salt in the samples hence not much ion pairs are formed. On the sample which was added with LiClO<sub>4</sub>, Al<sub>2</sub>O<sub>3</sub> and SiO<sub>2</sub>, some variation of the curves can be observed (Jana and Zhong, 2008).

As mentioned earlier, the dielectric constant plot from Figure 4.9 to 4.11 is plotted according to Equation 4.10. From these figures, the highest dielectric constant is achieved in the following samples:-

- PMMA-EC/PC with 25 wt% of LiClO<sub>4</sub>
- PMMA-EC/PC-LiClO<sub>4</sub> with 12 wt% of Al<sub>2</sub>O<sub>3</sub>
- PMMA-EC/PC-LiClO<sub>4</sub> with 12 wt% of SiO<sub>2</sub>

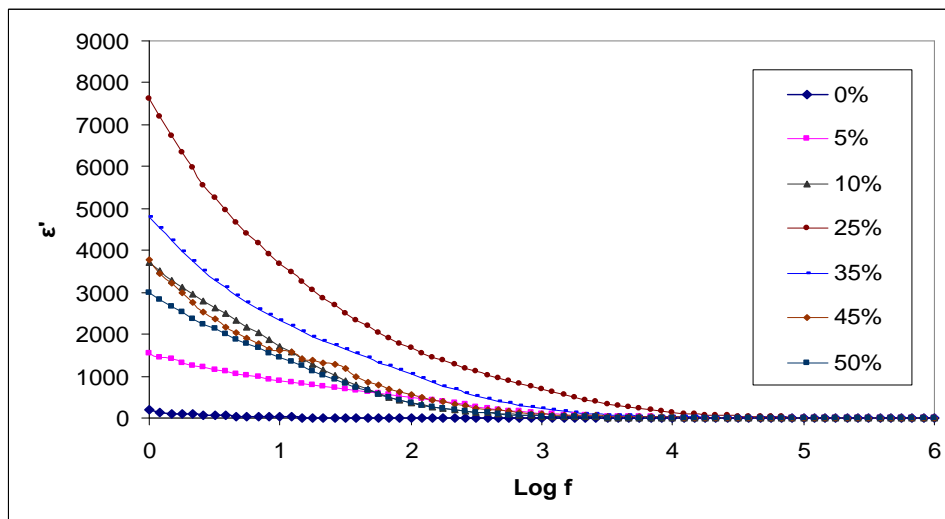
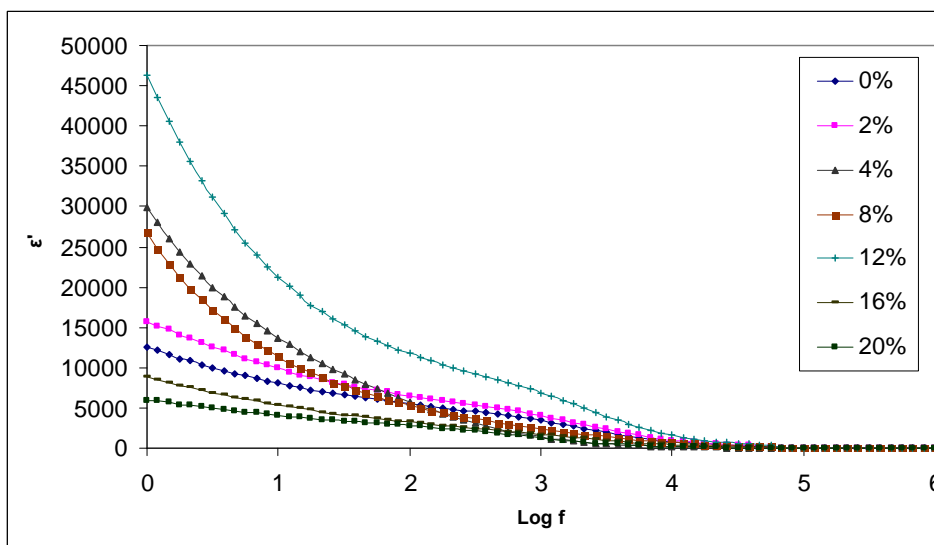
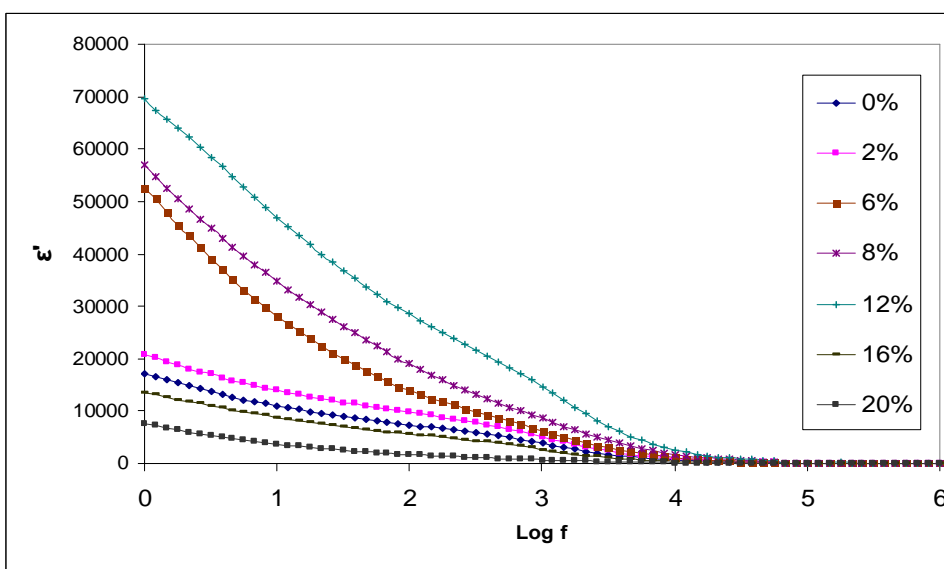


Figure 4.9: Real part of complex permittivity ( $\epsilon'$ ) for PMMA-EC/PC-(x wt%) LiClO<sub>4</sub> corresponding to frequency



**Figure 4.10: Real part of complex permittivity ( $\epsilon'$ ) for PMMA-EC/PC-LiClO<sub>4</sub>-(x wt%) Al<sub>2</sub>O<sub>3</sub> corresponding to frequency**



**Figure 4.11: Real part of complex permittivity ( $\epsilon'$ ) for PMMA-EC/PC-LiClO<sub>4</sub>-(x wt%) SiO<sub>2</sub> corresponding to frequency**

Due to the solvated Li<sup>+</sup> ions by plasticised effect and Lewis acid-base interaction on the surface of filler, the value of dielectric constant increase can be attributed to the increment at localised charge carrier concentration that boost the ionic conductivity. A further addition of electrolyte materials (LiClO<sub>4</sub>, Al<sub>2</sub>O<sub>3</sub> and SiO<sub>2</sub>) after the saturation level causes the dielectric constant

to decrease. This revealed the formation of ion aggregation which reduces the mobility of ions and hence reduces the ionic conductivity.

Besides that, the dielectric relaxation in the low frequency region is due to the electrode polarisation effect as a result of an accumulation of charge carrier at the electrode-electrolyte interface (Karan et al., 2008). Higher dielectric constant revealed the enhancement of charge carrier density at the space charge region. As a result, higher equivalent capacitance ( $C_p$ ) can be observed where the dielectric constant is directly proportional to the value of  $C_p$  (Ramesh et al., 2002).

When the operating frequency increases, it can be observed from Figure 4.9 to Figure 4.11 that the dielectric constant decreases. Due to the high periodic reversal of the electric field in higher frequencies, there is no excess ions diffusion in the direction of the electric field. The contribution of charge carriers towards the dielectric constant decreases at higher frequencies (Baskaran et al., 2004). Thus, the excess ions diffusion is lesser in the direction of electric field that induces the orientation of dipoles. This leads to decrease in polarisation and weaken the interaction of dipoles and electric field. This phenomenon can also be regarded that at low frequency range, the dipoles of molecules tend to reorient in the direction of applied field. But at high frequency, the dipoles may not have sufficient speed to reorient itself in the

direction of applied field thus dielectric constant decreases (Reicha et al., 1991).

The imaginary part of permittivity, called dielectric loss ( $\epsilon''$ ) is shown in Figures 4.12 to 4.14 which are generated according to Equation 4.11. Dielectric loss composed of an ionic transportation and a direct measurement of the energy is dissipated in the polymer electrolyte (Stephan et al., 2000). The  $\epsilon''$  measures the energy loss due to the orientation of dipoles and conduction of ionic species in the polymer electrolyte when an electrical field is applied (Jana and Zhong, 2008).

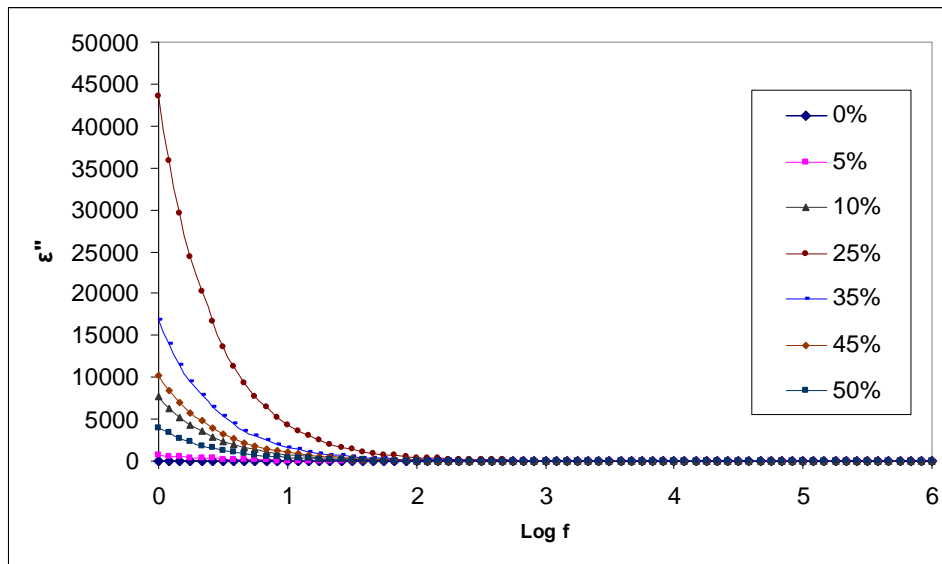


**Figure 4.12: Imaginary part of complex permittivity ( $\epsilon''$ ) for PMMA-EC/PC-(x wt%)  $\text{LiClO}_4$  corresponding to frequency**

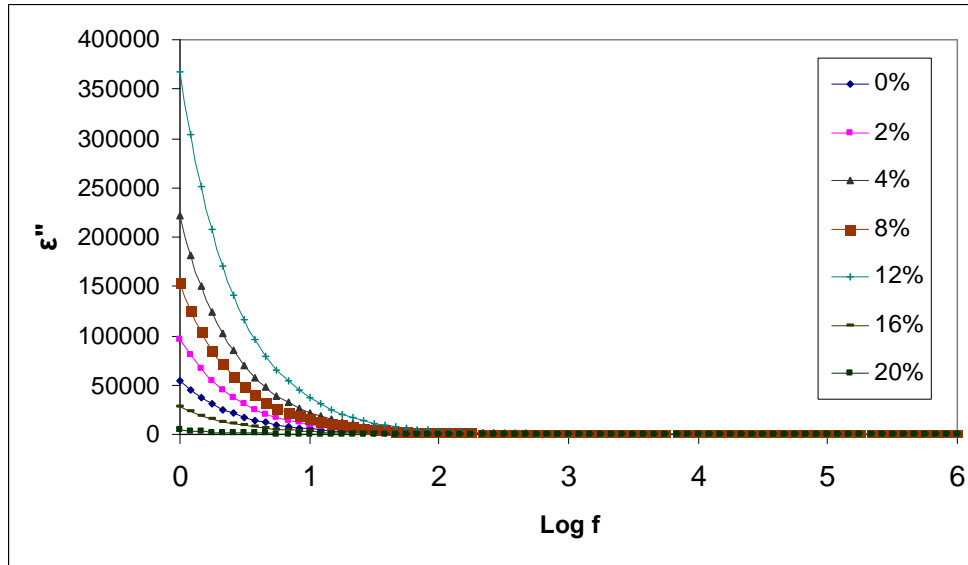


Figure 4.13: Imaginary part of complex permittivity ( $\epsilon''$ ) for PMMA-EC/PC-LiClO<sub>4</sub>-(x wt%) Al<sub>2</sub>O<sub>3</sub> corresponding to frequency

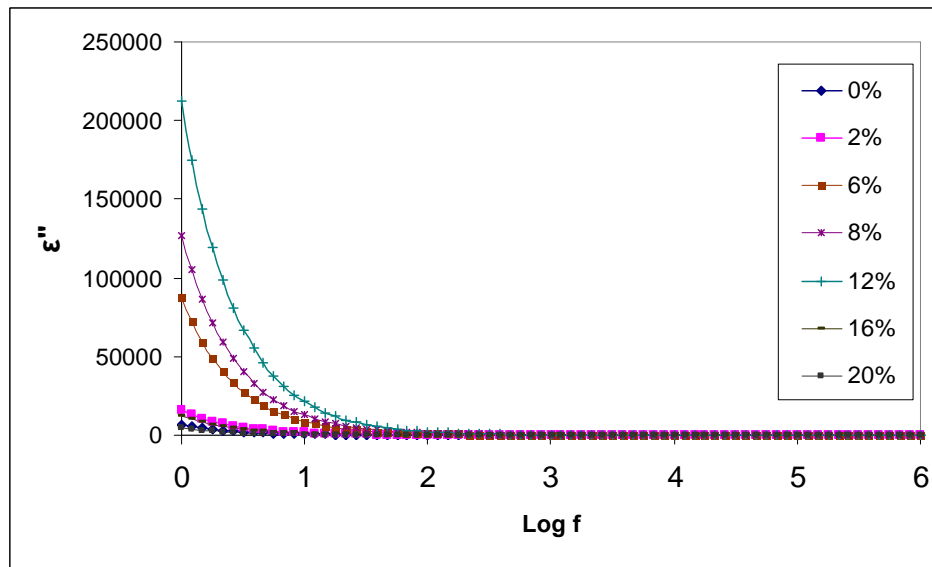


Figure 4.14: Imaginary part of complex permittivity ( $\epsilon''$ ) for PMMA-EC/PC-LiClO<sub>4</sub>-(x wt%) SiO<sub>2</sub> corresponding to frequency

In comparing the variation of dielectric loss for PMMA-EC/PC-LiClO<sub>4</sub>, PMMA-EC/PC-LiClO<sub>4</sub>-Al<sub>2</sub>O<sub>3</sub> and PMMA-EC/PC-LiClO<sub>4</sub>-SiO<sub>2</sub> systems at room temperature, the results are similar to dielectric constant where the

highest of the dielectric constant exhibit higher dielectric losses. High dielectric losses in complex films cause the ionic conductivity to increase (Jana and Zhong, 2008). In the present study, it can be observed from Figures 4.12 to 4.14 where the dielectric loss rises sharply towards low frequency region and the dielectric loss is decreased at higher frequencies. This mechanism is due to the free charge motion where the free charges are building up at the electrode and electrolyte interface (Arof, 1999). However, at the high frequency, the high periodic reversal of the electric field at the electrode and electrolyte interface causes no excess ion diffusion in the direction of the field (Baskaran et al., 2004).

The addition of electrolyte materials such as LiClO<sub>4</sub> salt, Al<sub>2</sub>O<sub>3</sub> filler and SiO<sub>2</sub> filler into PMMA-EC/PC system results in the overall increase of  $\epsilon'$  and  $\epsilon''$  due to both dipolar and free charge contributions. Therefore, any increases in the ionic mobility are reflected in the increase of free charge mobility that enhanced the ionic conductivity. The results from the dielectric studies are comparable to the ionic conductivity studies where the higher dielectric constant and dielectric losses revealed high ions mobility which generates a higher ionic conductivity.

#### 4.1.3.2 Dielectric Relaxation Studies on Polymer Electrolytes in the Temperature Range of 298 K to 373 K

The variation of permittivity ( $\epsilon'$ ) with respect to frequency for PMMA-EC/PC- 25 wt% of LiClO<sub>4</sub>, PMMA-EC/PC-LiClO<sub>4</sub>- 12 wt% of Al<sub>2</sub>O<sub>3</sub> and PMMA-EC/PC-LiClO<sub>4</sub>- 12 wt% of SiO<sub>2</sub> at different temperatures are depicted in Figures 4.15 to 4.17. From the figures, the value of dielectric constant ( $\epsilon'$ ) increases when increasing the temperature. This contributes to the higher carrier density whereby the ionic conductivity is increased (Othman et al., 2007). At higher temperature, the dipoles can orient easily compared to a highly cross-linked material (Jana and Zhong, 2008).

The higher values of dielectric constant at higher temperature can be attributed to the dissociation of ion aggregates and higher degree of salt dissociation. The crystallinity of the polymer electrolyte is reduced with an increase in the temperature. This in turn influences the polymer dynamics and the dielectric behaviour (Awadhia et al., 2006). From the figures, it can be observed that at low frequencies the dielectric constant is high. This is due to the accumulation of the charge carriers at electrode-electrolyte interface.

However, the dielectric constant is decreased at higher frequency which attributes to the high reversal of the applied field. The polarisation of the charge accumulation decreases leading to a decrease in the dielectric constant

(Ramya et al., 2008). The decrease in dielectric constant with increasing frequency can be associated to the inability of dipoles to rotate rapidly in the direction of the applied electric field (Nada et al., 2004). Hence, the polarisation due to charge accumulation decreases at the electrode-electrolyte interface and thus a decrease in dielectric constant.

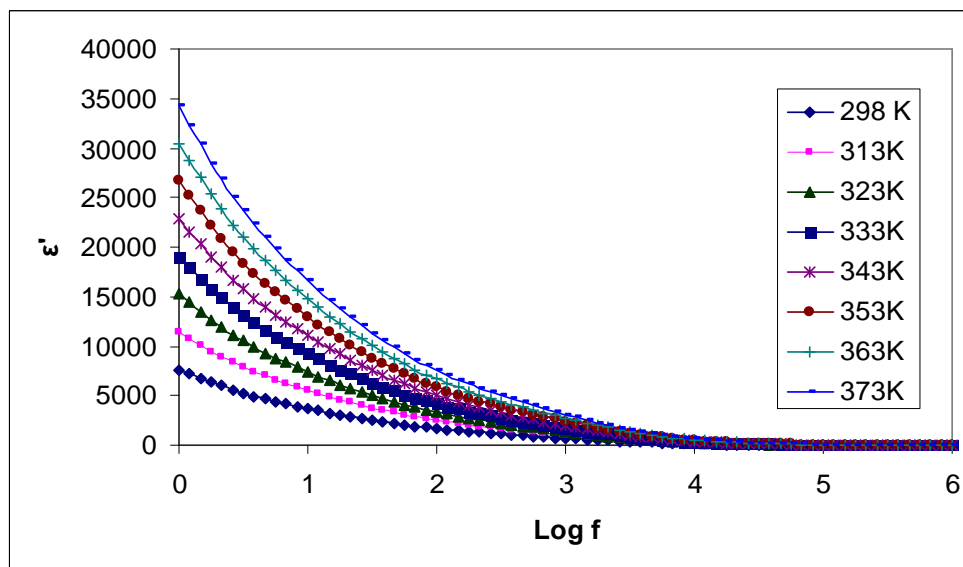


**Figure 4.15:** Real part of complex permittivity ( $\epsilon'$ ) for PMMA-EC/PC- 25 wt% of  $\text{LiClO}_4$  corresponding to frequency in the temperature range of 298-373K

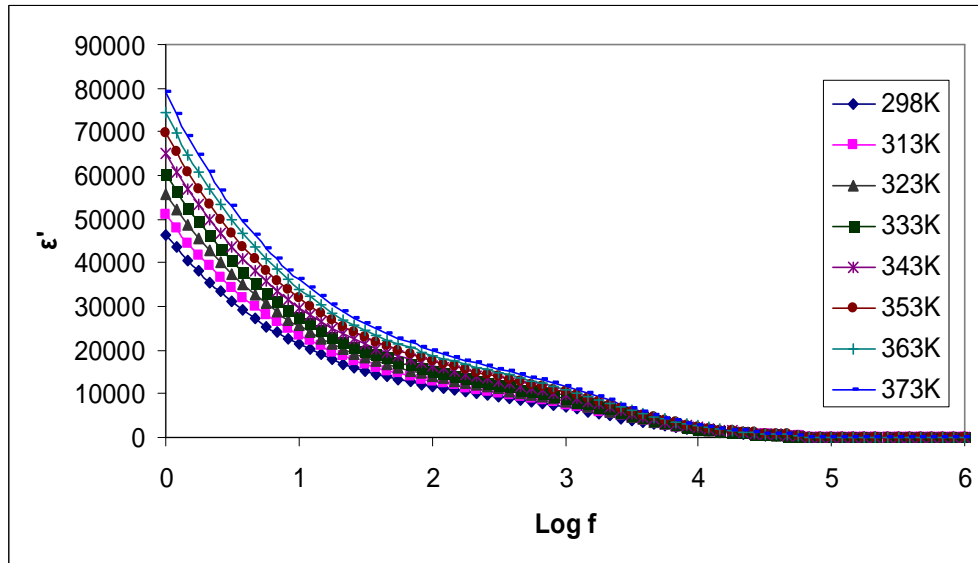


**Figure 4.16:** Real part of complex permittivity ( $\epsilon'$ ) for PMMA-EC/PC-LiClO<sub>4</sub>- 12 wt% of Al<sub>2</sub>O<sub>3</sub> corresponding to frequency in the temperature range of 298-373K

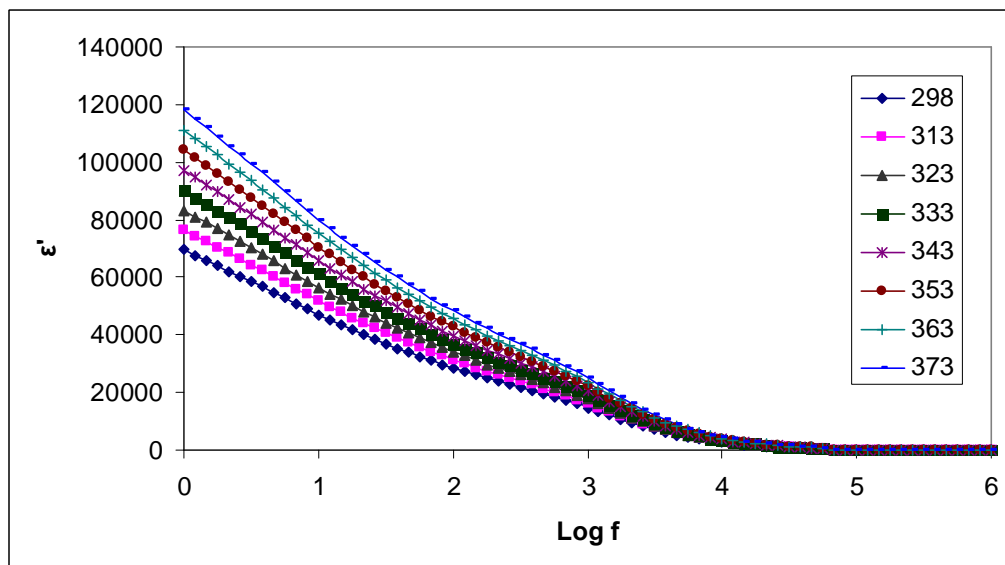


**Figure 4.17:** Real part of complex permittivity ( $\epsilon'$ ) for PMMA-EC/PC-LiClO<sub>4</sub>- 12 wt% of SiO<sub>2</sub> corresponding to frequency in the temperature range of 298-373K

In general, the dielectric loss is a direct measurement of energy dissipated and contributes to the ionic transport and the polarisation of the charge (Nithya et al., 2011). Figures 4.18 ó 4.20 show the variation of  $\epsilon''$  varies with temperature in PMMA-EC/PC- 25 wt% of LiClO<sub>4</sub>, PMMA-EC/PC-

LiClO<sub>4</sub>- 12 wt% of Al<sub>2</sub>O<sub>3</sub> and PMMA-EC/PC-LiClO<sub>4</sub>- 12 wt% of SiO<sub>2</sub> which operates at different frequencies.

The relationship between the conductivity and the dielectric loss factor can be determined by Equation 4.11. Both conductivity and dielectric loss are temperature dependence. The dielectric loss increased with respect to the increment of temperature (Schmidt-Rohr et al., 1994). At higher temperature, the dielectric loss value at lower frequency is higher than the value at high frequency. It may be caused by the movement of the main segments or the free charge motion within the electrolyte. At low frequency, there is sufficient time for the free ion to build up at the electrode-electrolyte interface before the electric field is reversed (Nithya et al., 2011).

At higher frequency, the dielectric loss decreases sharply. This is due to the side group dipoles and the nearest part of the backbone (Ramya et al., 2008). Hence, with an increase in operating frequency, the ions have insufficient time to build up on the electrode-electrolyte interface (Dyre, 1991;Kyristis et al., 1995).

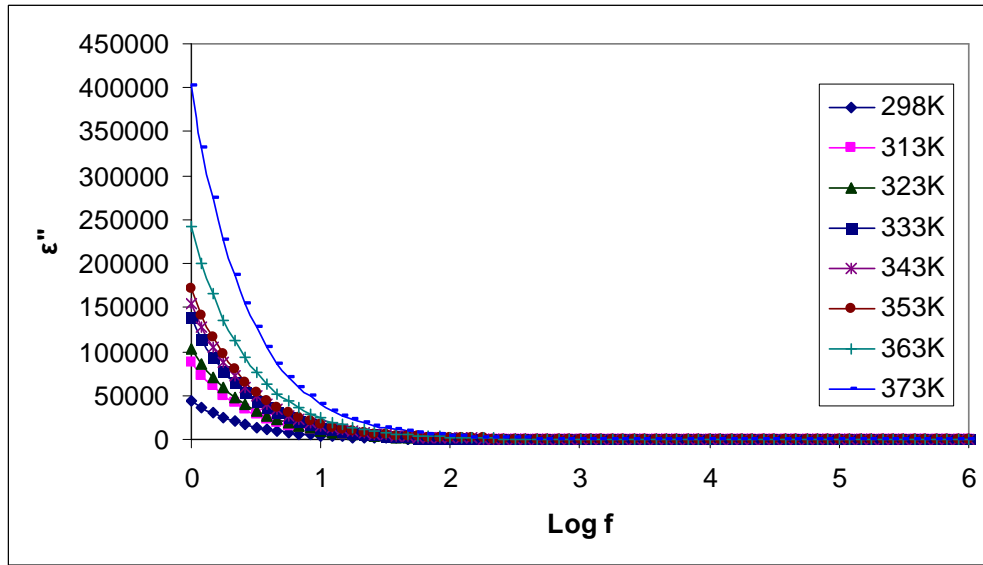


**Figure 4.18: Imaginary part of complex permittivity ( $\epsilon''$ ) for PMMA-EC/PC- 25 wt% of  $\text{LiClO}_4$  corresponding to frequency in the temperature range of 298-373K**

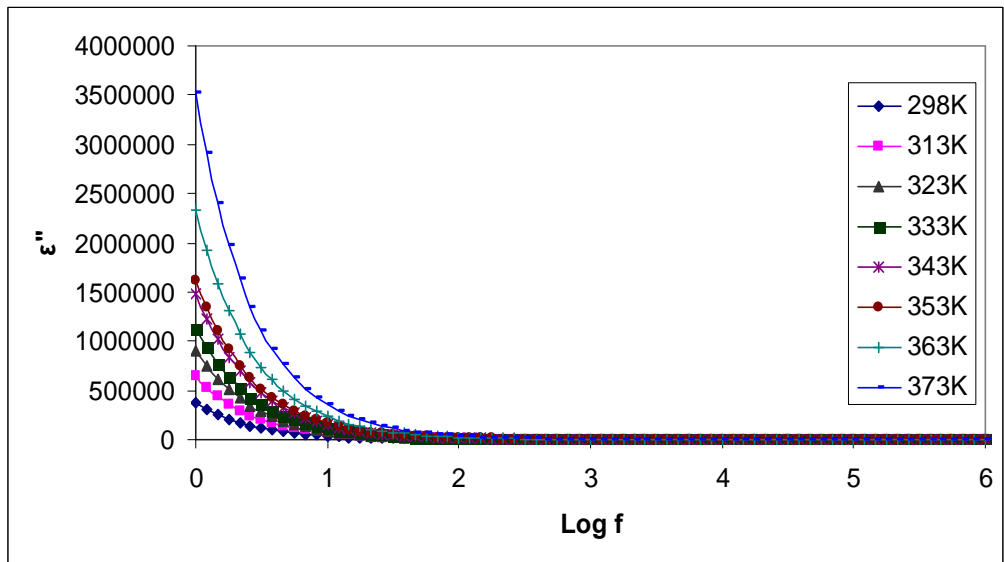


**Figure 4.19: Imaginary part of complex permittivity ( $\epsilon''$ ) for PMMA-EC/PC- $\text{LiClO}_4$ - 12 wt% of  $\text{Al}_2\text{O}_3$  corresponding to frequency in the temperature range of 298-373K**

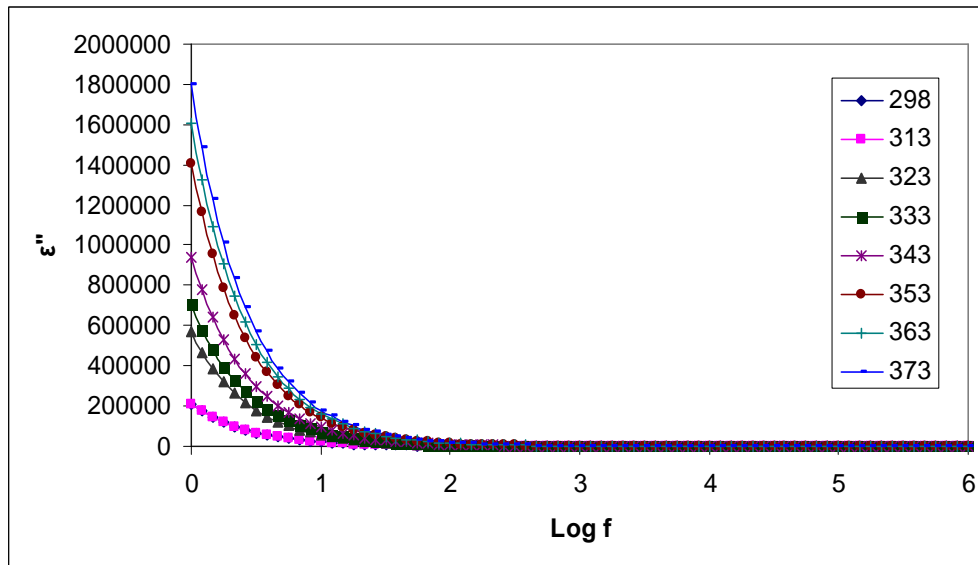


**Figure 4.20: Imaginary part of complex permittivity ( $\epsilon''$ ) for PMMA-EC/PC-LiClO<sub>4</sub>- 12 wt% of SiO<sub>2</sub> corresponding to frequency in the temperature range of 298-373K**

## 4.2 X-ray Diffraction (XRD) Studies

In order to investigate the effects of EC/PC plasticizer mixture, LiClO<sub>4</sub> lithium salt, Al<sub>2</sub>O<sub>3</sub> alumina filler and SiO<sub>2</sub> fumed silica filler in PMMA host polymer, XRD studies were carried out. The information about the crystalline nature and the structure changes of the solid materials were revealed through XRD patterns.

The spacing between layers of atom (d-spacing) is obtained according to Equation 4.12.

$$n \lambda = 2 d \sin \theta \quad (4.12)$$

where  $n$  = integer

$\lambda$  = wavelength of X-ray

$\theta$  = incident angle of the X-ray to the sample surface

#### 4.2.1 PMMA-EC/PC Samples XRD result

Figure 4.21 illustrates the XRD diffractograms of pure PMMA and PMMA-EC/PC up to 35 wt% of EC/PC mixtures added into PMMA. Table 4.2 shows the intensity obtained at diffraction peaks with respect to the PMMA-EC/PC system. The broad characteristic peaks of pure PMMA can be observed in the Figure 4.21 (a), where the broad peaks are obtained at angles of  $2\theta = 13.28^\circ$  and  $29^\circ$ .

By adding 5 wt% of EC/PC into PMMA, the broad peaks obtained from pure PMMA are shifted to  $2\theta$  angle of  $16.3^\circ$  and  $30^\circ$  with weaker intensities.

The shift of the peaks and the change of the intensities revealed the complexation of PMMA with EC/PC.

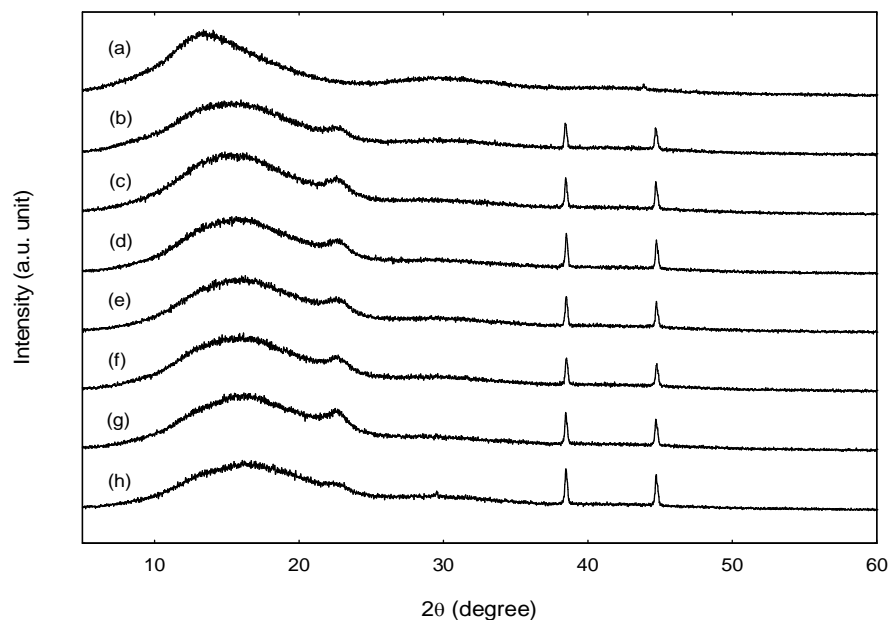


**Figure 4.21:** XRD patterns of (a) pure PMMA, (b) 5 wt% EC/PC, (c) 10 wt% EC/PC, (d) 15 wt% EC/PC, (e) 20 wt% EC/PC, (f) 25 wt% EC/PC, (g) 30 wt% EC/PC, (h) 35 wt% EC/PC added into PMMA

**Table 4.2:** Intensity peak obtained at diffraction Peaks for samples (1-x) PMMA – (x) EC/PC

		x							
		0 wt%	5 wt%	10 wt%	15 wt%	20 wt%	25 wt%	30 wt%	35 wt%
Intensity at diffraction peaks	13.28°	1150	-	-	-	-	-	-	-
	16.30°	-	1100	975	960	960	960	960	850
	23.00°	-	760	700	640	620	640	595	515
	29.00°	400	-	-	-	-	-	-	-
	30.00°	-	310	310	310	300	305	290	270
	38.45°	-	600	715	740	670	640	635	760
	44.70°	-	640	610	620	595	610	595	655

With the addition of EC/PC mixture into pure PMMS, the formation of shoulder peak are found at  $2\theta$  angle of  $23^\circ$  and this shoulder peak is shifted to lower the  $2\theta$  angle as the amount of EC/PC mixture increases with the addition

of EC/PC mixture, new intense peaks are observed at  $2\theta$  angle of  $38.45^\circ$  and  $44.7^\circ$ . This may be attributed to the EC/PC plasticised effect which softens and interacts with polymer backbone. Apparently, the polymer thin films became more flexible and the ionic conductivity is increased proportionally with the increment of EC/PC concentration.

The broader of  $2\theta$  peak and occurrence of new shoulder peak reveal that the amorphous nature of the film increases as a function of plasticisers concentration (Ragavendran et al., 2004). The changes of the intensities of the broad characteristic peak, shoulder peak and intense peaks give strong evidence that EC/PC mixture added into polymer matrices interact with the PMMA backbone and enhanced the amorphous nature of the plasticised polymer. The increase in the amorphous nature of plasticiser polymer causes a reduction in the energy barrier for the segmental motion in polymer electrolyte (Rajendran and Prabhu, 2010). Therefore, higher ionic conductivity could be obtained at higher amorphous nature of polymer. From Section 4.1.2, it gives a similar result to support the evidence which increases the amount of plasticiser thus give rise in the ionic conductivity. However, a further increase of EC/PC mixture into the PMMA host polymer altered the mechanical properties which changed a rigid and solid polymer to a more gel-liked mixture.

Figure 4.21 (g) and (h), show the changes of the broad peak and shoulder peak, where the shoulder peak tend to combine with the broad peak.

This is a clear evidence to show that the solid polymer electrolyte has behaved like a gelled electrolyte when added with EC/PC mixture beyond 30 wt%. The gelled type polymer electrolyte will give a better ionic conductivity due to the greater amorphous region in the polymer complex (Mahendran et al., 2005). In the present studies, the concern on the mechanical properties, mechanical integrity in between electrodes and practical application of polymer electrolyte are important factors with an objective to produce a solid type of polymer electrolyte. Therefore, the EC/PC content is fixed at 30 wt% to avoid the production of gelled type polymer electrolyte.

#### **4.2.2 PMMA-EC/PC-LiClO<sub>4</sub> Samples XRD result**

As illustrated in Figure 4.22 the sharp intense peaks obtained for LiClO<sub>4</sub> lithium salt at  $2\theta = 18.4^\circ, 23.18^\circ, 27.66^\circ, 33^\circ$  and  $36.42^\circ$  represent the crystalline character of LiClO<sub>4</sub>. Table 4.3 shows the intensity obtained at diffraction peaks for PMMA-EC/PC-LiClO<sub>4</sub> system. It is clearly illustrated in Figure 4.22 where most of the peak corresponding to lithium salt has disappeared in the plasticised PMMA polymer electrolyte, which reveals the complete dissolution of the lithium salt in the polymer matrix.

The diffraction pattern as shown in Figure 4.22 clearly indicates that the crystallinity in PMMA-EC/PC system is further disturbed by the addition of LiClO<sub>4</sub>. It is revealed that the PMMA polymer has undergone significant

structural reorganisation while adding the plasticiser and lithium salt. The plasticised effect may induce significant interaction with  $\text{LiClO}_4$  within the polymer matrix. The interaction between the PMMA, plasticiser and lithium salt contributes a much lower crystallinity and enhances the structural disorderliness.

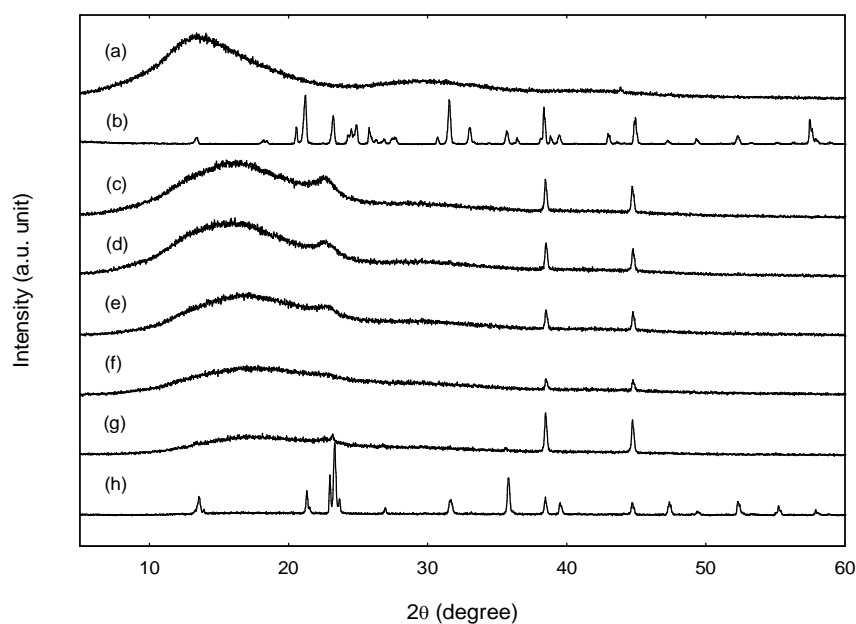


**Figure 4.22:** XRD patterns of (a) pure PMMA, (b) pure  $\text{LiClO}_4$ , (c) 0 wt%  $\text{LiClO}_4$ , (d) 5 wt%  $\text{LiClO}_4$ , (e) 15 wt%  $\text{LiClO}_4$ , (f) 25 wt%  $\text{LiClO}_4$ , (g) 35 wt%  $\text{LiClO}_4$ , (h) 50 wt%  $\text{LiClO}_4$  doped into PMMA-EC/PC system

**Table 4.3: Intensity peak obtained at diffraction peaks for (1-x)PMMA-EC/PC- (x) LiClO<sub>4</sub> system**

		X					
		0 wt%	5 wt%	15 wt%	25 wt%	35 wt%	50 wt%
Intensity at diffraction peaks	13.55 <sub>-</sub>	-	-	-	-	-	345
	16.30 <sub>-</sub>	960	750	570	510	360	75
	21.30 <sub>-</sub>	-	-	-	-	-	440
	23.00 <sub>-</sub>	595	560	470	-	320	700
	23.30 <sub>-</sub>	-	-	-	-	-	1240
	26.92 <sub>-</sub>	-	-	-	-	-	150
	30.00 <sub>-</sub>	290	310	270	270	180	300
	35.78 <sub>-</sub>	-	-	-	-	-	650
	38.45 <sub>-</sub>	635	500	700	350	760	340
	39.50 <sub>-</sub>	-	-	-	-	-	240
	44.70 <sub>-</sub>	595	470	590	320	640	240
	52.30 <sub>-</sub>	-	-	-	-	-	260
	55.23 <sub>-</sub>	-	-	-	-	-	180
	57.90 <sub>-</sub>	-	-	-	-	-	125

With reference to Figure 4.21 (PMMA-EC/PC system), the intense peak at 38.45° and 44.70° appeared with the addition of EC/PC. Therefore, similar peaks found in the following sample might refer to the crystalline character of EC/PC. However, the pure LiClO<sub>4</sub> shows the similar intense peak at 2° degree, which might be due to the LiClO<sub>4</sub> and EC/PC having the common functional group (oxide group). The result shows that the maximum matching of the LiClO<sub>4</sub> with PMMA-EC/PC while the optimum weight percentage (25 wt/%) shows a smaller peak. However the intense peak increases with respect to a higher concentration of LiClO<sub>4</sub>.

By comparing the diffraction patterns in Figure 4.22 (c) and (f), it is found that the intensity of the broad characteristic peak of PMMA is reduced and the shoulder peak is brought to a lower level and tends to disappear.

Eventually, the shoulder peak vanished at 25 wt% of  $\text{LiClO}_4$  and the PMMA broad peak becomes broader. The decrease in the intensities is caused by the increase of the amorphous region which leads to higher ionic conductivity (Ganesan et al., 2008). The intensities of sharp intense peaks observed at  $2\theta = 38.45^\circ$  and  $44.7^\circ$ . This implies that there is an interaction between lithium salt with the plasticisers as well as the host polymer. This shows that the EC/PC mixture provides the additional transit site in the polymeric matrix for ionic transportation. Therefore, the enhanced dissolvability of the  $\text{LiClO}_4$  is greater. The inducing of the amorphous region within the polymeric complexes can be described as the structural disorderliness that is attributed to the re-arrangement of the molecules and ions in the polymeric matrices. For the addition of  $\text{LiClO}_4$  up to 25 wt% into PMMA-EC/PC system results to a gradually decrease in overall intensities of the shoulder peak and sharp peak as well as consistent broadening of PMMA peak. The higher degree of amorphous polymer matrix contributes to more disorder arrangement of polymeric chain and thus increases flexibility of polymer matrix.

However, beyond the saturation level (25 wt% of  $\text{LiClO}_4$ ), the shoulder peak at  $2\theta = 23^\circ$  has reappeared (it is observed at 35 wt% of  $\text{LiClO}_4$  added into plasticized PMMA). This has clearly shown that optimum concentration limits for salt dissolution into the plasticiser PMMA matrix (Shukla and Thakur, 2009). The significant increase of the intensities show the increase of the crystallinity in the polymer complex. Upon the addition of 50 wt% into the PMMA-EC/PC polymer matrix, the polymer-salt phase separation has been

observed. Due to the insoluble lithium salt, the broad peak of PMMA has disappeared and the diffraction pattern is similar to pure  $\text{LiClO}_4$  which can be contrasted from Figure 4.22 (b) and (h). As discussed in EIS, due to the increment of the crystallinity of polymer electrolyte, the energy barrier for ionic transport is increased hence the ionic conductivity is decreased.

### **4.2.3 PMMA-EC/PC-LiClO<sub>4</sub>-Al<sub>2</sub>O<sub>3</sub>Samples XRD result**

The changes in the diffraction pattern and intensity of diffraction peaks for PMMA-EC/PC-LiClO<sub>4</sub>-Al<sub>2</sub>O<sub>3</sub> systems are illustrated in Figure 4.23 and Table 4.4, respectively. As seen from the figures, the dispersion of alumina filler (Al<sub>2</sub>O<sub>3</sub>) is significantly changing the diffraction pattern of all system. The changes of diffraction pattern reveals the interaction between polymer with nano-sized filler as well as plasticiser and lithium salt. The  $2\theta$  angles at 25.56°, 37°, 43°, 52.54°, 57° represent the sharp intense peaks of pure alumina filler as shown in figure 4.23 (b).

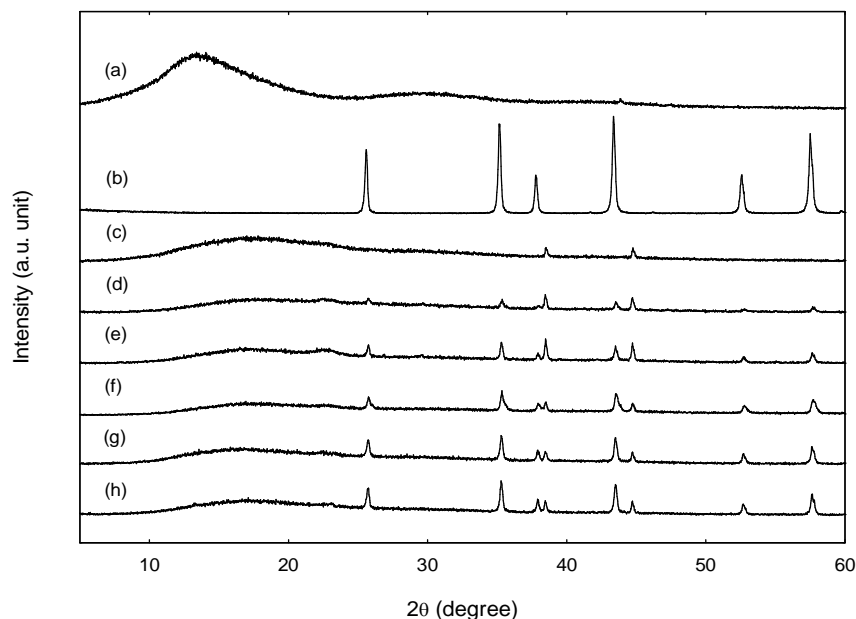


**Figure 4.23:** XRD patterns of (a) pure PMMA, (b) pure  $\text{Al}_2\text{O}_3$ , (c) 0 wt%  $\text{Al}_2\text{O}_3$ , (d) 4 wt%  $\text{Al}_2\text{O}_3$ , (e) 8 wt%  $\text{Al}_2\text{O}_3$ , (f) 12 wt%  $\text{Al}_2\text{O}_3$ , (g) 16 wt%  $\text{Al}_2\text{O}_3$ , (h) 20 wt%  $\text{Al}_2\text{O}_3$ , dispersed into PMMA-EC/PC- $\text{LiClO}_4$  system

**Table 4.4:** Intensity peak obtained at diffraction peaks for (1-x)PMMA-EC/PC- $\text{LiClO}_4$ - (x) $\text{Al}_2\text{O}_3$  system

		x					
		0 wt%	4 wt%	8 wt%	12 wt%	16 wt%	20 wt%
Intensity at diffraction peaks	16.30_	510	300	310	270	250	340
	23.00_	-	340	310	200	210	295
	25.7_	-	330	410	310	370	580
	30.00_	270	200	180	130	150	190
	35.3_	-	320	400	360	500	720
	38.45_	350	400	525	285	280	320
	43.50_	-	270	390	350	450	620
	44.70_	320	340	450	270	250	320
	52.70_	-	125	175	160	210	265
	57.70_	-	165	240	270	330	470

From Figure 4.23, it clearly shows that the interaction between  $\text{Al}_2\text{O}_3$  with PMMA, EC/PC and  $\text{LiClO}_4$ . When 4 wt% of alumina filler was integrated into the polymer electrolyte, and the intensity of broad peak of PMMA is decreased. This shows that the filler is eventually interacted with polymeric

matrix whereby the formations of new peaks appeared in the diffraction pattern when  $\text{Al}_2\text{O}_3$  filler is dispersed. The change in the diffraction pattern infer that the nature of  $\text{Al}_2\text{O}_3$  filler. From the observation, the intensity of the intense peak of characteristic  $\text{Al}_2\text{O}_3$  filler decreases with increasing concentration of  $\text{Al}_2\text{O}_3$ . Moreover, with the dispersion of 12 wt % alumina filler, the broad peak is broadened and intensity is decreased. As a result, the broadened peak decreased in the intensity of the peaks which reveal the decreasing in crystallinity (Saikia et al., 2008). Higher amorphous degree of polymer matrix attributes to more disorder arrangement of polymeric chain and increases the flexibility of polymer matrix. The formation of three-dimensional networks for ionic transportation, the mobility of ions is enhanced hence the ionic conductivity is increased (Ahmad et al., 2006). As a result, the ionic conductivity with 12 wt %  $\text{Al}_2\text{O}_3$  dispersion exhibits the highest conductivity value.

However, a further increase in the concentration of the  $\text{Al}_2\text{O}_3$  filler into the PMMA-EC/PC- $\text{LiClO}_4$  complex causes the interaction within the  $\text{Al}_2\text{O}_3$  filler to be stronger. As shown in the Figure 4.23 (g) and (h), the intense peak of  $\text{Al}_2\text{O}_3$  filler is increased toward an increment of concentration of alumina filler. From the EIS characterisation, the ionic conductivity is dropped beyond 12 wt% of  $\text{Al}_2\text{O}_3$  filler dispersed into polymer matrix. This may be due to the strong interaction in between the  $\text{Al}_2\text{O}_3$  filler to produce the ion pairs, aggregates and ion clusters causing the blocking effect in the polymer electrolyte. As the three-dimensional networks is created at a low concentration

of  $\text{Al}_2\text{O}_3$  filler, a higher concentration of  $\text{Al}_2\text{O}_3$  might cause the conduction path to be more viscous and decrease in ionic mobility. In fact, the crystallinity of this composite solid polymer electrolyte system is increased with the dispersion of  $\text{Al}_2\text{O}_3$  beyond the saturation level (12 wt% of  $\text{Al}_2\text{O}_3$  filler). As the ionic conduction is generally conducted in an amorphous region, the decrease in amorphous region in polymeric matrix revealed the decrease in the ionic conductivity.

#### **4.2.4 PMMA-EC/PC-LiClO<sub>4</sub>-SiO<sub>2</sub>Samples XRD result**

Figure 4.24 (b) depicts the diffraction pattern and crystalline nature of pure fumed silica filler ( $\text{SiO}_2$ ). The dispersion of this type of ceramic fillers into the polymer matrix does have some interactions with the polymer chain and polymer backbone. It is clearly indicated in Figure 4.24 and Table 4.4 the overall changes in the diffraction pattern and intensity for PMMA-EC/PC-LiClO<sub>4</sub>-SiO<sub>2</sub> system.

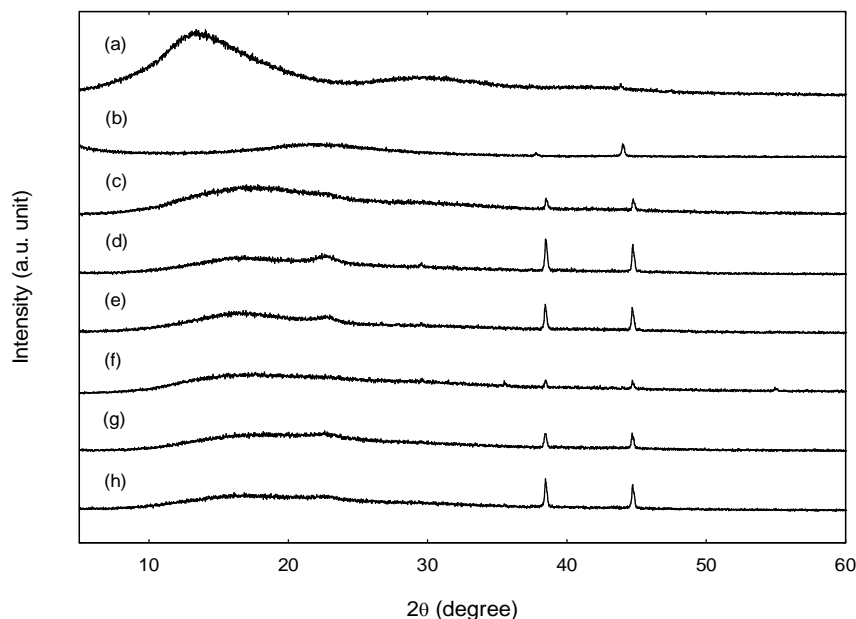


**Figure 4.24:** XRD patterns of (a) pure PMMA, (b) pure SiO<sub>2</sub>, (c) 0 wt% SiO<sub>2</sub>, (d) 4 wt% SiO<sub>2</sub>, (e) 8 wt% SiO<sub>2</sub>, (f) 12 wt% SiO<sub>2</sub>, (g) 16 wt% SiO<sub>2</sub>, (h) 20 wt% SiO<sub>2</sub> dispersed into PMMA-EC/PC-LiClO<sub>4</sub> system

**Table 4.5:** Intensity obtained at diffraction peaks for (1-x)PMMA-EC/PC-LiClO<sub>4</sub>- (x)SiO<sub>2</sub> system

		x					
		0 wt%	4 wt%	8 wt%	12 wt%	16 wt%	20 wt%
Intensity at diffraction peaks	16.30_	510	310	370	310	320	310
	23.00_	-	350	330	-	350	290
	30.00_	270	180	200	170	160	170
	38.45_	350	640	530	250	345	580
	44.70_	320	550	480	250	360	480

Apparently, the shoulder peak has disappeared and caused the broad peak of polymer to become wider or broader in the peak area upon addition of the SiO<sub>2</sub> filler. The intensities of the sharp peak are brought to a lower level. This is an indication of reduction in the degree of crystallinity. The formation of three-dimensional network among aggregates contributes to the distortion of the arrangement (amorphous) of polymer matrix. In general, the polymer

segmental motion and flexibility of polymer backbone is improved due to the enhancement in the amorphous phase. From these effects, the ion diffusivity eventually improved with a higher ionic conductivity. From the figure, no new peak appears in all diffraction patterns. This inferred that the SiO<sub>2</sub> filler may be a better ceramic filler candidate compared to Al<sub>2</sub>O<sub>3</sub> filler. This result is well metered with EIS studies where the ionic conductivity for the sample dispersed with SiO<sub>2</sub> filler is slightly higher than the sample added Al<sub>2</sub>O<sub>3</sub> filler.

As a higher concentration of SiO<sub>2</sub> filler is being dispersed into the polymer electrolyte, the shoulder peak re-appears and the intensities for sharp peaks are increased due to the reduction of amorphous region and formation of SiO<sub>2</sub> clusters (Pandey et al., 2008). Consequently, the reduction in the amorphous region might cause the conduction path to become more viscous and block the motion in polymeric matrices. Therefore the ionic conductivity is dropped.

#### **4.2.5 Summary of XRD characterisation**

The overall variation of the diffraction pattern of highest polymer electrolyte sample in particular electrolyte system is illustrated in Figure 4.25. The diffraction pattern of pure PMMA is disturbed by the addition of 30 wt% of EC/PC mixture. The reduction of intensity in the broad peak and a slight

shift of the PMMA peak as well as the existence of new shoulder and sharp peak. This is the evidence to show that the EC/PC plasticiser is interacted with PMMA backbone.

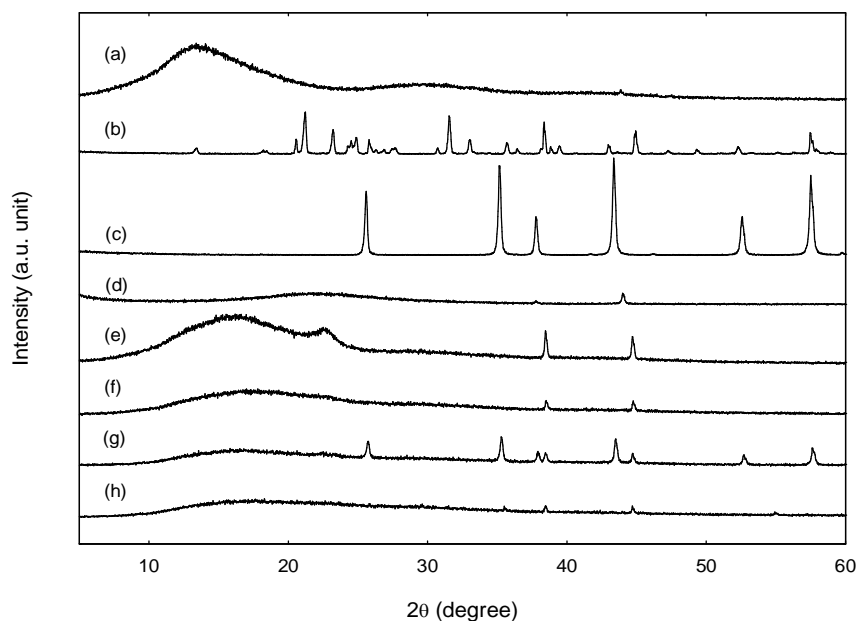


**Figure 4.25: XRD patterns of (a) pure PMMA, (b) pure LiClO<sub>4</sub>, (c) pure Al<sub>2</sub>O<sub>3</sub>, (d) pure SiO<sub>2</sub>, (e) PMMA (70):EC/PC (30), (f) PMMA-EC/PC (75): LiClO<sub>4</sub> (25), (g) PMMA-EC/PC-LiClO<sub>4</sub> (88): Al<sub>2</sub>O<sub>3</sub> (12), (h) PMMA-EC/PC- LiClO<sub>4</sub> (88): SiO<sub>2</sub> (12)**

With the addition of 25 wt% of LiClO<sub>4</sub> salt into PMMA-EC/PC system, significant changes of diffraction pattern are observed as shown in Figure 4.25 (f). The broad characteristic peak of PMMA is broadened upon the addition of LiClO<sub>4</sub>. Besides that, the intensities of sharp peaks are reduced. This effect is inferred to the solubility (high dielectric constant) of EC/PC mixture which is dissolved and interacts with LiClO<sub>4</sub>. The reduction in the intensities gives the evidence that the crystallinity of polymer matrix is further decreased hence

leads to a higher ionic conductivity (Ganesan et al., 2008). Higher degree of amorphous region in polymer matrix might contribute to more disorder arrangement of polymeric chain and increases the flexibility of polymer matrix. Therefore more solvated ions can travel along these paths and increase the mobility. As a result, the higher conductivity is achieved due to a higher mobility of ion transportation in the amorphous region.

Further dispersing of the ceramic filler eventually brings some effects to the polymer electrolytes such as improving the mechanical properties as well as enhancing the ionic conductivity. In Figure 4.25 (g) and (h), both ceramic fillers clearly altered the diffraction pattern, the broad peak is further reduced and the shoulder peak is vanished to broaden the broad characteristic peak of PMMA. The intensities of the sharp peaks in the diffraction pattern are reduced. This may be evidence to conclude that there are some structures which are undergoing changes in the polymeric matrix, such as the formation of three dimension network for ionic transportation (Ahmad et al., 2006). By comparing the diffraction pattern of both ceramic filler, it can be seen that the crystalline nature of the system with SiO<sub>2</sub> filler is lower than Al<sub>2</sub>O<sub>3</sub> filler system. This infers that the new peak exhibit in the Al<sub>2</sub>O<sub>3</sub> filler system has a slight distinction in the crystallinity (amorphous). It may be caused by the deficiency interaction between this ceramic filler with other electrolyte materials. This shows that the interaction between PMMA-EC/PC-LiClO<sub>4</sub> with SiO<sub>2</sub> filler is better when the amorphous region is enhanced and no significant

new peak is observed. Therefore, the ionic conductivity for PMMA-EC/PC-LiClO<sub>4</sub>-SiO<sub>2</sub> system is higher than the PMMA-EC/PC-LiClO<sub>4</sub>-Al<sub>2</sub>O<sub>3</sub> system.

### 4.3 Fourier Transform Infrared (FTIR) Studies

The FTIR spectroscopy is used to analyse the structure of polymer and the interaction between electrolyte materials and host polymer. These interactions can induce changes in the vibration modes of the molecules in the polymer electrolyte. The FTIR spectrum pattern may show noticeable changes in vibrational modes which are observed in term of shifting the band position, band width, and intensity. In the present samples, the FTIR spectrum is studied at the range of 400-4000 cm<sup>-1</sup>.

#### 4.3.1 FTIR for PMMA-EC/PC samples

The FTIR spectrum of pure PMMA is shown in Figure 4.26 and the assignments of vibration modes and wavenumber are indicated in Table 4.6. The wavenumber at 750, 1191, 1240 and 1433 cm<sup>-1</sup> are assigned to CH<sub>2</sub> rocking, CH<sub>2</sub> twisting, CH<sub>3</sub> Symmetric bending and CH<sub>3</sub> asymmetric bending for PMMA. The vibrational peaks at 1071, 1150, 1722 and 2951 cm<sup>-1</sup> are

assigned to O-CH<sub>2</sub> stretching, C-O-C asymmetric stretching, C=O symmetric stretch and CH<sub>3</sub> asymmetric stretching of PMMA.

In order to investigate the interaction of molecules between plasticiser and host polymer, the pure plasticiser such as EC and PC is priority investigated from FTIR. The vibration peaks for pure EC is illustrated in Figure 4.27 and the vibrational mode and wavenumber is depicted in Table 4.7. The structure CH<sub>2</sub> in EC is undergoing wagging and bending at a frequency of 1392 and 1477 cm<sup>-1</sup>, respectively. The frequency of 1780 are assigned to C=O stretching in EC. From figure 4.27, the Ring breathing and skeletal stretching for EC is observed at 891, 967 and 1074 cm<sup>-1</sup>.

The spectrum of pure PC is illustrated in Figure 4.28 and the assigning of vibrational mode and wavenumber is indicated in Table 4.8. The vibration modes such as ring deformation, CH<sub>2</sub> rocking, CH<sub>2</sub> wagging and C=O stretching are found in the frequency at 711 and 776, 954 and 1222, 848, and 1790, respectively. The observed peaks for pure PMMA, EC and PC were comparable with the wavenumber found by other researchers as shown in Table 4.6 ó 4.8.

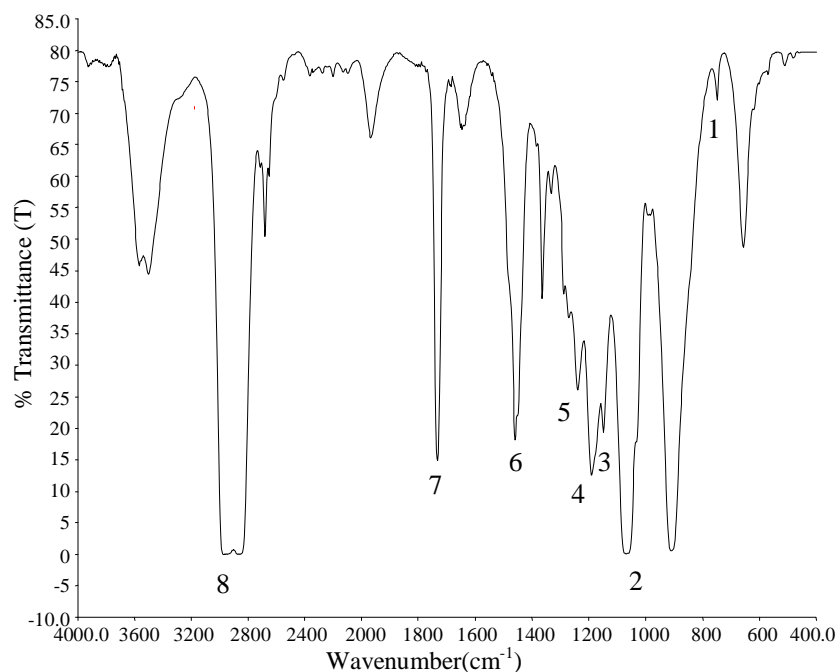


**Figure 4.26: FTIR spectrum for pure PMMA**

**Table 4.6: Vibration modes and wavenumber of pure PMMA**

No.	Vibration mode	Wavenumber (cm <sup>-1</sup> )	Reference	Wavenumber obtained (cm <sup>-1</sup> )
1	CH <sub>2</sub> rocking	750	Rajendran and Mahendran, 2001	751
2	O-CH <sub>2</sub> stretching	1070	Mahendran et al., 2005 ; Mahendran and Rajendran, 2003	1071
3	C-O-C asymmetric stretching	1151	Deka and Kumar,2010	1150
4	O-CH <sub>3</sub> stretching	1191	Ramesh et al., 2007	1191
5	C-O stretching	1235	RajendranMahendran and Kannan (2002)	1238
6	CH <sub>3</sub> asymmetric bending	1452	Tan et al., 2007	1433
7	C=O stretching	1725	Deka and Kumar,2010	1722
8	CH <sub>3</sub> asymmetric stretching	2954	Rajendran et al., 2003	2951

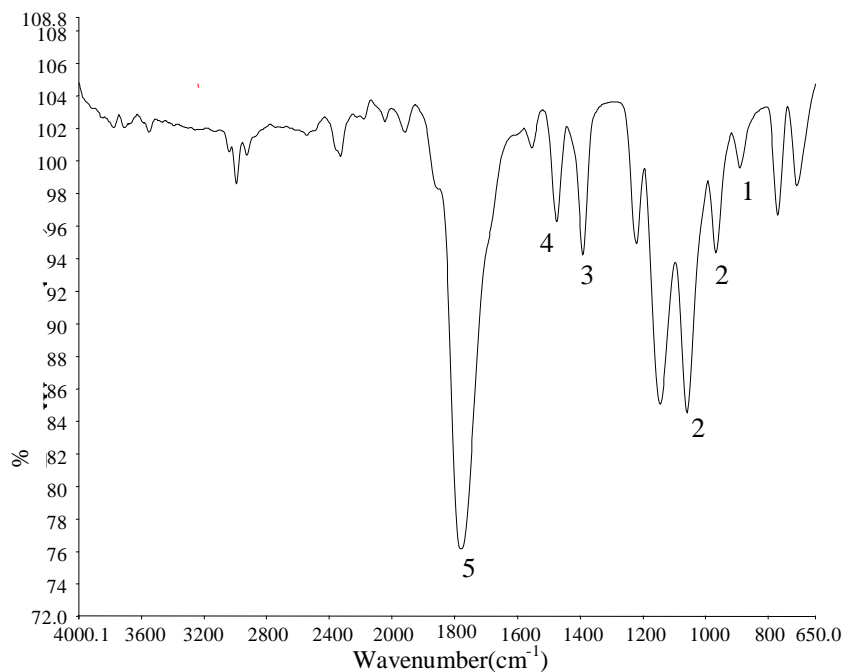


**Figure 4.27: FTIR spectrum for pure EC**

**Table 4.7: Vibration modes and wavenumber of pure EC**

No.	Vibration mode	Wavenumber (cm <sup>-1</sup> )	Reference	Wavenumber obtained (cm <sup>-1</sup> )
1	Ring breathing	890	Wang et al., 1996	891
2	Skeletal Stretching	970, 1076	Angell, 1956	967, 1074
3	CH <sub>2</sub> wagging	1394	Wang et al., 1996	1392
4	CH <sub>2</sub> bending	1480	Angell, 1956	1477
5	C=O stretching	1778	Fini and Mirone, 1973	1780

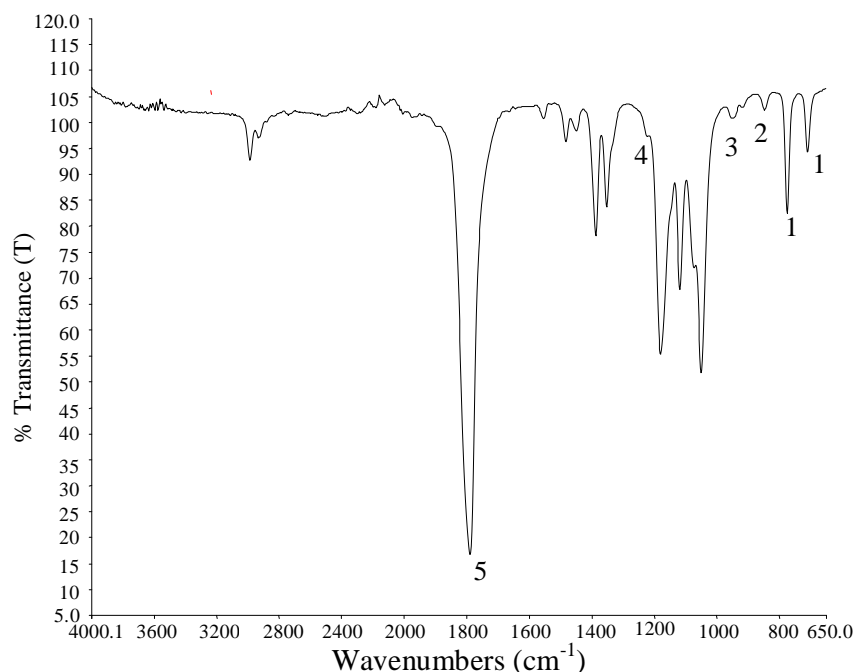


**Figure 4.28: FTIR spectrum for pure PC**

**Table 4.8: Vibration modes and wavenumber of pure PC**

No.	Vibration mode	Wavenumber (cm <sup>-1</sup> )	Reference	Wavenumber obtained (cm <sup>-1</sup> )
1	Ring deformation	712, 777	Stephan et al., 1999	711, 776
2	CH <sub>2</sub> wagging	840	Rajendran and Sivakumar, 2008	848
3	CH <sub>2</sub> rocking	956	Stephan et al., 2000	954
4	CH <sub>2</sub> rocking	1224	Rajendran and Sivakumar, 2008	1222
5	C=O stretching	1789	Rajendran and Prabhu, 2010	1790

Figure 4.29 illustrates the FTIR spectrum of a pure PMMA added with EC/PC up to 35 wt%. The overall changes in the complexation of PMMA-EC/PC are clearly indicated. From the spectrum, it can be seen that the intensity of absorption peaks in transmittance mode varies according to the

weight percentage of EC/PC mixture added into the pure PMMA host polymer. Besides, some disappearance of absorption peak can also be observed.

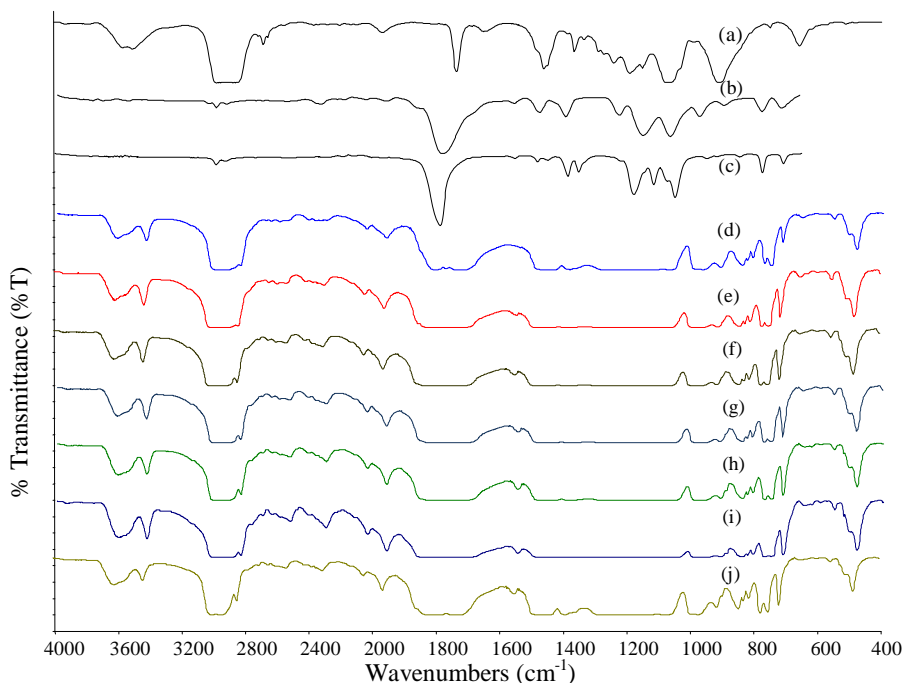


**Figure 4.29: FTIR spectrum for a) pure PMMA, b) pure EC, c) pure PC, d) 5wt%, e) 10 wt%, f) 15 wt%, g) 20wt%, h) 25 wt%, i) 30 wt%, j) 35 wt%, of EC/PC added into PMMA**

From the observation, there are some disappearances of absorption peaks located at 1150, 1191, 1238, and 1433  $\text{cm}^{-1}$  which were assigned to C-O-C asymmetric stretching, O-CH<sub>3</sub> stretching, C-O stretching and asymmetric bending, respectively with 30 wt% of EC/PC mixture in PMMA. The disappearance of absorption peaks which can be observed from Figure 4.30 indicates the formation of complexation between PMMA and EC/PC mixture. The PMMA sample added with 30 wt% of EC/PC, O-CH<sub>2</sub> stretching obtained

at the  $1071\text{ cm}^{-1}$  are shifted to  $1086\text{ cm}^{-1}$ . Figure 4.31 depicts the shift of the  $\text{CH}_2$  rocking from  $751$  to  $745\text{ cm}^{-1}$  as 30 wt% of EC/PC was added into PMMA. As observed in Figure 4.32, the absorption peak at  $1722\text{ cm}^{-1}$  is broaden and shifted to  $1805\text{ cm}^{-1}$  which is referred to the addition of 30 wt% of plasticiser. This shift can be observed in the reliable carbonyl ( $\text{C}=\text{O}$ ) stretching frequency of the complexes as compared to pure PMMA which indicates the formation of complex (Mahendran et al., 2005).

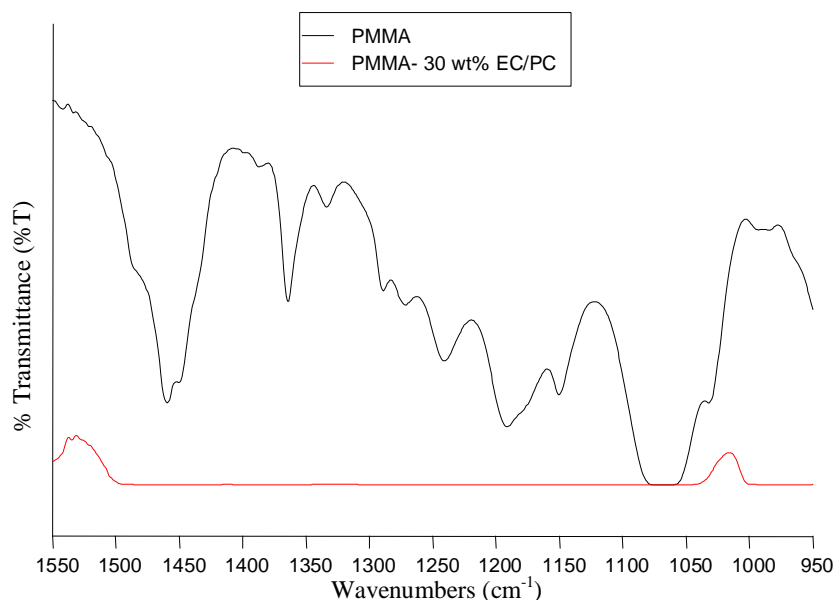


**Figure 4.30: FTIR spectrum for pure PMMA and PMMA- 30wt% EC/PC in the range of  $1000\text{-}1550\text{cm}^{-1}$**

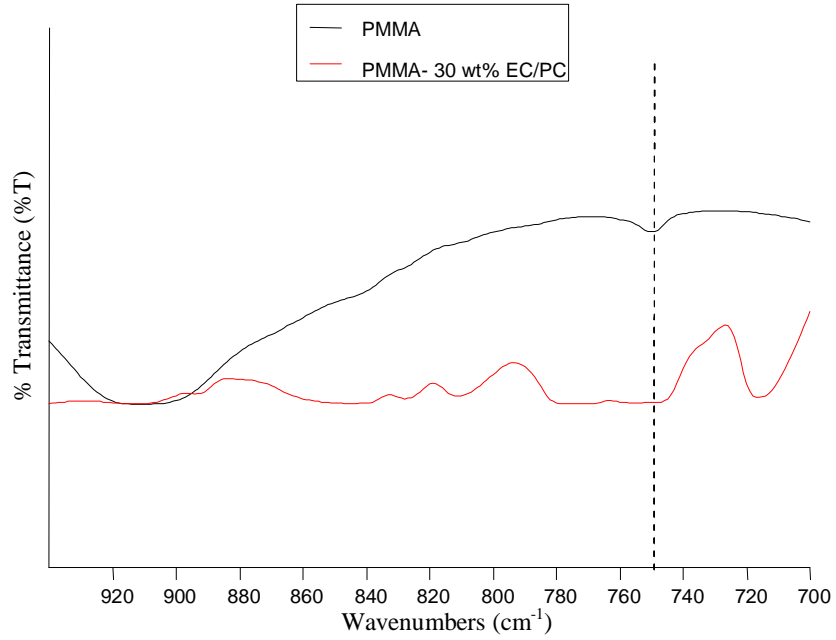


**Figure 4.31: FTIR spectrum for pure PMMA and PMMA- 30wt% EC/PC in the range of 700-930  $\text{cm}^{-1}$**

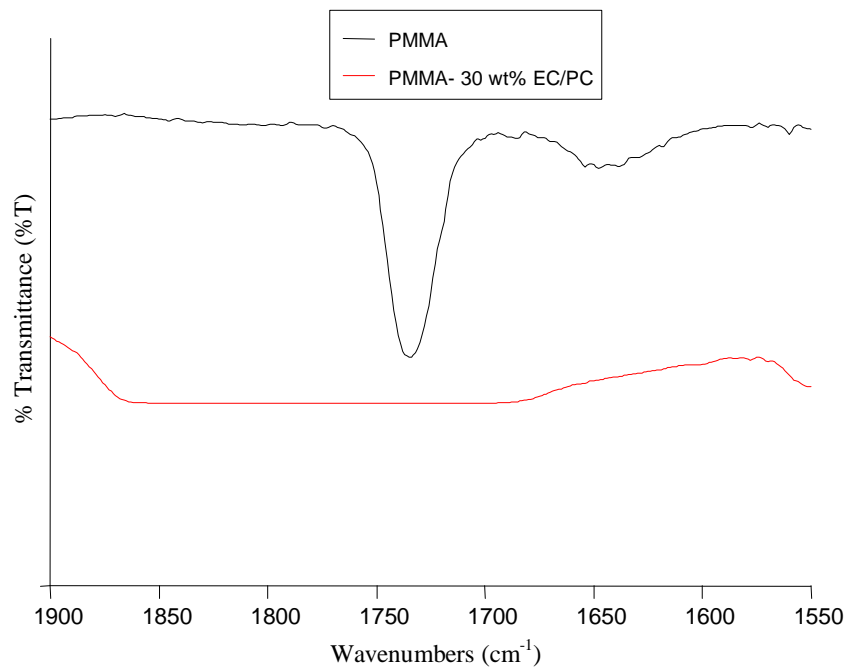


**Figure 4.32: FTIR spectrum for pure PMMA and PMMA- 30wt% EC/PC in the range of 1550-1900  $\text{cm}^{-1}$**

As noticed in Figure 4.29, the intensity of the absorption peak is reduced when in transmittance mode. This may infer that a favourable interaction has happened between PMMA and EC/PC. From the investigation, some of this absorption peaks have re-appeared in the complexation where 35 wt% of EC/PC are added into PMMA. This inferred that the polymer is changed from solid types to gelled types. The overall intensity of FTIR spectrum in the range of 400-1100 $\text{cm}^{-1}$  is decreased when the concentration of EC/PC mixture is increased up to 30 wt%. But the intensity of the peaks in 400-1100  $\text{cm}^{-1}$  is increased again when 35 wt% of EC/PC is added into the host polymer. This may be evidence to show that the characteristic of solid polymer becomes gelled. Based on the changes in shift, changes in intensity and disappearance of the characteristic peaks, it can be concluded that there is a complexation between PMMA and the EC/PC mixture in PMMA-EC/PC system. The appearance of the new peak and changes of intensity concluded that an addition of 35 wt% EC/PC into the host polymer can alter the characteristic of solid polymer and behave like a gelled polymer. The information obtained is similar and comparable with the results of XRD.

#### **4.3.2 FTIR for PMMA-EC/PC-LiClO<sub>4</sub> samples**

Figure 4.33 shows the FTIR spectrum of the pure LiClO<sub>4</sub> salt and Table 4.9 depicts its assignments of important bands. The vibration modes such as

$\text{ClO}_4^-$  anti-symmetric stretching and Pure  $\text{LiClO}_4$  vibration mode are found at a vibration frequency of 1095 and 1635  $\text{cm}^{-1}$ .

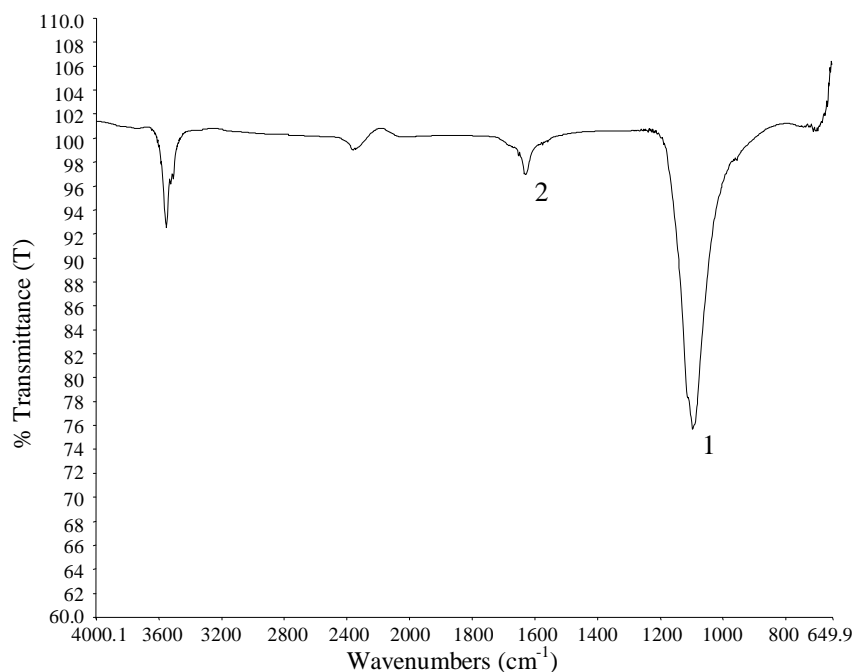


**Figure 4.33: FTIR spectrum for pure  $\text{LiClO}_4$**

**Table 4.9: Vibration modes and wavenumber of pure  $\text{LiClO}_4$**

No.	Vibration mode	Wavenumber ( $\text{cm}^{-1}$ )	Reference	Wavenumber obtained ( $\text{cm}^{-1}$ )
1	$\text{ClO}_4^-$ antisymmetric stretching	1092	Mahendran et al., 2005	1095
2	Pure $\text{LiClO}_4$ vibration mode	1630	Rajendran et al., 2002	1635

From Figure 4.34, it can be seen that the integration of  $\text{LiClO}_4$  lithium salt into PMMA-EC/PC system have changed all the FTIR spectrum pattern of sample deposited with  $\text{LiClO}_4$ . With the addition of 15 wt% of  $\text{LiClO}_4$ , there is

no significant absorption peak which can be observed between 400-600  $\text{cm}^{-1}$ . The absorption peaks between 3400-3700  $\text{cm}^{-1}$  have disappeared and are broaden. It can be inferred the formation of complexation between PMMA-EC/PC with  $\text{LiClO}_4$ . The vibration mode of the sample exhibits the highest conductivity value (25 wt%  $\text{LiClO}_4$ ) is shown in Figure 4.34 (h)

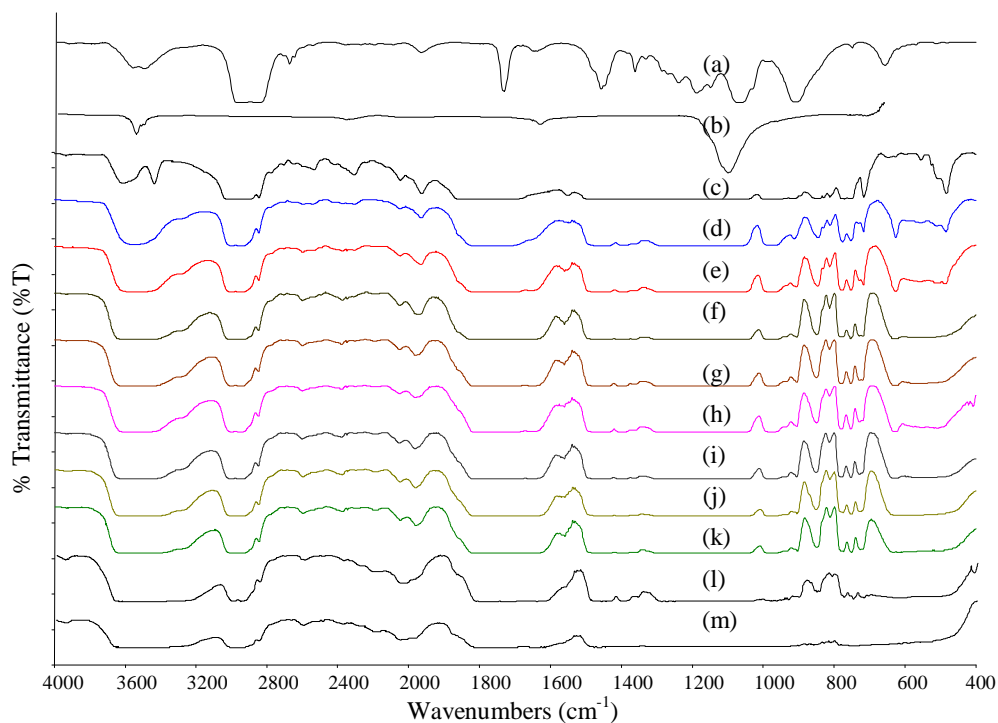


**Figure 4.34: FTIR spectrum for a) pure PMMA, b) pure  $\text{LiClO}_4$ , c) 0wt%, d) 5wt%, e) 10 wt%. f) 15 wt%. g) 20wt%,h) 25 wt%. i) 30 wt%. j) 35 wt%. k) 40wt%. l) 45wt%. m) 50 wt% of  $\text{LiClO}_4$  doped into PMMA-EC/PC system**

The stretching mode for  $\text{ClO}_4^-$  for pure  $\text{LiClO}_4$  vibration mode obtained at 628  $\text{cm}^{-1}$  is shifted to 629  $\text{cm}^{-1}$  (Deka and Kumar, 2010). The addition of lithium salt after the saturation level have caused the band to disappear. This provides evidence for the formation of ion pairs, ion aggregates and ion

clusters. The  $\text{ClO}_4^-$  anti-symmetric stretching observed at  $1095\text{ cm}^{-1}$  has disappeared due to the complete dissolution of lithium salt into the polymer electrolyte system. This may be caused by the interaction of  $\text{ClO}_4^-$  anion with polar group on PMMA backbone (O-CH<sub>2</sub> molecules at  $1070\text{ cm}^{-1}$ ). A new absorption peak at the vibration frequency of  $1386\text{ cm}^{-1}$  might refer to the interaction between lithium salt with EC and PC whereas, the polar group in PC providing additional free volume and transit site for  $\text{Li}^+$  ion. Besides, the frequency of  $2988\text{ cm}^{-1}$  might refer to the interaction of PMMA backbone. As seen in Figure 4.35, the formation of doublet peak is observed at  $751$  and  $778\text{ cm}^{-1}$ . These frequencies might refer to the ring deformation for EC/PC mixture where the ionic association is stronger through the redistribution of charge accompanying the formation of ionic pairs and aggregations (Stephan et al., 1999).

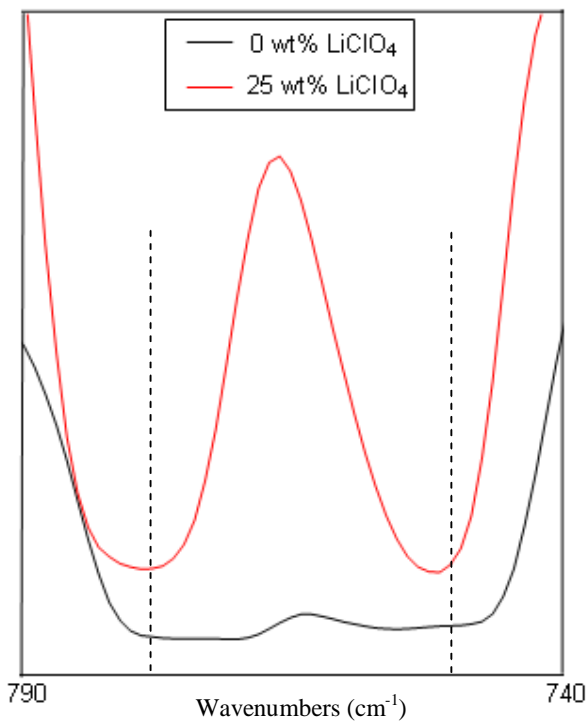


**Figure 4.35: Formation of doublet peak for PMMA-EC/PC-25 wt% LiClO<sub>4</sub> in the range of 740-790 cm<sup>-1</sup>**

The appearance of spectrum at 844 cm<sup>-1</sup> is assigned to a combination of CH symmetrical stretching and C-O-C symmetrical stretching. It can be observed that this band has been shifted to a higher frequency side with respect to increasing the LiClO<sub>4</sub> salt concentration. The formation of a weak doublet peak can be observed at an absorption peak of 2951 cm<sup>-1</sup> which is depicted in Figure 4.36. The intensity of this doublet peak is lower compared to the sample without any addition of LiClO<sub>4</sub> salt. Due to the interaction of CH<sub>3</sub> molecules with LiClO<sub>4</sub> salt which leads to better lithium salt dissolution followed by better ionic conductivity. Moreover, the C=O symmetric stretching is found shifted to a lower frequency (1779 cm<sup>-1</sup> as 25wt% of LiClO<sub>4</sub> salt is added into the polymer electrolyte). This observation inferred the interaction between

lithium salt with PMMA and EC/PC, the  $\text{Li}^+$  may break the covalent bonding and attach to oxide ion ( $\text{O}^{2-}$ ). The overall intensity of the absorption peaks is decreased with respect to the increment of  $\text{LiClO}_4$  salt up to 25 wt%. Beyond this saturation point, the overall intensity of the absorption peaks is increased again after this saturation level. The increases in the intensity can be explained by the  $\text{ClO}_4^-$  ions favouring for re-association of ions or the formation of ion pair (Mahendran et al., 2005). This inferred that the ionic conductivity is increased before its saturation level and is dropped after its saturation level.

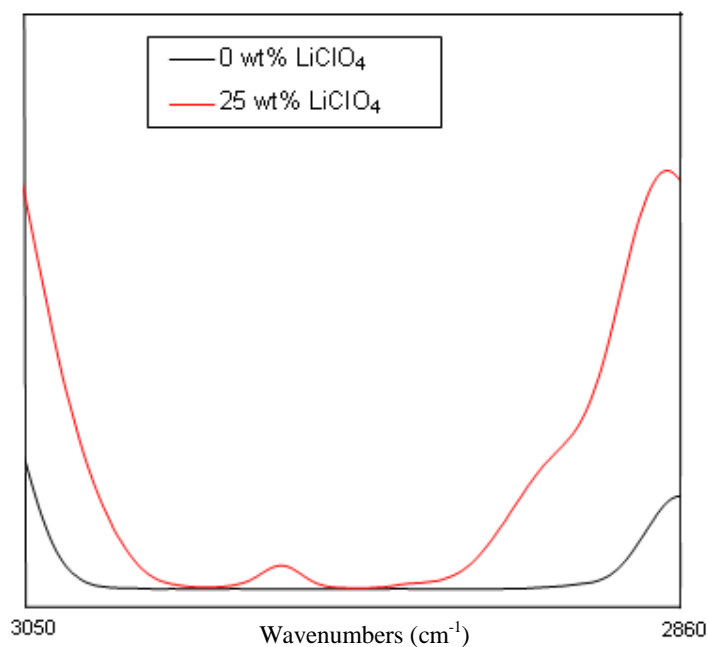


**Figure 4.36: PMMA-30 wt% EC/PC and PMMA-EC/PC-25 wt% LiClO<sub>4</sub> in the range of 2860-3050 cm<sup>-1</sup>**

According to Figure 4.34 (l) and (m), it shows that the unfavourable vibrational bands representing 45 wt% and 50 wt% of  $\text{LiClO}_4$  salt added into

PMMA-EC/PC complex. It revealed that further addition of LiClO<sub>4</sub> salt into the solid polymer electrolyte, the spectrum or main peaks (characteristic peaks) of PMMA has almost disappeared. It may be due to the insoluble LiClO<sub>4</sub> salt which forms a crystalline structure in the particular polymer electrolyte sample which is confirmed by XRD and SEM. The amorphous characteristic of plasticised PMMA is totally replaced by the crystalline structure of LiClO<sub>4</sub> salt. As the amorphous region in the electrolyte system is reduced, the ionic conductivity is dropped significantly. Besides that, another structure modification can be observed at 2951 cm<sup>-1</sup>. The doublet peak has disappeared as the excessive lithium salt is doped into the polymer electrolyte. This may be due to the insoluble lithium salt which produces the ion aggregates, ion pair and ion clouds along the polymeric backbone. Hence no significant characteristic peak for PMMA can be obtained.

All of these observations indicate that the interaction occurred between PMMA-EC/PC and LiClO<sub>4</sub> salt. With careful dopant of LiClO<sub>4</sub> into the PMMA-EC/PC system, optimised ionic conductivity behaviour can be obtained.

### 4.3.3 FTIR for PMMA-EC/PC-LiClO<sub>4</sub>-Al<sub>2</sub>O<sub>3</sub> samples

In the PMMA-EC/PC-LiClO<sub>4</sub> system doped with Al<sub>2</sub>O<sub>3</sub> filler, the FTIR spectrum for pure Al<sub>2</sub>O<sub>3</sub> is shown in Figure 4.37 as a reference sample and the information about the assignment of vibrational mode and wavenumber is depicted in Table 4.10. From these observation, it reveals that the H<sub>2</sub>O rocking vibration and O-H stretching is obtained at 1623 and 3490 cm<sup>-1</sup>, respectively. These observed peaks are similar to the wavenumber suggested by other researchers as shown in Table 4.10

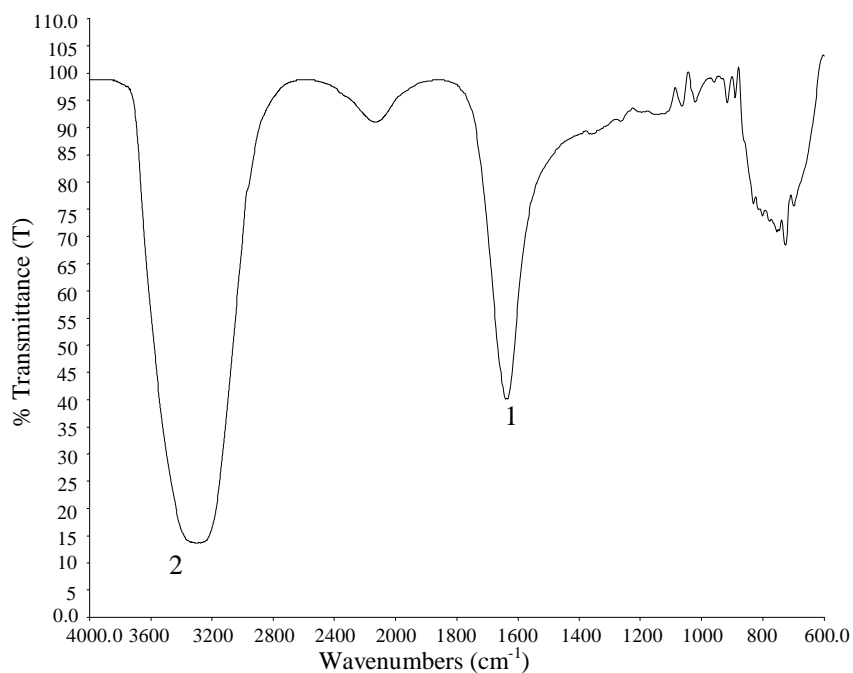


**Figure 4.37: FTIR spectrum for pure Al<sub>2</sub>O<sub>3</sub>**

**Table 4.10: Vibration modes and wavenumber of pure Al<sub>2</sub>O<sub>3</sub>**

No.	Vibration mode	Wavenumber (cm <sup>-1</sup> )	Reference	Wavenumber obtained (cm <sup>-1</sup> )
1	H <sub>2</sub> O rocking vibration	1600	Raveh et al., 1997	1623
2	O-H stretching	3500	Ozer et al., 1999	3490

Figure 4.28 shows the variation of spectrums of Al<sub>2</sub>O<sub>3</sub> added into PMMA-EC/PC-LiClO<sub>4</sub> system. The Addition of Al<sub>2</sub>O<sub>3</sub> eventually alter the FTIR spectrum which inferred the structure changes and forming the complexation in the polymeric matrix. In Figure 4.39, it can be seen that the characteristic peaks in vibration band of 550-900 cm<sup>-1</sup> have disappeared and the band is broader when 25 wt% of Al<sub>2</sub>O<sub>3</sub> concentration is dispersed into composite solid polymer electrolyte (CSPE). This is the evidence to show the formation of complexation between Al<sub>2</sub>O<sub>3</sub> filler with PMMA-EC/PC-LiClO<sub>4</sub>. As discussed in EIS and XRD, dispersing Al<sub>2</sub>O<sub>3</sub> filler significantly increases the ionic conductivity and enhances the amorphous region which is attributed to the formation of three dimension network within the polymer complexes.

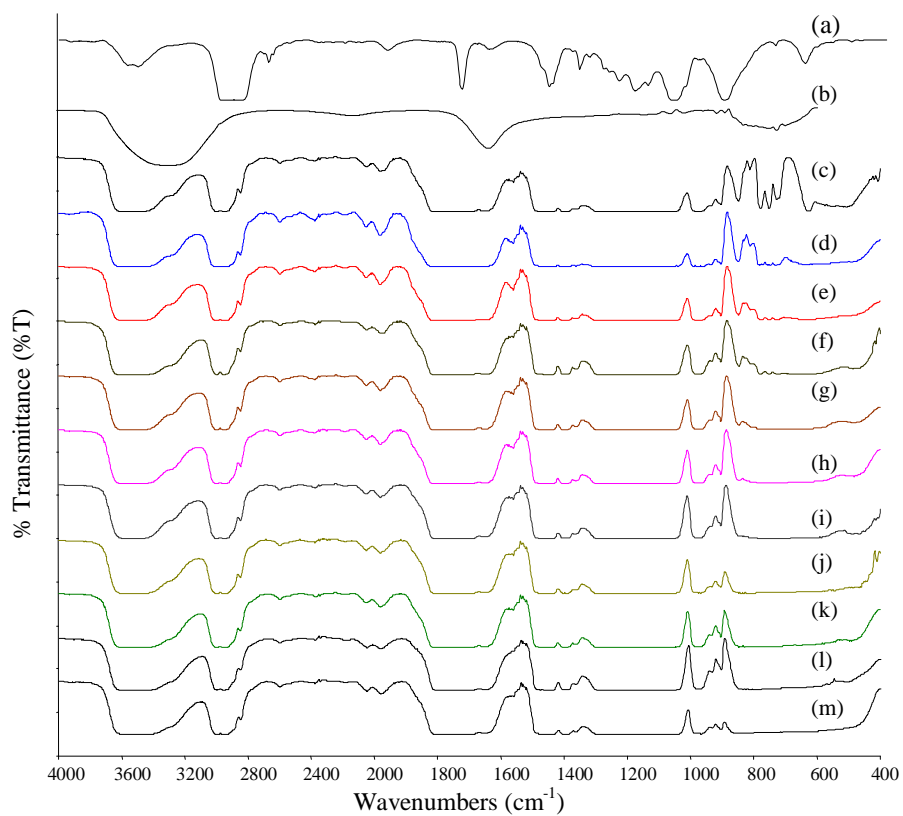


**Figure 4.38:** FTIR spectrum for a) pure PMMA, b) pure Al<sub>2</sub>O<sub>3</sub>, c) 0wt%, d) 2wt%, e) 4 wt%, f) 6 wt%, g) 8wt%, h) 10 wt%, i) 12 wt%, j) 14 wt%, k) 16wt%, l) 18wt%, m) 20 wt%, of Al<sub>2</sub>O<sub>3</sub> dispersed into PMMA-EC/PC-LiClO<sub>4</sub> system

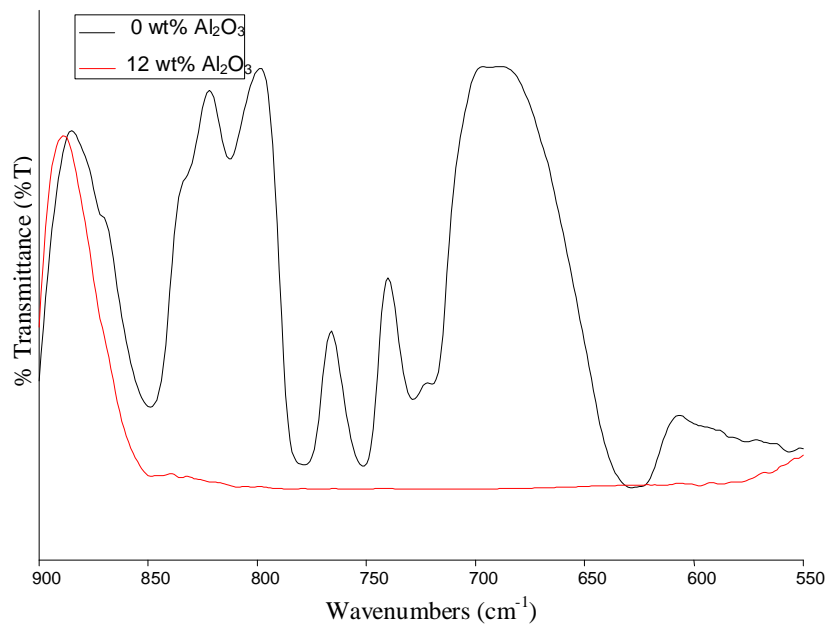


**Figure 4.39: PMMA-EC/PC-LiClO<sub>4</sub> with 12 wt% and without Al<sub>2</sub>O<sub>3</sub> in the range of 550-900cm<sup>-1</sup>**

Besides that, the CH<sub>3</sub> bending, C=O symmetric stretching and CH<sub>3</sub> asymmetric stretching of PMMA have all been shifted to 1460, 1727 and 2953 cm<sup>-1</sup>, respectively. From the investigation of these spectrums, there are no significant changes along the vibration frequency at 1800 to 2800 cm<sup>-1</sup>, only a slight shift of some characteristic peak and slight change of intensity is observed. For the vibration mode in pure Al<sub>2</sub>O<sub>3</sub>, the vibration mode of H<sub>2</sub>O rocking has disappeared and the O-H stretching is shifted to 3548 cm<sup>-1</sup>. The shift of the O-H stretching revealed the information about the interaction between alumina filler and lithium salt (LiClO<sub>4</sub>). The appearance of O-H stretching vibration indicates the presence of the oxygen-hydrogen (O-H) group at the surface of Al<sub>2</sub>O<sub>3</sub> surface (Song et al., 2006). Therefore, it is suggested that the Lewis acid-base type OH surface groups on alumina grains interact with the ions of the lithium salt.

#### 4.3.4 FTIR for PMMA-EC/PC-LiClO<sub>4</sub>-SiO<sub>2</sub> samples

The FTIR spectrum for pure SiO<sub>2</sub> filler is plotted in Figure 4.40 and the detail of assignation of vibration mode and wavenumber is depicted in Table 4.11. The O-H bending modes of hydrogen-bonded and isolated silanolic groups are identified at wavenumber of 808 and 975 cm<sup>-1</sup>. The vibration frequency at 1108, 1638, 3428 cm<sup>-1</sup> is assigned to Si-O stretching, O-H deformation vibration of surface hydroxyl group of fumed silica and O-H stretching mode of surface hydroxyl group of fumed silica, respectively. The O-H deformation vibration of surface hydroxyl group indicates the existence of OH surface groups for the Lewis acid-base interaction.

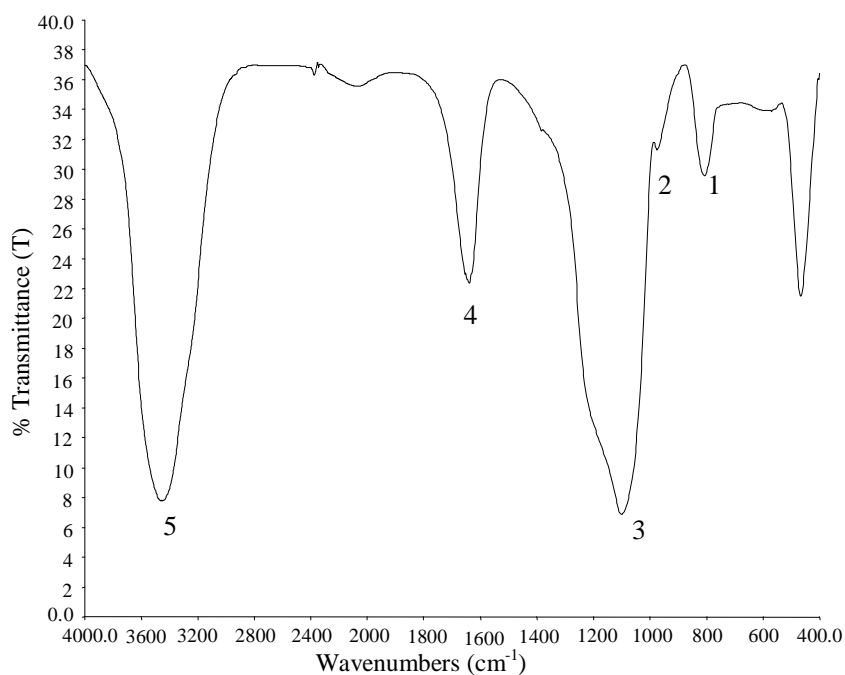


**Figure 4.40: FTIR spectrum for pure SiO<sub>2</sub>**

**Table 4.11: Vibration modes and wavenumber of pure SiO<sub>2</sub>**

No.	Vibration mode	Wavenumber (cm <sup>-1</sup> )	Reference	Wavenumber obtained (cm <sup>-1</sup> )
1	O-H bending mode of hydrogen bonded silanolic group	813	Arico et al., 2003	808
2	O-H bending mode of hydrogen isolated silanolic group	972	Arico et al., 2003	975
3	Si-O stretching	1104	Arico et al., 2003	1108
4	O-H deformation vibration of surface hydroxyl group of fumed silica	1639	Sharma and Sekhon 2007	1638
5	O-H stretching mode of surface hydroxyl group of fumed silica	3423	Ramesh and Wen, 2010	3428

From the Figure 4.41, the overall intensity of absorption peaks decreases with respect to the increment of SiO<sub>2</sub> filler which is dispersed into the polymer electrolyte complexes. This phenomenon occurred at the vibration frequencies range in between 1300-1450 cm<sup>-1</sup>. In the spectrum with 12 wt% of SiO<sub>2</sub> filler was dispersed into PMMA-EC/PC-LiClO<sub>4</sub> system, The shifting of CH<sub>2</sub> rocking, C-O-C bending, CH<sub>3</sub> bending and CH<sub>3</sub> asymmetric stretching of PMMA is observed at 750, 849, 1452 and 2952 cm<sup>-1</sup>, respectively. Moreover, the Shifting of CH<sub>2</sub> rocking is depicted in Figure 4.42. This shifted the peak to reveal the presence of the interaction and coordination of CH<sub>2</sub> bond with SiO<sub>2</sub>.

It can be observed that, after dispersion of SiO<sub>2</sub> filler into the polymer electrolyte, the absorption peaks for O-H bending mode of hydrogen bonded and isolated the silanolic group, and O-H stretching mode of surface hydroxyl group of fumed silica are shifted to 811, 978 and 3477 cm<sup>-1</sup>, respectively. These might attribute to the polar surface group of filler grain which helps to dissolve and interact with lithium salt. For the vibration frequency shifting to 1095 cm<sup>-1</sup> as observed in spectrum of 12 wt% of SiO<sub>2</sub> filler (spectrum i) and dispersed into PMMA-EC/PC-LiClO<sub>4</sub> system, this inferred to the interaction of Si-O molecules with LiClO<sub>4</sub>, whereby producing more favourable of lithium salt dissolution in the polymer electrolyte. Figure 4.43 depicts the change in shape of vibrational peak from a single peak to doublet peaks, it is confirmed that the Lewis acid-based interaction where the surface groups of SiO<sub>2</sub> filler are likely to compete with the ClO<sub>4</sub><sup>-</sup> for the formation of complexes with the polymer chains.

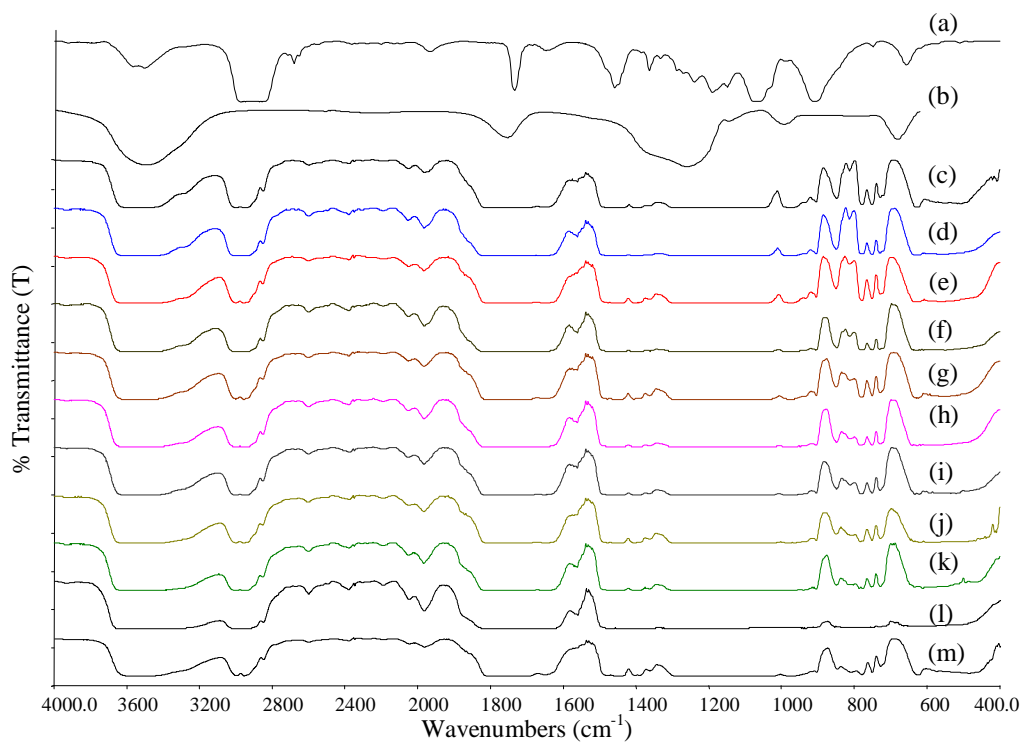


**Figure 4.41: FTIR spectrum for a) Pure PMMA, b) SiO<sub>2</sub>, c) 0wt%, d) 2wt%, e) 4 wt%, f) 6 wt%, g) 8wt%, h) 10 wt%, i) 12 wt%, j) 14 wt%, k) 16wt%, l) 18wt%, m) 20 wt%, of SiO<sub>2</sub> dispersed into PMMA-EC/PC-LiClO<sub>4</sub> system**

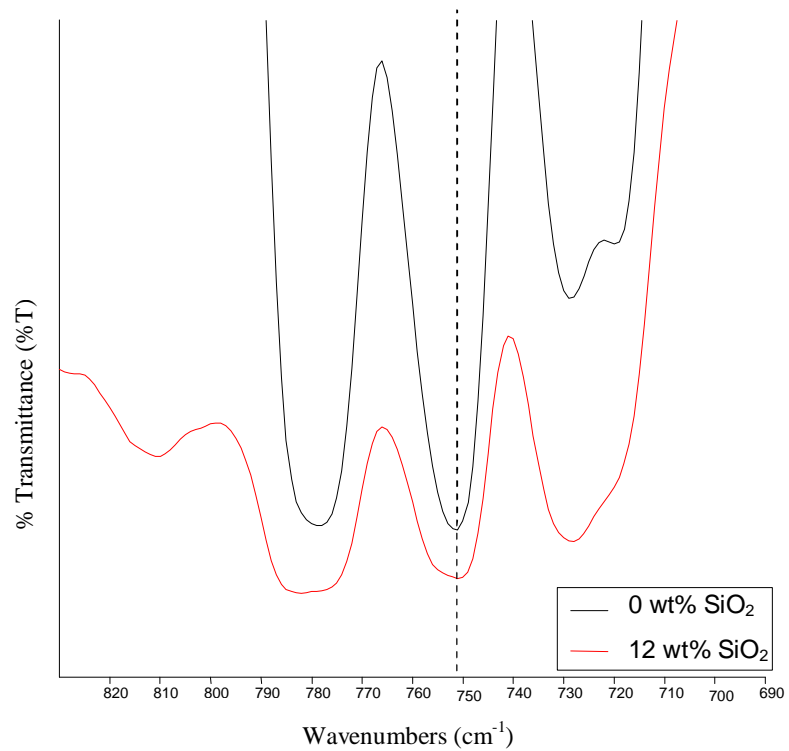


**Figure 4.42: Comparison of shifting in vibration peak of CH<sub>2</sub> rocking mode of PMMA in without SiO<sub>2</sub> and 12 wt% of SiO<sub>2</sub>**

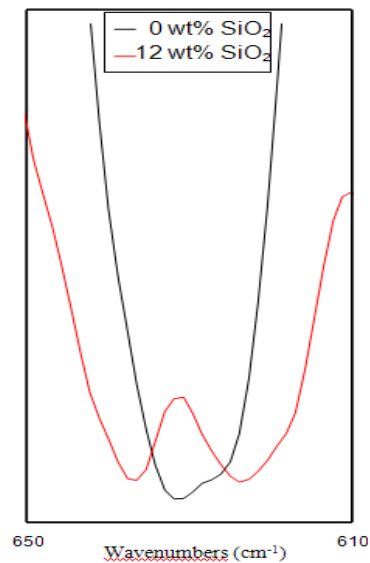


**Figure 4.43: Comparison of change in shape of vibrational peak in the range of 610-650cm<sup>-1</sup>**

Eventually, there are not much changes on the FTIR spectrum pattern along the vibrational frequency as illustrated in figures. But the increase of intensity and some shifting of the absorption peaks may be the evidence to show the interaction of SiO<sub>2</sub> filler with the polymeric matrices. It is believed that the dispersion of SiO<sub>2</sub> filler might favourably enhance the properties and re-organise the structures of the composite solid polymer electrolyte. As explained in EIS, the Lewis acid-base O-H surface group is favourably dissolved and avoid the re-association of LiClO<sub>4</sub> at a certain amount of SiO<sub>2</sub> filler.

#### **4.3.5 Summary of FTIR Spectroscopy**

In this study, FTIR spectra of various compositions of PMMA-based polymer electrolytes were shown in Figure 4.44. Referring to Figure 4.44, CH<sub>2</sub> rocking at 750 cm<sup>-1</sup>, C-O-C bending at 844 cm<sup>-1</sup>, C-O-C asymmetric stretch at 1152 cm<sup>-1</sup>, C-O-C symmetric stretching at 1287 cm<sup>-1</sup>, CH<sub>3</sub> bending at 1456 cm<sup>-1</sup>, C=O symmetric stretch at 1724 cm<sup>-1</sup>, CH<sub>3</sub> asymmetric stretching at 2954 cm<sup>-1</sup> are observed for PMMA.

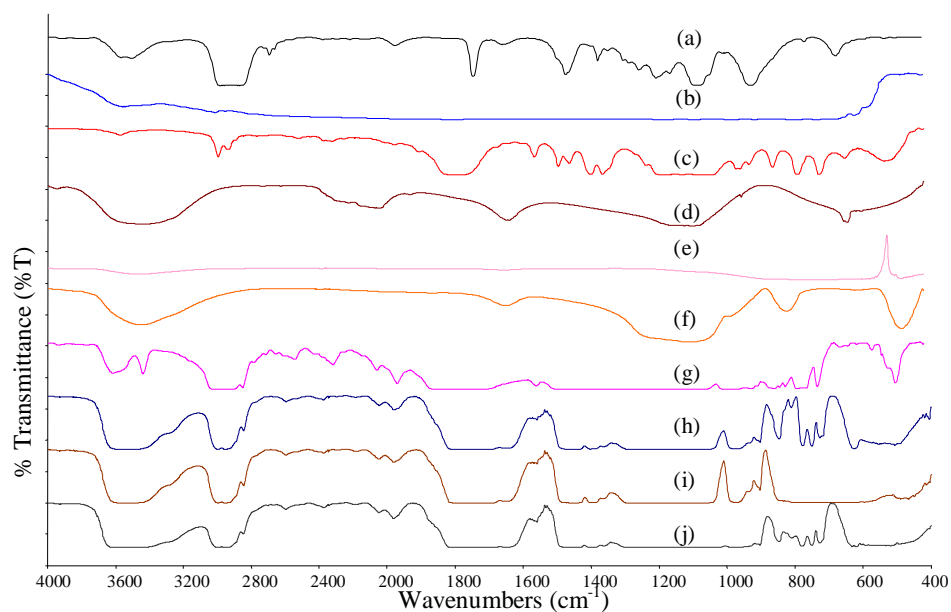


**Figure 4.44:** FTIR spectrum for a) pure PMMA, b) pure EC c) pure PC d) pure LiClO<sub>4</sub> e) pure Al<sub>2</sub>O<sub>3</sub> f) pure SiO<sub>2</sub> g) PMMA-30wt% EC/PC h) PMMA-EC/PC-25wt% LiClO<sub>4</sub> i) PMMA-EC/PC-LiClO<sub>4</sub>-12wt% Al<sub>2</sub>O<sub>3</sub>, j) PMMA-EC/PC-LiClO<sub>4</sub>-12wt% SiO<sub>2</sub>

C-O-C bending which appears at 844 cm<sup>-1</sup> is shifted to 843 cm<sup>-1</sup> caused by the additional of EC/PC mixture into the system. Due to the effect of the EC/PC mixture plasticiser, the absorption peak at 1070 cm<sup>-1</sup> of pure PMMA was shifted to 1086 cm<sup>-1</sup> is referred to the O-CH<sub>2</sub> stretching mode. The absorption peaks have disappeared at 1152 and 1287 cm<sup>-1</sup> which were assigned to C-O-C asymmetric stretching and C-O-C symmetric stretching of PMMA as 30 wt% of EC/PC mixture added into the host polymer.

While adding LiClO<sub>4</sub> salt into the system, the stretching mode for ClO<sub>4</sub><sup>-</sup> and pure LiClO<sub>4</sub> vibration mode obtained at 628 and 1637 cm<sup>-1</sup> are shifted to 629 and 1648 cm<sup>-1</sup>, respectively. The ClO<sub>4</sub><sup>-</sup> anti-symmetric stretching observed

at  $1089\text{ cm}^{-1}$  is shifted to  $1093\text{ cm}^{-1}$ . The formation of weak doublet peak can be observed through investigation at the absorption peak at  $2954\text{ cm}^{-1}$ . The intensity of the doublet peak obtained is lower than the sample without addition of  $\text{LiClO}_4$  salt. This may be due to the interaction of  $\text{CH}_3$  molecules with  $\text{LiClO}_4$  salt which leads to better lithium salt dissolution hence better ionic conductivity. Moreover, the  $\text{C}=\text{O}$  symmetric stretching is shifted to  $1779\text{ cm}^{-1}$  as 25 wt% of  $\text{LiClO}_4$  salt is added into polymer electrolyte. This may infer the interaction between lithium salt with PMMA and EC/PC. Thereby, the  $\text{Li}^+$  may break the covalent bonding and attach to  $\text{O}^{2-}$ . The overall intensity of the absorption peaks are decreased according to increment in the concentration of  $\text{LiClO}_4$  salt up to 25 wt% and the overall intensity of the absorption peaks has increased again after this saturation level. The increases in the intensity can be explained by the  $\text{ClO}_4^-$  ions in favour for the re-association of ions or the formation of ion pair (Mahendran et al., 2005). This inferred that the ionic conductivity is increased before its saturation level and is dropped after its saturation level.

The vibration modes of  $\text{H}_2\text{O}$  rocking vibrations and O-H stretching of the  $\text{Al}_2\text{O}_3$  were found at  $1623\text{ cm}^{-1}$ , and  $3490\text{ cm}^{-1}$ . The appearance of O-H stretching vibration indicates the presence of the oxygen-hydrogen (O-H) group at the  $\text{Al}_2\text{O}_3$  surface (Song et al., 2006). Therefore, it is suggested that the Lewis acid-base type OH surface groups on alumina grains interacts with the ions of the lithium salt. Upon the dispersion of  $\text{Al}_2\text{O}_3$  filler, the  $\text{CH}_3$  bending,  $\text{C}=\text{O}$  symmetric stretching and  $\text{CH}_3$  asymmetric stretching of PMMA

is shifted to 1460, 1727 and 2953  $\text{cm}^{-1}$ , respectively. The vibration mode in pure  $\text{Al}_2\text{O}_3$ , the vibration mode of  $\text{H}_2\text{O}$  rocking has disappeared and the O-H stretching has shifted to 3548  $\text{cm}^{-1}$ . The shift of the O-H stretching revealed the information about the interaction between the polar group of alumina filler and lithium salt ( $\text{LiClO}_4$ ).

For the samples doped with  $\text{SiO}_2$ , the O-H bending modes of hydrogen-bonded and isolated silanolic groups at wavenumber of 808 and 975  $\text{cm}^{-1}$  are shifted to 811, 978  $\text{cm}^{-1}$ . The shift of O-H stretching mode of surface hydroxyl group of fumed silica is found at 3477  $\text{cm}^{-1}$ . The shifting of these absorption peaks gives the evidence that the polar surface group of filler grain helps to dissolve and interacts with lithium salt. The vibration frequency at 1095  $\text{cm}^{-1}$  which can be observed from spectrum (i) where this shifting inferred the interaction of Si-O molecules with  $\text{LiClO}_4$  to provide more favourable of lithium salt dissolution in the polymer. Besides that, the  $\text{CH}_2$  rocking, C-O-C bending,  $\text{CH}_3$  bending and  $\text{CH}_3$  asymmetric stretching of PMMA is shifted to 750, 849, 1452 and 2952  $\text{cm}^{-1}$ , respectively. The changes of intensity and shifting of the absorption peaks may be due to the interaction of  $\text{SiO}_2$  filler with the polymeric matrices. Therefore, it is believed that the dispersion of  $\text{SiO}_2$  filler might favourably enhance the properties and re-organise the structures of the composite solid polymer electrolyte.

## **4.4 Scanning Electron Microscopy (SEM) Studies**

SEM is used to investigate the structure, morphology, grain size and distribution of elements (Smart and Moore, 2005). As explained in section 3.3.4, the electron beam produced is scanned across the polymer surface at the point of interest. The SEM image can be produced by the exchange of energy between the electron beam and the sample causing an emission of secondary electrons and electromagnetic radiation that can be detected.

### **4.4.1 PMMA-EC/PC SEM**

The SEM image of pure PMMA electrolyte is shown in Figure 4.45. Several craters were found on the surface of the electrolyte caused by the rapid evaporation of THF solvent used in the preparation of the film (Stephan et al., 2000). As shown in Figure 4.46, the craters eventually disappeared when 10 wt% of EC/PC mixture was added into the PMMA host polymer. This may attribute to the nature of PC plasticiser which slows down the drying process and prolongs the solvent evaporation time.

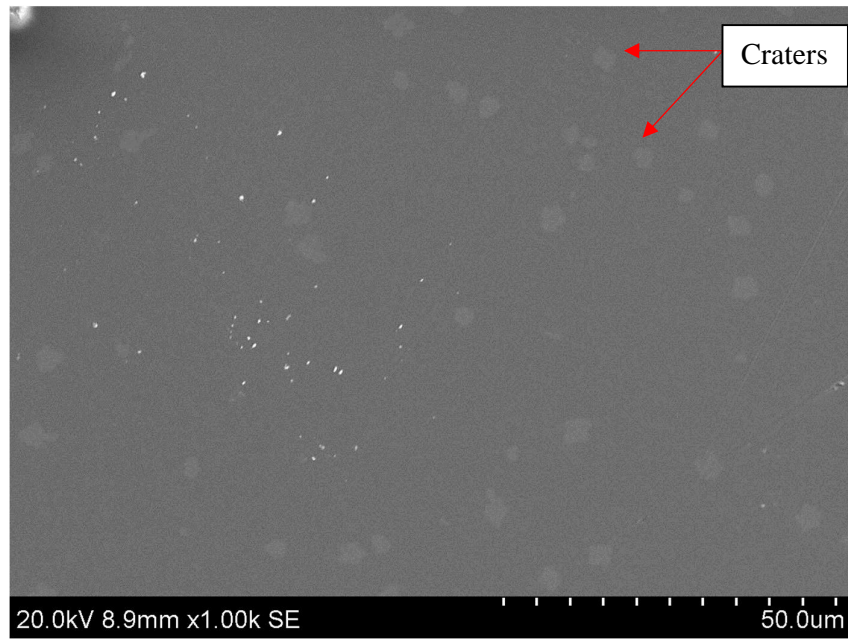


**Figure 4.45: SEM image of pure PMMA**

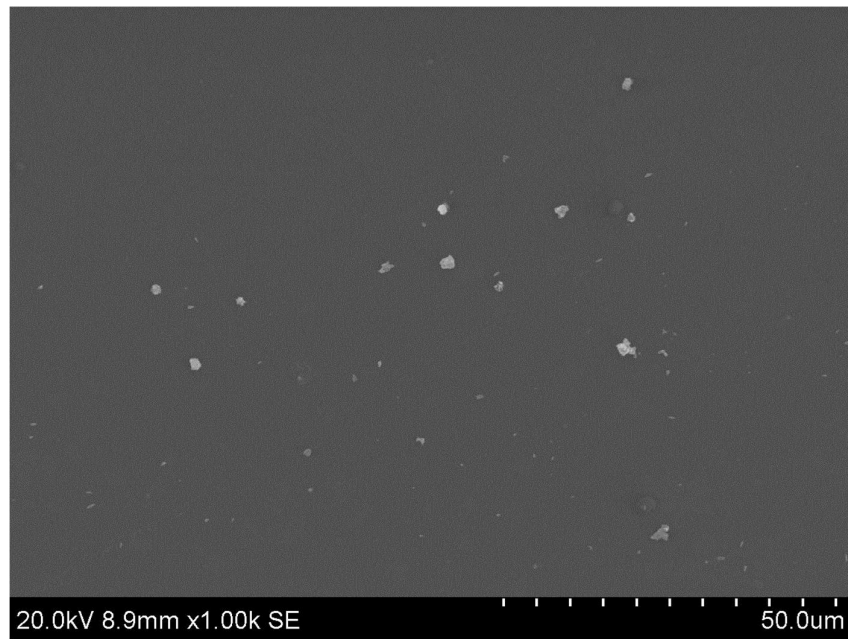


**Figure 4.46: SEM image of PMMA- 10wt% EC/PC**

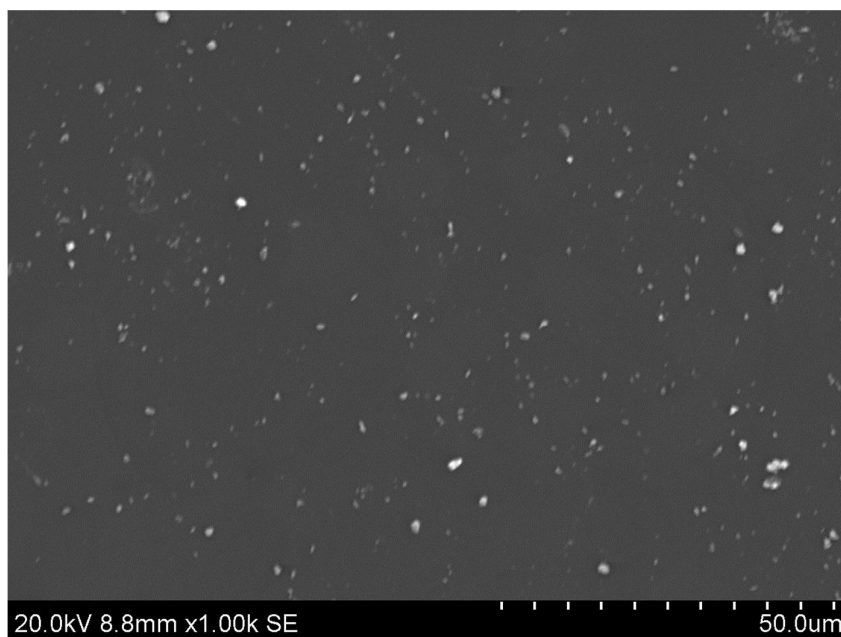


**Figure 4.47:** SEM image of PMMA- 30wt% EC/PC

As the EC/PC increases, the existence of pores are more obvious. As shown in Figure 4.47, a further increase of EC/PC mixtures up to 30 wt%, will cause the existing pores to increase significantly. The association of these pores that serve as a connecting path in the polymer matrix can enhance the ionic conductivity of the sample. As the porosity increases, the microstructure of the sample has become rougher. This inferred that the EC/PC tends to disorder the structure and increase the amorphous region in the polymeric matrix.

As discussed in the XRD study, the higher the amorphous in nature, the higher ionic conductivity could be obtained. The conducting ions and polymer segments can move more freely in the electrolyte within a smooth surface and therefore caused enhancement in the conductivity (Low et al., 2010). This

result matches with the conductivity study where the EC/PC mixture is added into the PMMA which exhibits a slight increase in conductivity as compared to the pure PMMA. When the EC/PC is added into the polymer matrix up to 35 wt%, the sample turns gelled. Hence, 30 wt% of EC/PC is selected to be the optimised composition where no phase separation occurs and the electrolyte remains solid.

#### **4.4.2 PMMA-EC/PC-LiClO<sub>4</sub> SEM**

Figure 4.48 to 4.50 depicted the SEM images of PMMA-EC/PC-5wt%, 25wt% and 50wt% of LiClO<sub>4</sub> lithium salt polymer electrolyte, respectively. From Figure 4.48, the surface morphology is changed due to a small quantity of LiClO<sub>4</sub> salt doped into the PMMA-EC/PC system. This quantity of LiClO<sub>4</sub> salt in the PMMA matrix has brought substantial modification to the microstructure pattern as contrasted with plasticised PMMA (Shukla and Thakur, 2009). Besides, it can be noticed from Figure 4.48 that the LiClO<sub>4</sub> salt is dispersed uniformly in the polymer matrix. Hence, as the charge carrier is increased in the free volume, the ionic conductivity is also increased.

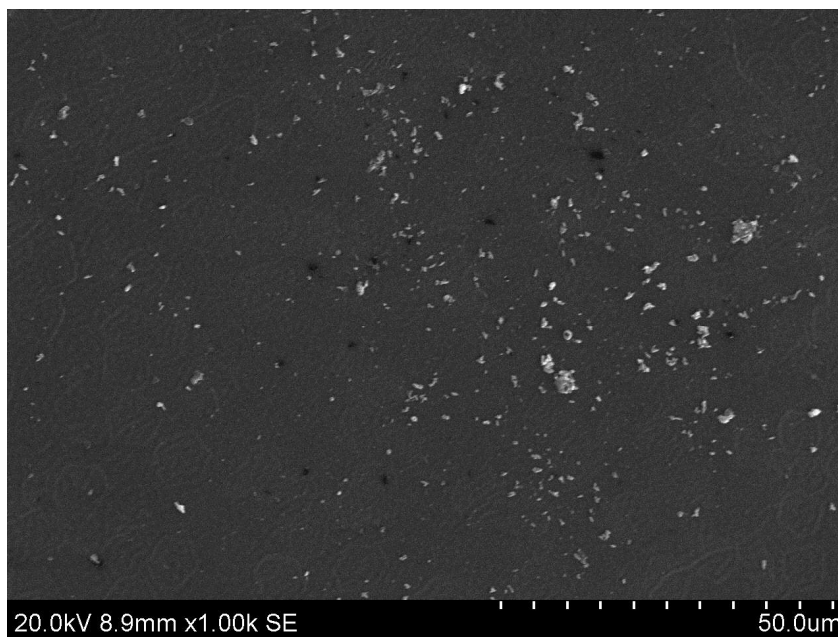


**Figure 4.48:** SEM image of PMMA-EC/PC- 5 wt% LiClO<sub>4</sub>

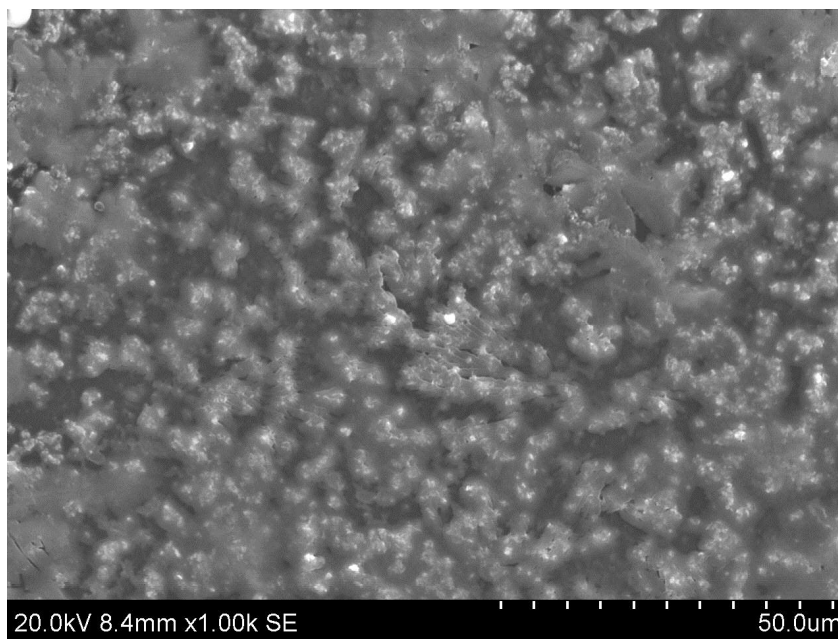


**Figure 4.49:** SEM image of PMMA-EC/PC- 25 wt% LiClO<sub>4</sub>

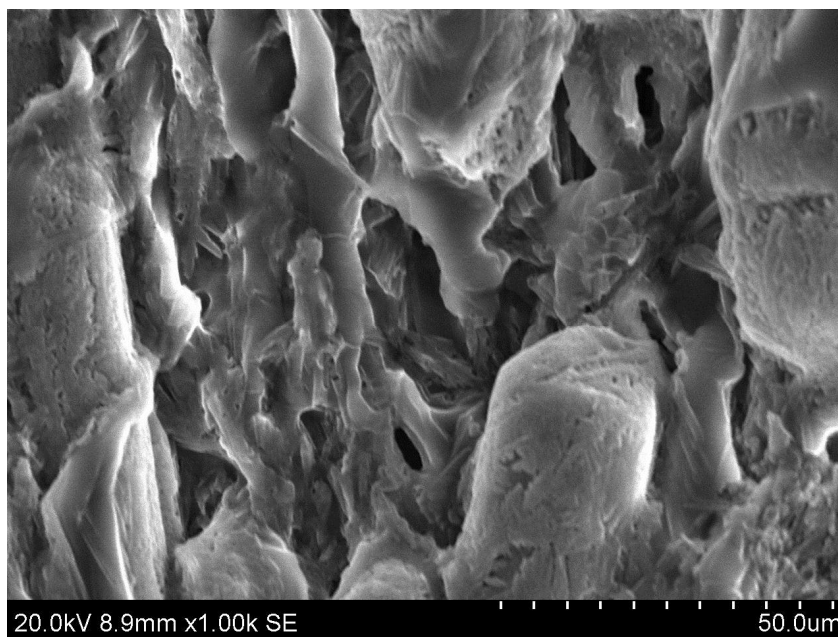


**Figure 4.50:** SEM image of PMMA-EC/PC- 50 wt% LiClO<sub>4</sub>

As shown in Figure 4.49, it can be observed that the addition of 25 wt% of LiClO<sub>4</sub> salt into the PMMA-EC/PC system forms a sphere-like surface. This is mainly due to the disruption of LiClO<sub>4</sub> salt onto the plasticised polymer. This indicates that the interaction between LiClO<sub>4</sub> salt with PMMA-EC/PC polymer complex is a result of the competitive interaction (Yen et al., 2008). The effect of high dielectric constant of EC/PC mixture plasticiser helps to dissociate more lithium salt and provides more charge carrier in the polymer matrix. Hence, a greater number of charge carriers within the polymer electrolyte further enhance the ionic conductivity of the solid polymer electrolyte. As the LiClO<sub>4</sub> is evenly dispersed in polymer matrix, the mobility of ionic transport and polymer segmental motion is greater with no barrier, thus the ionic conductivity is able to reach about  $10^{-05} \text{ Scm}^{-1}$ . As indicated in Figure 4.49, the film containing 25 wt% of LiClO<sub>4</sub> salt shows a more dispersed phase which indicates the higher amorphous nature as compared to 5 wt% and 50 wt%

LiClO<sub>4</sub> salt. The SEM image for 25 wt% of LiClO<sub>4</sub> doped into PMMA-EC/PC is almost similar to the work done by Mahendran and Rajendran, 2003.

Further addition of LiClO<sub>4</sub> salt into the PMMA-EC/PC system, caused the polymer-salt phase separation and the coarse surface morphology to be observed. From the Figure 4.50, at high LiClO<sub>4</sub> salt loadings, the salt tends to exist in ion pairs rather than form complexation between PMMA-EC/PC polymer matrices. As explained in XRD and FTIR, these aggregated ions lead to a more crystalline phase in this polymer electrolyte. Due to the increment in the crystallinity of polymer electrolyte, the energy barrier for ionic transport is increased hence the ionic conductivity is decreased. Upon the addition of LiClO<sub>4</sub> salt after its saturation level, the ionic mobility is hindered. Therefore, the existence of blocking effect might cause the ionic conductivity to drop. Moreover, the changes in micro-structure revealed in SEM agree well with the XRD pattern and unfavourable interaction between high concentrations of LiClO<sub>4</sub> salt with PMMA-EC/PC complexes as discussed in FTIR.

#### **4.4.3 PMMA-EC/PC-LiClO<sub>4</sub>-Al<sub>2</sub>O<sub>3</sub> SEM**

Figures 4.51 to 4.53 show SEM images for 4 wt%, 12wt% and 20wt% of Al<sub>2</sub>O<sub>3</sub> filler have dispersed into the predetermined PMMA-EC/PC-LiClO<sub>4</sub> system. The effect of Al<sub>2</sub>O<sub>3</sub> filler could be seen from Figure 4.51, the tiny

white dots represent the nano-sized  $\text{Al}_2\text{O}_3$  filler, where the  $\text{Al}_2\text{O}_3$  filler is insoluble and dispersed in the polymer matrix. As discussed in the EIS study, the  $\text{LiClO}_4$  salt can be dissociated due to the Lewis acid groups such as the -OH groups on the  $\text{Al}_2\text{O}_3$  surface that have some interaction with the lithium cations. Further, the ion pair, ion aggregation and ionic clusters are able to dissociate upon the dispersion of this filler.

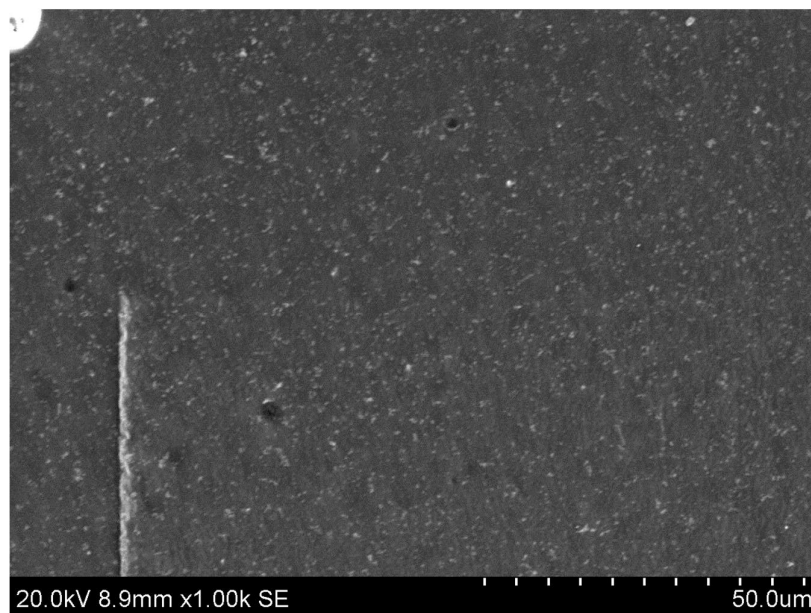


**Figure 4.51:** SEM image of PMMA-EC/PC-LiClO<sub>4</sub>-4 wt% Al<sub>2</sub>O<sub>3</sub>

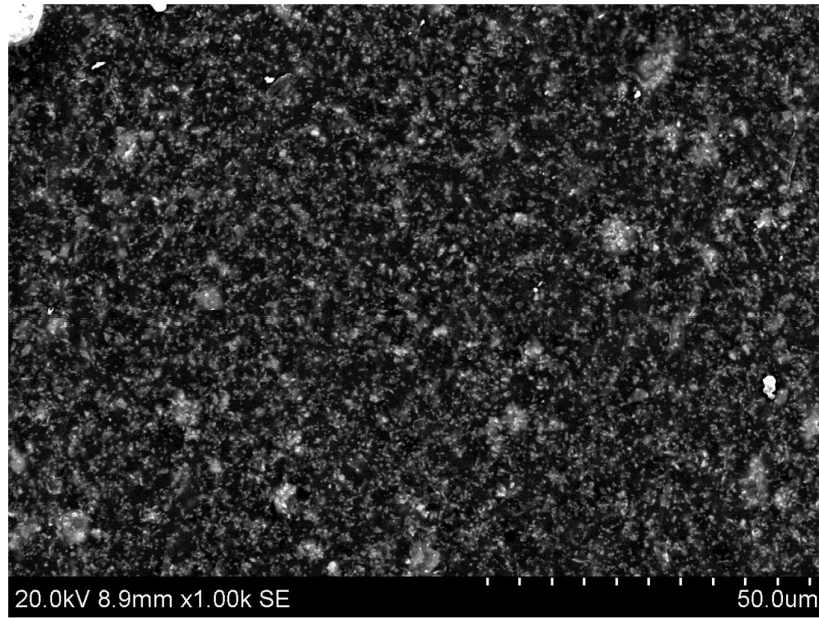


**Figure 4.52:** SEM image of PMMA-EC/PC-LiClO<sub>4</sub>-12 wt% Al<sub>2</sub>O<sub>3</sub>

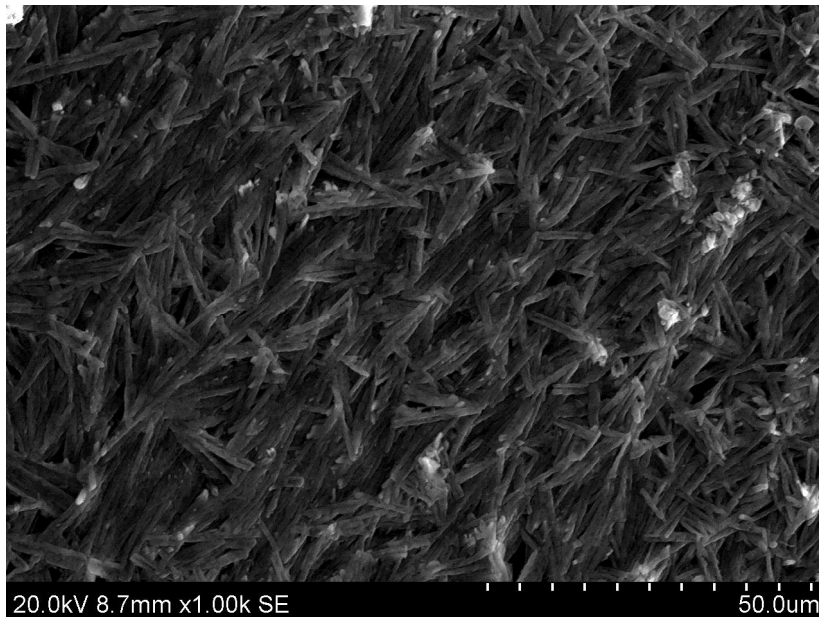


**Figure 4.53:** SEM image of PMMA-EC/PC-LiClO<sub>4</sub>-20 wt% Al<sub>2</sub>O<sub>3</sub>

By increasing the Al<sub>2</sub>O<sub>3</sub> filler up to 12 wt% of Al<sub>2</sub>O<sub>3</sub> fillers, the Al<sub>2</sub>O<sub>3</sub> grains are dispersed evenly across the polymeric matrices and the Al<sub>2</sub>O<sub>3</sub> grains are getting closer to one another which can be observed from Figure 4.52. As

the  $\text{Al}_2\text{O}_3$  grains are getting closer, the formations of three dimensional networks are established. The ionic conduction could be performed between the adjacent nano-sized grains. Therefore, the ionic conductivity is increased. Besides that, appropriate quantity of  $\text{Al}_2\text{O}_3$  filler is able to weaken the tendency of  $\text{LiClO}_4$  salt re-association. Consequently, the number of charge carriers is enhanced due to the tendency to dissociate with lithium salt and the ionic mobility is increased. Other than that, the sphere-like surface in Figure 4.52 has disappeared as 12 wt% of  $\text{Al}_2\text{O}_3$  fillers are integrated into the polymeric matrices. The sphere-like surface is then replaced by the tiny  $\text{Al}_2\text{O}_3$  filler grains as observed. This type of appearance reveals the amorphous region in the polymer electrolytes.

A further increase of the  $\text{Al}_2\text{O}_3$  filler beyond its saturation level (12 wt%), phase separation on the polymer surface is discovered as seen in Figure 4.53. As the  $\text{Al}_2\text{O}_3$  filler grains are getting closer to each other, the three dimensional transportation networks become more and more packed with  $\text{Al}_2\text{O}_3$  filler. This blocking effect is creating a barrier for ionic conduction, and for conductivity to be decreased. The formation of ion pairs and ion aggregates which do not assist in ionic conduction might also act as a barrier for ionic transport. The SEM studies agree with the result in XRD and FTIR that an appropriate quantity of  $\text{Al}_2\text{O}_3$  filler, in the amorphous region is increased but at higher  $\text{Al}_2\text{O}_3$  filler concentration, the amorphous region is reduced by the formation of aggregates.

#### 4.4.4 SEM of PMMA-EC/PC-LiClO<sub>4</sub>-SiO<sub>2</sub> system

The morphologies of sample doped with 4 wt%, 12wt% and 20wt% of SiO<sub>2</sub> filler are illustrated in Figure 4.54 to Figure 4.56. The morphology of PMMA-EC/PC-LiClO<sub>4</sub> is altered by dispersion of SiO<sub>2</sub> filler which can be observed in figure 4.54. The SiO<sub>2</sub> filler is dispersed across the surface of the composite solid polymer electrolyte. At the sample doped with 4 wt% of SiO<sub>2</sub> filler, the SiO<sub>2</sub> grains has started to attract each other due to the Lewis acid-base interaction and the three dimensional transportation channels are established. Due to the smaller grain size, the SiO<sub>2</sub> filler is dispersed uniformly in the polymer electrolyte.

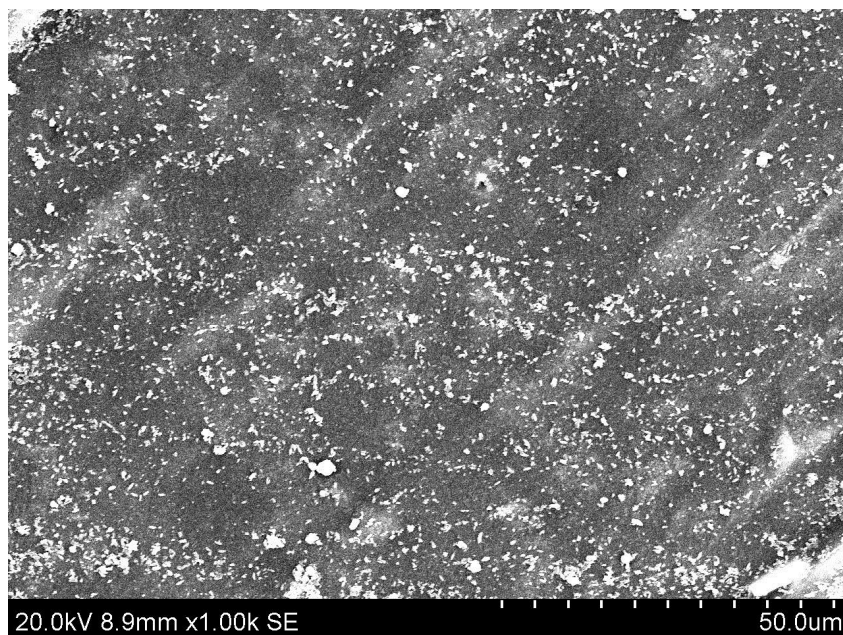
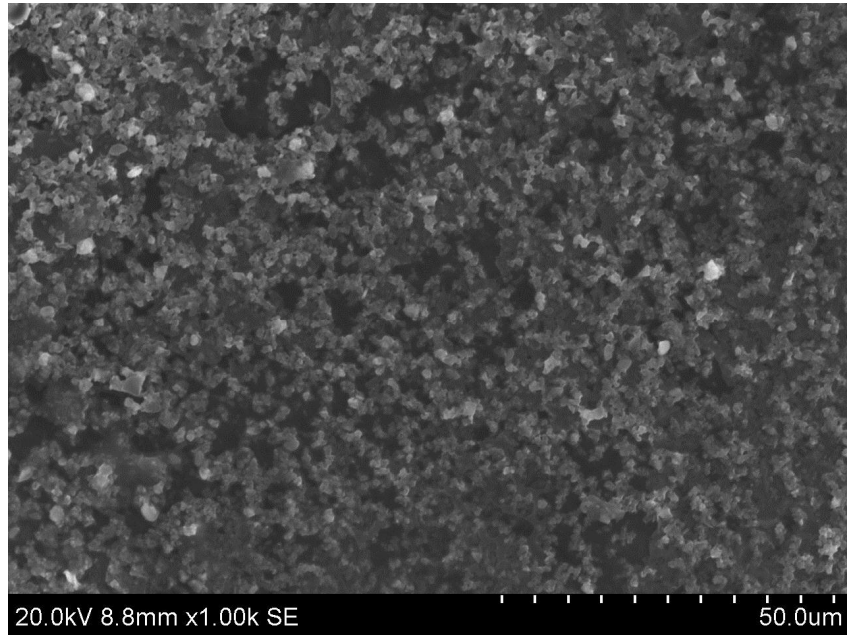
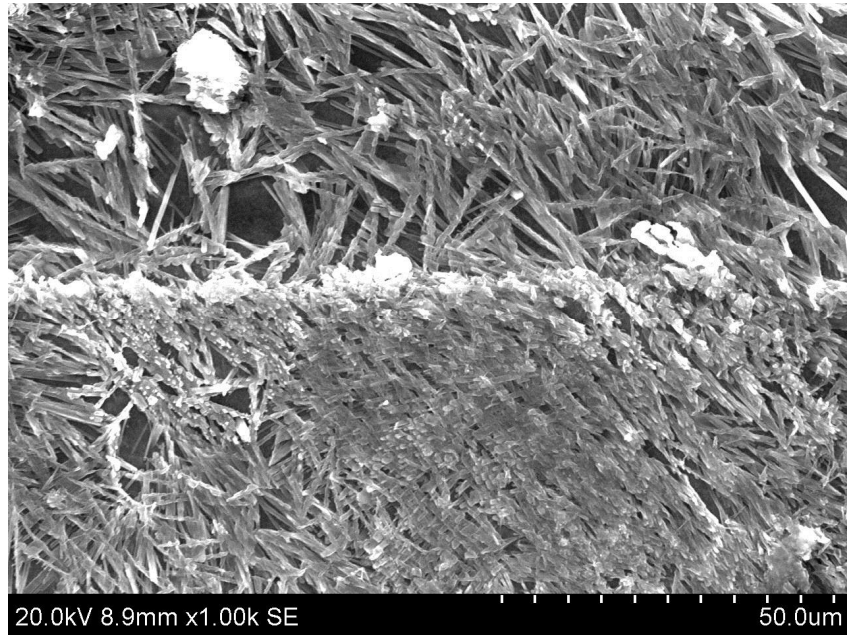


Figure 4.54: SEM image of PMMA-EC/PC-LiClO<sub>4</sub>-4 wt% SiO<sub>2</sub>



**Figure 4.55:** SEM image of PMMA-EC/PC-LiClO<sub>4</sub>-12 wt% SiO<sub>2</sub>



**Figure 4.56:** SEM image of PMMA-EC/PC-LiClO<sub>4</sub>-20 wt% SiO<sub>2</sub>

As the SiO<sub>2</sub> filler concentration is increased up to 12 wt%, the formation of three dimension transportation network is established. From Figure 4.55, the black cavities is observed, these black cavities might represent the evidence of three dimensional transportation network for ionic conduction. Hence, the ionic conduction is favourable as compared to lower filler concentrations. This inferred that the three dimensional transportation channels are fully established at 12 wt% of SiO<sub>2</sub> filler. Besides that, the ionic conductivity observed in this composite solid polymer electrolyte is elevated to 10<sup>-4</sup> Scm<sup>-1</sup>. As a result from the FTIR studies, the LiClO<sub>4</sub> salt is able to dissociate due to the Lewis acid groups -OH groups on the SiO<sub>2</sub> surface which indicates the lithium cations. Therefore, the charge carriers in this polymer electrolyte are increased. Moreover, with the new ionic transportation path, the ionic mobility in this polymer electrolyte is enhanced. Therefore, more Li<sup>+</sup> ions finds it favourable to use this path for ionic conduction.

From Figure 4.56, the phase separation in polymeric matrices is observed. This may be inferred to the excessive SiO<sub>2</sub> fillers (20 wt%) that blocked the conducting path along the three dimensional transportation networks. Besides that, the formation of ions aggregates and ions pairs due to excessive SiO<sub>2</sub> fillers have reduced the ionic mobility. As a result, the ionic conductivity has decreased to a very low level. The reduction of amorphous nature in the polymer is also further confirmed by XRD and FTIR studies.

#### **4.4.5 SEM images for Highest Ionic Conductivity Samples in Each System**

Figure 4.57 shows the highest conductivity sample as compared to the pure PMMA. As seen from Figure 4.57 (a), the pure PMMA sample shows the formation of several craters on the surface. This might be inferred to the rapid evaporation of THF solvent used in the preparation of the film (Stephan et al., 2000). These craters have disappeared (Figure 4.57b) as the EC/PC mixture is integrated into the host polymer. This may be due to the nature of liquid PC plasticiser slowing the drying process hence prolonged the solvent evaporation time which was carried out inside the fumed hood.

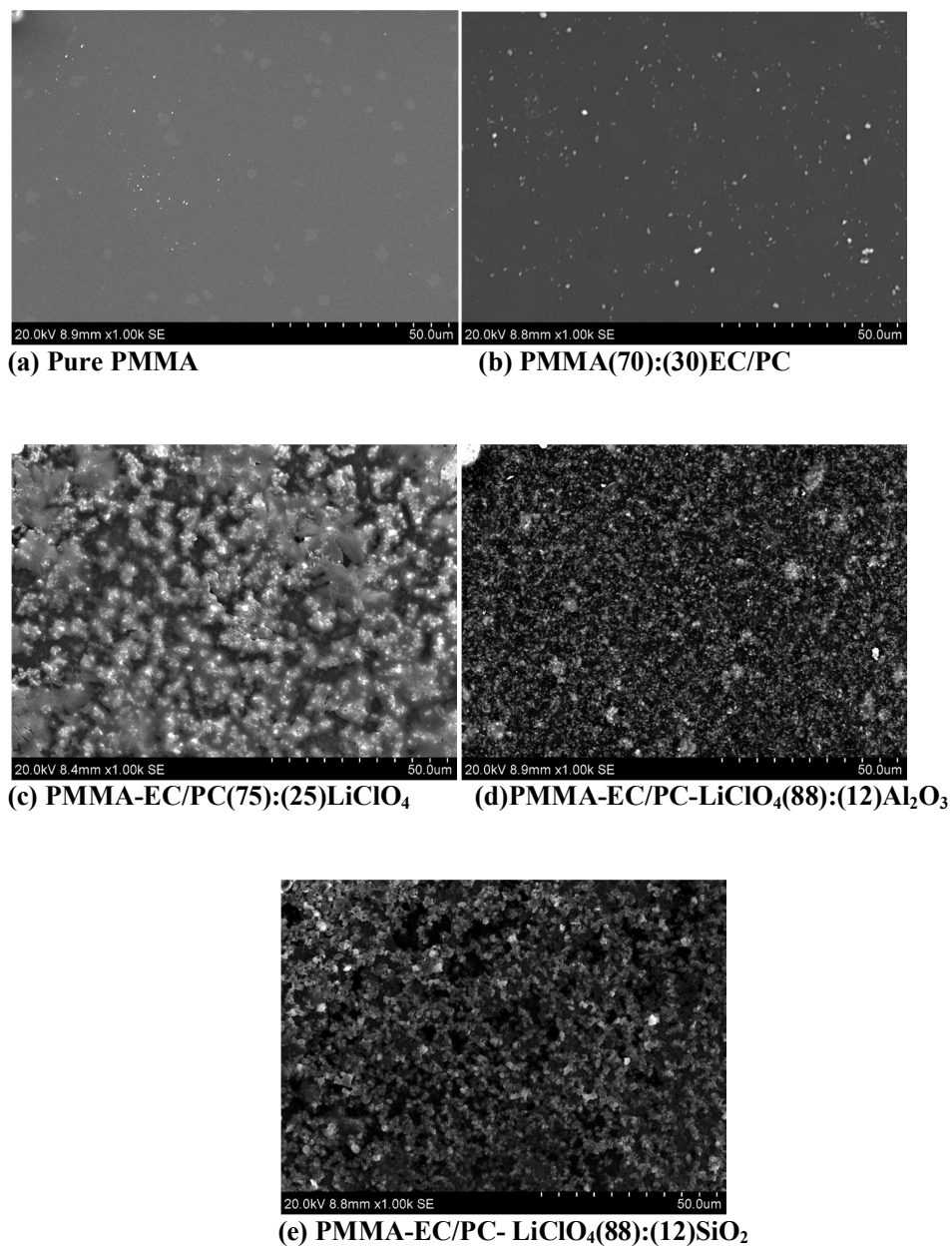


**Figure 4.57: SEM images for highest ionic conductivity sample of each system**

When the lithium salt is further added into the PMMA-EC/PC system as shown in Figure 4.57 (c), the sphere-like surface morphology is evenly spread across the polymer electrolyte surface at 25 wt% of LiClO<sub>4</sub> salt. From Figure 4.57 (c), the disruption of LiClO<sub>4</sub> salt onto the plasticised polymer is

mainly attributed to the interaction between  $\text{LiClO}_4$  salt with PMMA-EC/PC polymer complex as a result of the competitive interaction (Yen et al., 2008).

From the observation from Figure 4.57 (d) and (e), the  $\text{Al}_2\text{O}_3$  fillers (40-47nm) and  $\text{SiO}_2$  filler (7nm) are getting closer to one another as the filler concentration has increased. Upon dispersion of an appropriate quantity of ceramic filler (both systems are 12 wt%), a new ionic transportation pathway so-called three dimensional transportation network has generated. The black cavities observed in the figures might represent the evidence of three dimensional transportation networks. Hence, the ionic conduction is favourable to be conducted in this ionic transportation pathway. Due to the Lewis acid-based interaction, the  $\text{LiClO}_4$  salt is able to dissociate with the Lewis acid groups -OH groups on the fillers surface with the Lewis acid lithium cations. The roles of ceramic fillers in the polymer electrolyte are weakening the tendency of  $\text{Li}^+\text{-ClO}_4^-$  re-association. Therefore, the charge carriers in this polymer electrolyte have increased which leads to a higher ionic conductivity. For both types of ceramic filler integrated into the polymer electrolyte system, the composite solid polymer electrolyte has remained in the amorphous region whereby the dispersion of these ceramic filler may disorder and then reorganise the structure. The dispersion phase with  $\text{SiO}_2$  filler is better than  $\text{Al}_2\text{O}_3$  fillers. This may be attributed to the formation of three dimensional network which has formed better  $\text{SiO}_2$  filler as compared to  $\text{Al}_2\text{O}_3$  fillers. As a result, the ionic conductivity for  $\text{SiO}_2$  filler is higher than  $\text{Al}_2\text{O}_3$  fillers.

## 4.5 Mechanical Properties

In general, the stress-strain test is employed for the characterisation of the mechanical parameters for many polymeric materials (Billmeyer, 1984). The understanding of the deformation mechanism of polymers (stress and strain test) is important for managing the mechanical characteristics of the polymer membranes. Callister (2000) revealed that the response toward the tensile stresses is the elongation of the chain molecules in the direction of the applied stress. Besides, the tensile stress and tensile strain can be calculated by the following equation:

$$\sigma = \frac{F}{A} \quad (4.13)$$

$$\varepsilon = \frac{\ell_i}{\ell_o} \quad (4.14)$$

Where  $\sigma$  = Tensile Stress

F = Applied Force

A = Area

$\varepsilon$  = Tensile Strain

$\ell_i$  = Elongated Length

$\ell_o$  = Original Length

In this study, the mechanical properties of the polymer electrolyte are carried out by tensile stress-strain characterisation. The results of tensile stress-strain plots for the best ionic conductivity in each system are depicted in Figure 4.58 - 4.62. From the Figure 4.58, it shows that the pure PMMA film is rigid and fragile. The tensile stress-strain result shows that the pure PMMA have high mechanical strength but low ductility. However, due to the amorphous structure, the flexibility of the PMMA thin film is better over other polymers such as PVC, PEMA, PEO etc. The high molecular weight of host polymer mainly contributes to the mechanical integrity to the polymer itself. In order to make the polymer thin film become more flexible, plasticiser is introduced into the polymer matrix. From Figure 4.59, it is depicted that the polymer film becomes more elastic with an addition 30 wt% of EC/PC. The tensile strain is increased from 2.25 % to 60.17%. However, the tensile stress has decreased from 62 MPa to 18.67 MPa. The synergist effect of EC/PC has softened and has improved the mechanical properties. This effect is attributed to the reduction in the cohesive force of attraction between PMMA. The enhancement of elasticity can be ascribed to the inducement of amorphous regions and disordering of the structure of the polymer complex.

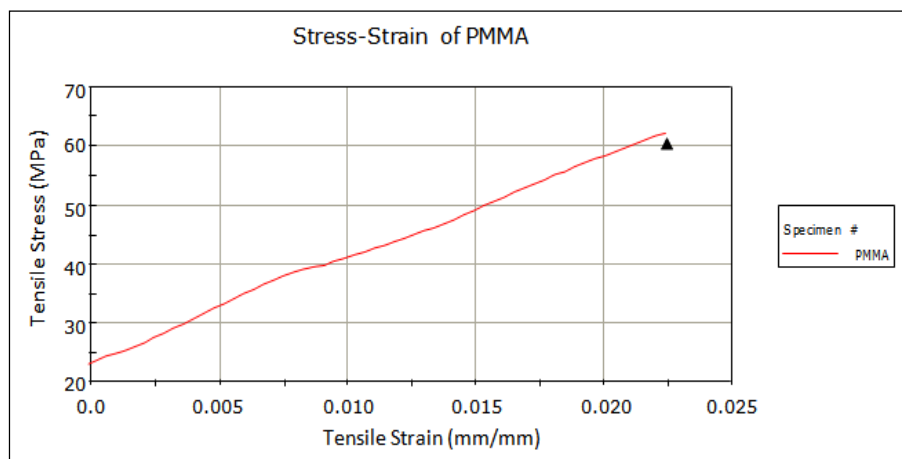


**Figure 4.58: Tensile stress and strain result of pure PMMA**

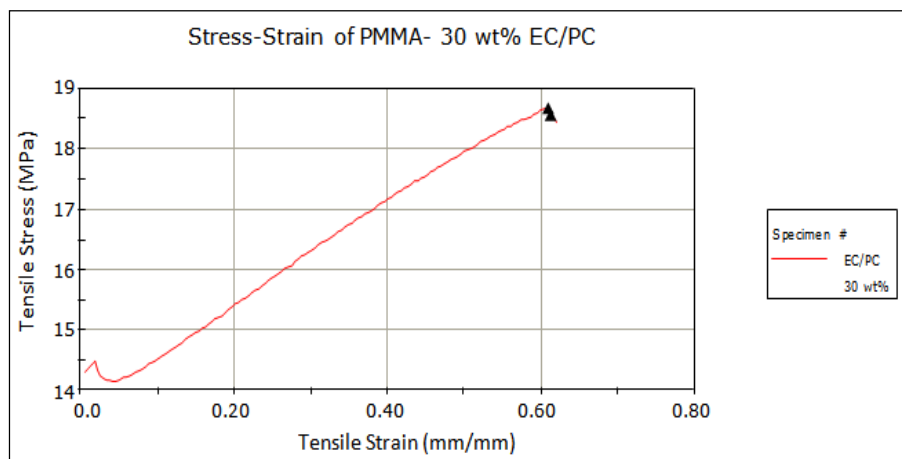


**Figure 4.59: Tensile stress and strain result of PMMA- 30 wt% of EC/PC**

For the PMMA-EC/PC-LiClO<sub>4</sub> system, the elongation capability is enhanced at 25 wt% of LiClO<sub>4</sub> into polymeric matrices. The changes of the tensile stress and strain can be observed at Figure 4.60. The polymer electrolyte has become more flexible as the tensile strain is enhanced from 60.17% to 278%. However, the enhancement of elasticity eventually reduces the mechanical strength of the polymer electrolyte. In comparing Figure 4.59 with Figure 4.60, the tensile stress is reduced to 0.94 MPa. This result agreed with

the XRD characterisation where the addition of 25 wt% LiClO<sub>4</sub> has induced and enhanced the amorphous region. The disorderliness of the structure makes the polymer electrolyte more elastical and ductile. The enhancement on the flexibility may attribute to the interaction between LiClO<sub>4</sub> with polymer backbone. As reported by Mahendran and Rajendran (2003), the low lattice energy with large anion LiClO<sub>4</sub> favourably promotes better dissolution in the polymer matrices. Therefore, the dispersed phase or constructed amorphous region by LiClO<sub>4</sub> may act as a barrier before the polymer electrolyte is fractured. Besides, the structure changes and the interaction between PMMA with LiClO<sub>4</sub> are confirmed by XRD, FTIR and SEM.

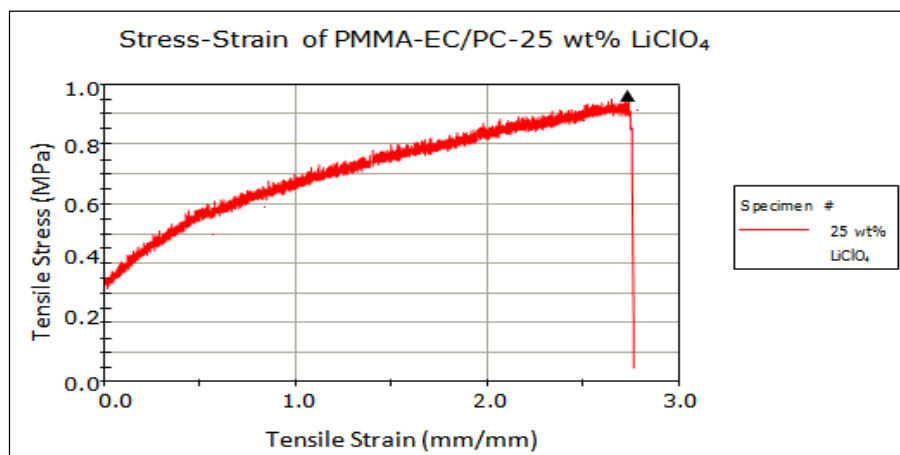


**Figure 4.60: Tensile stress and strain result of PMMA-EC/PC- 25 wt% LiClO<sub>4</sub>**

The tensile stress and tensile strain results together with the dispersion of Al<sub>2</sub>O<sub>3</sub> and SiO<sub>2</sub> are depicted in Figure 4.61 and Figure 4.62, respectively. The mechanical strength has improved to 1.61 MPa and 4.47 MPa for 12 wt% of Al<sub>2</sub>O<sub>3</sub> and 12 wt% of SiO<sub>2</sub>. For the tensile strain properties, the elasticity has

improved to 288% and 331% for 12 wt% of  $\text{Al}_2\text{O}_3$  and 12 wt% of  $\text{SiO}_2$ . From these results, it is proven that the dimensional stability and mechanical properties of the polymer electrolyte have improved with the dispersion of both ceramic fillers. Ahmad et al. (2006) reported that the toughness of the polymer electrolyte can be increased through the addition of ceramic fillers. Whereby, the presence of the fillers can reduce the fracture strength of the polymer and the elongation to failure. This may infer that the dispersion of the ceramic fillers changes the structure of the polymer complex. The effect of disordering the structure can induce the amorphous region in the polymeric matrices which is confirmed by the XRD result. This ascribes that the flexibility of the polymer electrolyte has improved due to the enhancement in the amorphous phase. Whereas the enhancement of amorphous region in the polymer electrolytes has destroyed the crystalline portion and disrupted the interaction of polymer chain. Besides, the aggregation of ceramic fillers might reinforce the fracture strength of the polymer electrolyte. At the same time, the disorderliness of structure improves the elongation property of the polymer electrolyte.

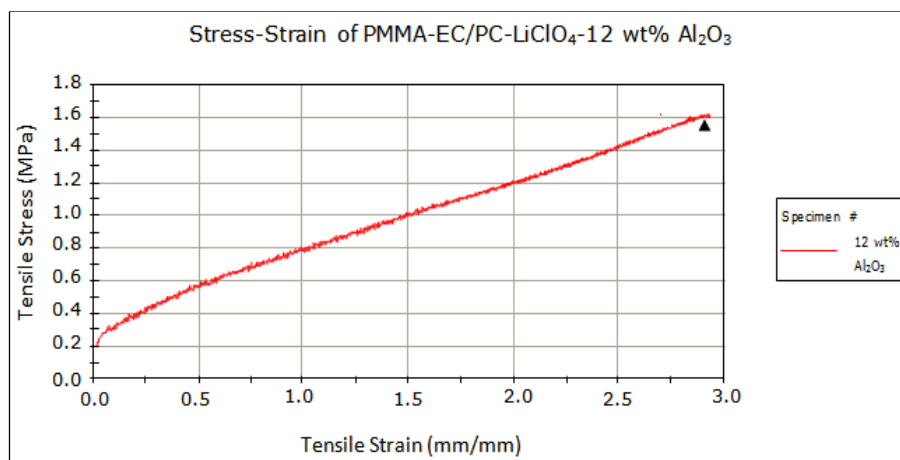


**Figure 4.61: Tensile stress and strain result of PMMA-EC/PC- LiClO<sub>4</sub>- Al<sub>2</sub>O<sub>3</sub>**

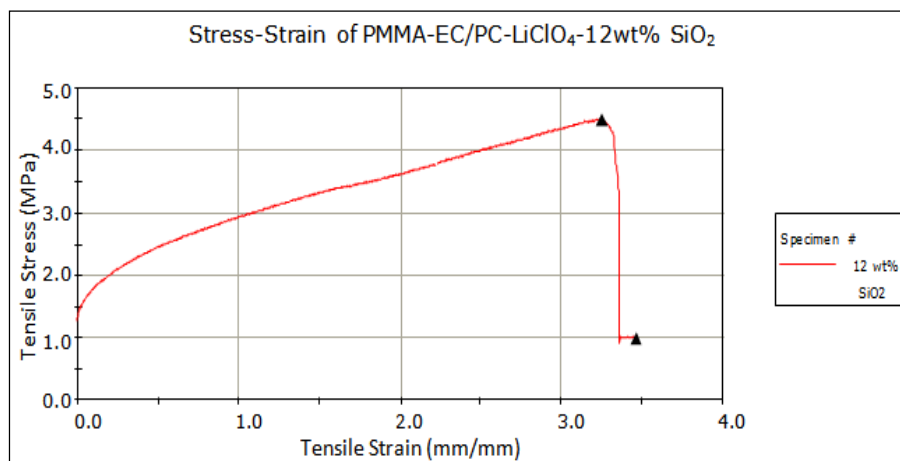


**Figure 4.62: Tensile stress and strain result of PMMA-EC/PC- LiClO<sub>4</sub>- SiO<sub>2</sub>**

For the summary of the mechanical tensile stress and strain test, the addition of EC/PC into the rigid PMMA basically improves the flexibility of the polymer electrolyte. However, the mechanical strength is reduced. A further addition of LiClO<sub>4</sub> in the sample, resulting to the mechanical strength being further reduced due to the enhancement of flexibility in the sample. With the dispersing of the nano-size ceramic filler into the polymer electrolyte, both mechanical strength and flexibility have increased. The Figure 4.63, Figure 4.64 and Table 4.12 show that the sacrifice of the tensile strength in turn enhances the tensile strain of polymer electrolyte. This is more preferred when the flexibility of the polymer electrolyte has improved the practical application of the lithium rechargeable battery.

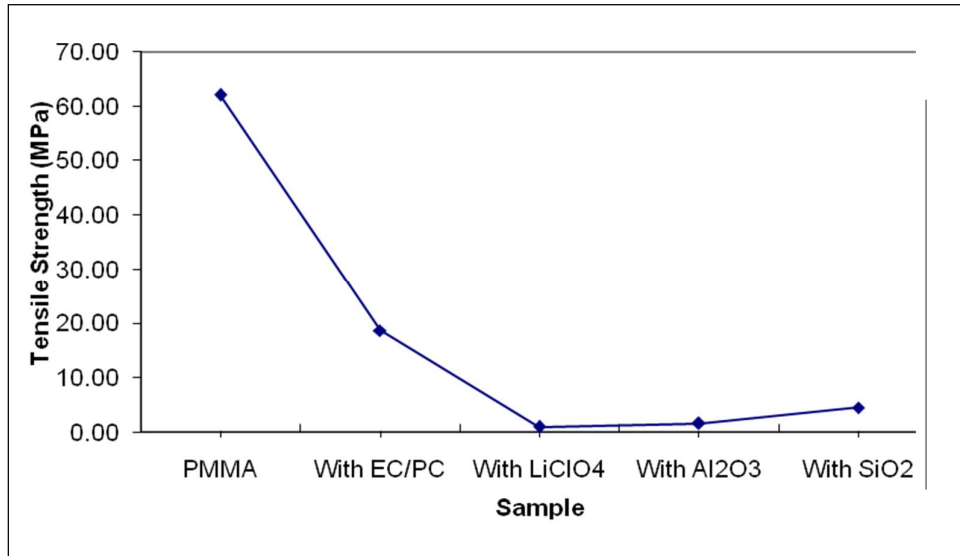


**Figure 4.63: Overall tensile stress of the best ionic conductivity sample**

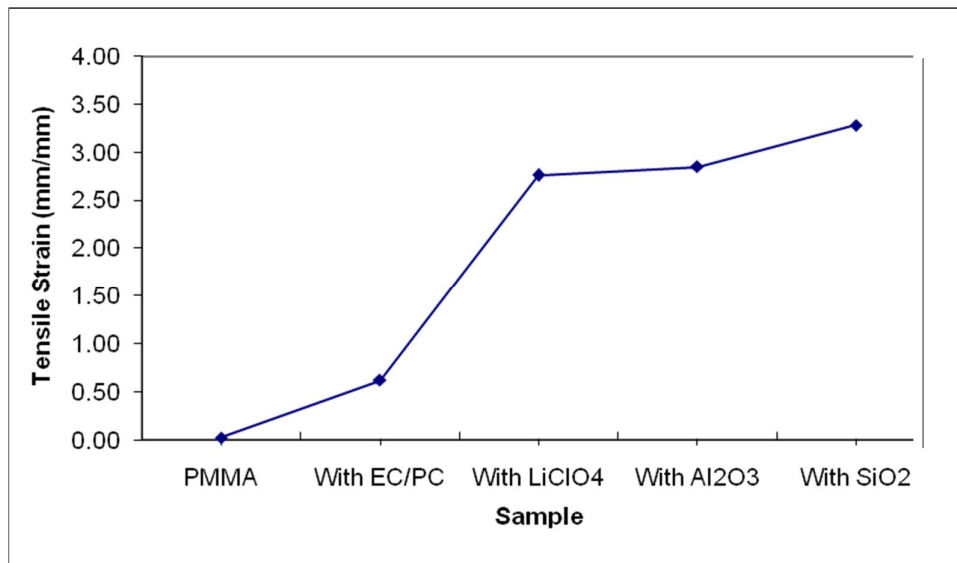


**Figure 4.64: Overall tensile strain of the best ionic conductivity sample**

**Table 4.12: Overall tensile strength and tensile strain for the best ionic conductivity sample**

Sample	Tensile Stress	Tensile Strain
Pure PMMA	62 Mpa	0.0225 mm/mm
70 wt% PMMA : 30% EC/PC	18.6 Mpa	0.62 mm/mm
75 wt% PMMA-EC/PC : 25 wt% LiClO <sub>4</sub>	0.92 Mpa	2.76 mm/mm
88 wt% PMMA-EC/PC-LiClO <sub>4</sub> : 12 wt% Al <sub>2</sub> O <sub>3</sub>	1.6 Mpa	2.85 mm/mm
88 wt% PMMA-EC/PC-LiClO <sub>4</sub> : 12 wt% SiO <sub>2</sub>	4.5 Mpa	3.28 mm/mm

## CHAPTER 5

### CONCLUSION

#### 5.1 Summary

Four groups of PMMA based polymer electrolyte consisting of PMMA-EC/PC, PMMA-EC/PC-LiClO<sub>4</sub>, PMMA-EC/PC-LiClO<sub>4</sub>-Al<sub>2</sub>O<sub>3</sub> and PMMA-EC/PC-LiClO<sub>4</sub>-SiO<sub>2</sub> have been prepared using solution-cast technique. These thin films are flexible in nature without losing its mechanical integrity. In this work, a high molecular weight PMMA of 996,000 is used as a host polymer. The optimum ratio of EC/PC mixture was at 70:30 through the EIS characterisation.

When 30 wt% of EC/PC mixture is added into the host polymer, the ionic conductivity is enhanced from  $3.19 \times 10^{-11} \text{ S cm}^{-1}$  to  $7.57 \times 10^{-10} \text{ S cm}^{-1}$  at ambient temperature. This effect can be attributed to the plasticiser effect which makes the polymer electrolyte more flexible and amorphous for ionic transportation and polymer segmental motion. A further addition of EC/PC mixture can cause the film to turn into a gel type polymer thin film.

Upon the addition of 25 wt% of LiClO<sub>4</sub> into PMMA-EC/PC, the ionic conductivity is enhanced to  $3.95 \times 10^{-05} \text{ S cm}^{-1}$  at ambient temperature. The enhancement in ionic conductivity is achieved by increasing the number of charge carriers and the mobility of ionic transportation. A further addition of 12 wt% of Al<sub>2</sub>O<sub>3</sub> and SiO<sub>2</sub> into PMMA-EC/PC-LiClO<sub>4</sub> is to generate two different composite solid polymer electrolyte systems. The highest ionic conductivity at ambient temperature obtained was  $1.02 \times 10^{-04} \text{ S cm}^{-1}$  and  $2.48 \times 10^{-04} \text{ S cm}^{-1}$ , respectively. The ionic conductivity is enhanced due to the interaction between the Lewis acid-base type oxygen and the OH surface groups on filler grains with cations and anions. The ionic conductivity is found to be at a decreased level. This might be attributed to the formation of ion pairs and ion aggregates which contribute to the blocking effects. In comparing the ionic conductivity obtained in this study with Table 5.1, the ionic conductivity of polymer electrolyte samples generated in this study is eventually enhanced. This may attribute to the synergised effect of EC and PC which reduces the mobility restriction in the polymer electrolyte samples and the Lewis acid base interaction from Al<sub>2</sub>O<sub>3</sub> and SiO<sub>2</sub> that provide greater Li<sup>+</sup> ions available to transport in the three dimensional network. Therefore, the objective of generating high ionic conductivity in the solid polymer electrolyte is achieved.

**Table 5.1 Work done by other researchers on the solid polymer electrolyte system**

Composition	Ionic Conductivity (Scm <sup>-1</sup> )	Reference
PVC(25)-PEG(75)-LiClO <sub>4</sub> (5)-TiO <sub>2</sub> (15)	1.158 x 10 <sup>-6</sup>	Rajendran et al., 2009
PMMA-LiCF <sub>3</sub> SO <sub>3</sub> (98)-SiO <sub>2</sub> (2)	7.30 x 10 <sup>-5</sup>	Ramesh and Wen, 2010
PMMA(49)-Li <sub>2</sub> B <sub>4</sub> O(21)-DBP(30)	1.58 x 10 <sup>-7</sup>	Ramesh and Chao, 2010
PEO-LiClO <sub>4</sub> (16:1)- SiO <sub>2</sub> (10)	2.3 x 10 <sup>-5</sup>	Ji et al., 2003
[PMMA-EC]-LiBF <sub>4</sub> (30)	4.07 x10 <sup>-7</sup>	Othman et al., 2007
[PMMA-EC]-LiCF <sub>3</sub> SO <sub>3</sub> (35)	3.4 x 10 <sup>-5</sup>	Othman et al., 2007
[PMMA-PEO-EC]-LiPF <sub>4</sub> (30)	~1.0 x 10 <sup>-6</sup>	Osman et al., 2005
[PMMA-EC-LiCF <sub>3</sub> SO <sub>3</sub> ]- Al <sub>2</sub> O <sub>3</sub> (5)	2.05 x 10 <sup>-4</sup>	Tan et al., 2007
[PMMA-EC-LiCF <sub>3</sub> SO <sub>3</sub> ]- SiO <sub>2</sub> (10)	2.15 x 10 <sup>-5</sup>	Tan et al., 2007

The ionic conductivity of all polymer electrolyte samples is enhanced when the temperature is increased. From the Arrhenius behaviour and the free volume theory that increases the operating temperature it will also increase the free volume in the polymeric matrix. The overall mobility of ionic transportation and polymer segmental motion is enhanced; therefore the ionic conductivity is increased. Besides that, the study on the complex permittivity of the samples reveals that the dielectric constant and loss in each system are increased accordingly with an increment of ionic conductivity.

FTIR results indicated that the complexation has occurred between the host polymer, plasticiser, lithium salts and ceramic fillers. The occurrence of complexation is determined based on the changes in the shifting of the peak, peak intensity and formation of new peaks. The XRD results also implied that the amorphous nature of polymer electrolyte is increased with the best sample

in each system as the intensity of the characteristic peaks is reduced. The changes in the amorphous nature are determined through the changes in the peak intensity and the diffraction peaks in the results obtained. For the SEM characterisation, the microstructure studies clearly showed that complexation has occurred in the samples as the electrolyte materials are integrated into the polymer complex. The SEM images proved that the formation of three dimensional transportation channel for ionic conduction upon dispersion of the inorganic ceramic filler reveal the improved ionic migration in the polymer electrolyte samples.

## **5.2 Suggestions For Future Work**

In the current study, the polymer electrolytes are generated based on a single type of host polymer (PMMA). Thus, for future work, the blending of polymer hosts such as PMMA/PVDF (Mahendran et al., 2005), PVC/PEG (Rajendran et al., 2009), PMMA/grafted natural rubber (Low et al., 2010), PVAc/PMMA (Rajendran et al., 2010) and others might be considered in the development of a solid type of polymer electrolytes. Due to the concern for the environment impact, the biodegradable polymer might be a good candidate to replace the conventional liquid electrolyte and polymer electrolyte in order to reduce the impact to environment (Ng et al., 2011).

Different types of lithium dopant salts, such as lithium triflate ( $\text{LiCF}_3\text{SO}_3$ ), lithium hexafluoroarsenate ( $\text{LiAsF}_6$ ), lithium tetrafluoroborate ( $\text{LiBF}_4$ ) and lithium trifluoromethanesulfonimide ( $\text{LiN}(\text{DF}_3\text{SO}_2)_2$ ), and also other types of ceramic fillers, such as titanium dioxide ( $\text{TiO}_2$ ) and zirconium dioxide ( $\text{ZrO}_2$ ) might be incorporated into the polymer host in order to study the effects of different types of lithium dopant salt and ceramic fillers, with the current samples as the reference materials.

More characterisation methods can be used to enhance the knowledge in this study. The thermal property of the polymer electrolyte can be observed from the results of the Differential Scanning Calorimeter (DSC) and Thermogravimetric Analysis (TGA) to determine the glass transition temperature ( $T_g$ ), thermal stability and thermal degradation of the samples. Rheological studies might be carried out to further clarify the relationship between the viscosities with ionic conductivity in the samples. The physical properties of the samples have also been thoroughly studied in order to understand the effects of the physical characteristics on the bulk ionic transportation.

## LIST OF REFERENCES

- Adebahr, J. et al., 2003. Enhancement of ion dynamics in PMMA-based gels with addition of TiO<sub>2</sub> nano-particles. *ElectrochimicaActa*, 48, pp. 2099-2103.
- Ahmad, S., Ahmad, S. and Agnihotry, S.A., 2003. Composite polymeric electrolytes based on PMMA-LiCF<sub>3</sub>SO<sub>3</sub>-SiO<sub>2</sub>. *Ionics*, 9, pp. 439-443.
- Ahmad, S. et al., 2006. Role of fumed silica on ion conduction and rheology in nanocomposite polymeric electrolytes. *Polymer*, 47, pp. 3583-3590.
- Ahmad, S., 2009. Polymer electrolytes: characteristics and peculiarities. *Ionics*, 15, pp. 309-321.
- Angell, C.L., 1956. The infra-red spectra and structure of ethylene carbonate. *Transactions of the Faraday Society*, 52, pp. 1178-1183.
- Appetecchi, G.B., Croce, F. and Scrosati, B., 1995. Kinetics and stability of the lithium electrode in poly(methylmethacrylate)-based gel electrolytes. *ElectrochimicaActa*, 40, pp. 991-997.
- Arico, A.S. et al., 2003. FTIR spectroscopic investigation of inorganic filler for composite DMFC membranes. *Electrochemistry Communications*, 5, pp. 862-866.
- Arof, A.K., 1999. Impedance Spectroscopy. In A. K. Arof (Ed.), *Proceedings of the Workshop on Current Problems in Batteries* (pp.59-80). Kuala Lumpur: Penerbit Universiti Malaya.

Awadhia, A., Patel, S.K. and Agrawal, S.L., 2006. Dielectric investigations in PVA based gel electrolytes. *Progress in Crystal Growth and Characterization of Materials*, 52, pp. 61-68.

Baskaran, R. et al., 2004. Vibrational, ac impedance and dielectric spectroscopic studies of poly(vinylacetate)-*N,N*-dimethylformamide-LiClO<sub>4</sub>. *Journal of Power Sources*, 134, pp. 235-240.

Bernson, A. and Lindgren, J., 1993. Free ions pairing/clustering in the system LiCF<sub>3</sub>SO<sub>3</sub>-PPO<sub>n</sub>. *Solid State Ionics*, 60, pp. 37-41.

Berthier, C. et al., 1983. Microscopic investigation of ionic conductivity in alkali metal salts-poly(ethylene oxide) adducts. *Solid State Ionics*, 11, pp. 91-95.

Billmeyer, F.W., 1984. Textbook of Polymer Science, 3<sup>rd</sup> ed. New York: Wiley-Interscience.

Bohnke, O. et al., 1993. Fast Ion transport in new lithium electrolytes gelled with PMMA. Influence of polymer concentration. *Solid State Ionics*, 66, pp. 97-104.

Callister, W. D., 2000. Materials Science and Engineering. 5<sup>th</sup> ed. New York: John Wiley & Sons, Inc.

Chintapalli, S. and Frech, R., 1996. Effect of plasticizers on high molecular weight PEO-LiCF<sub>3</sub>SO<sub>3</sub> complexes. *Solid State Ionics*, 86-88, pp. 341-346.

Chung, S.H. et al., 2001. Enhancement of ion transport in polymer electrolytes by addition of nanoscale inorganic oxides. *Journal of Power Sources*, 97-98, pp. 644-648

Croce, F., 1999. Physical and chemical properties of nanocomposite polymer electrolytes. *Journal of Physical Chemistry B*, 103, pp. 10632-10638.

Croce, F., Sacchetti, S., and Scrosati, B., 2006. Advanced high-performance composite polymer electrolytes for lithium batteries. *Journal of Power Sources*, 161(1), pp. 560-564.

Croce, F., Settini, L., and Scrosati, B., 2006. Superacid ZrO<sub>2</sub> added, composite polymer electrolytes with improved transport properties. *Electrochemistry Communications*, 8(2), pp. 364-368.

Deepa, M. et al., 2002. Conductivity and viscosity of liquid and gel electrolytes based on LiClO<sub>4</sub>, LiN(CF<sub>3</sub>SO<sub>2</sub>)<sub>2</sub> and PMMA. *Solid State Ionics*, 152-153, pp. 253-258.

Deka, M. and Kumar, A., 2010. Enhanced ionic conductivity in novel nanocomposite gel polymer electrolyte based on intercalation of PMMA into layered LiV<sub>3</sub>O<sub>8</sub>. *Journal of Solid State Electrochemistry*, 14, pp. 1649-1656

Dissanayake, M.A.K.L. et al., 2003. Effect of concentration and grain size of alumina filler on the ionic conductivity enhancement of the (PEO)<sub>9</sub>LiCF<sub>3</sub>SO<sub>3</sub>: Al<sub>2</sub>O<sub>3</sub> composite polymer electrolyte. *Journal of Power Sources*, 119, pp. 409-414.

Dyre, J.C., 1991. Some remarks on ac conduction in disordered solid. *Journal Of Non-Crystalline Solid*, 135, pp. 219-226.

Fini, G. and Mirone, P., 1973. Evidence for short-range orientation effects in dipolar aprotic liquids from vibrational spectroscopy. Part 1.-Ethylene and propylene carbonates. *Journal of the Chemical Society, Faraday Transaction 2*, 69, pp. 1243-1248.

Fenton, D. E., Parker, J. M., and Wright, P. V., 1973. Complexes of alkali metal ions with poly(ethylene oxide). *Polymer*, 14(11), pp. 589.

Forsyth, M., et al., 1997. Ionic conductivity in poly(diethylene glycol carbonate)/sodium triflate complexes. *Solid State Ionics*, 99(3-4), pp. 257 - 261.

Ganesan, S., et al., 2008. Performance of a new polymerelectrolyte incorporated with diphenylamine in nanocrystalline dye-sensitized solar cell. *Solar Energy Materials and Solar Cells*, 92, pp. 1718-1722.

Gray, F.M., 1991. Polymer Electrolytes-Based Devices. *Solid polymerelectrolytes: Fundamentals of technological application*. (pp. 1-30). United Kingdom: Wiley-VCH.

Gray, F.M., 1997a. What are Polymer Electrolytes? *Polymer Electrolyte*. (pp.1-30). Cambridge: The Royal Society of Chemistry.

Gray, F.M., 1997b. What Materials are suitable as Polymer electrolyte? *Polymer Electrolyte*. (pp. 31-78). Cambridge: The Royal Society of Chemistry.

Harris, C.S., Shriver, D.S. and Ratner, M.A., 1986. Complex formation of polyethylenimine with sodium triflate and conductivity behavior of the complex. *Macromolecules*, 19, pp. 987-989.

Huang, B. et al., 1994. Lithium ion conduction in polymer electrolytes based on PAN. *Solid State Ionics*, 85, pp. 79-84.

Ito, Y., Kanehori, K., Miyauchi, K. and Kuda, T., 1987. Ionic conductivity of electrolytes formed from PEO-LiCF<sub>3</sub>SO<sub>3</sub> complex low molecularweight poly(ethylene glycol). *Journal of Materials Science*, 22, pp. 1845-1849.

Jana, S. and Zhong, W.-H., 2008. Electrical conductivity enhancement of a polymer using butyl glycidyl ether (BGE)-lithium hexafluorophosphate ( $\text{LiPF}_6$ ) complex. *Journal of Material Science*, 43, pp. 4607-4617.

Jeon, J.D., Kwak, S.Y. and Cho, B.W., 2005. Solvent-free polymer electrolytes -I. Preparation and characterization of polymer electrolytes having pores filled with viscous P(EO-EC)/ $\text{LiCF}_3\text{SO}_3$ . *Journal of the Electrochemical Society*, 152, pp. A1583-A1589.

Ji, K.S., Moon, H.S., Kim, J.W. and Park, J.W., 2003. Role of Functional nano-sized inorganic filler in poly(ethylene) oxide-based polymer electrolytes. *Journal of Power Sources*, 117, pp. 124-130.

Jiang, J., Gao, D., Li, Z. and Su, G., 2006. Gel polymer electrolytes prepared by in situ polymerization of vinyl monomers in room-temperature Ionic liquids. *Reactive and Functional Polymers*, 66, pp. 1141-1148.

Jiang, Z., Carroll, B. and Abraham, K.M., 1997. Studies of some poly(vinylidene fluoride) electrolytes. *Electrochimica Acta*, 42, pp. 2667-2677.

Jung, S. et al., 2009. Filler for solid-state polymer electrolyte: highlight. *Bulletin of Korean Chemical Society*, 30, pp. 2355-2360.

Kakahana, M., Schantz, S. and Torell, L.M., 1990. Raman Spectroscopic study of ion-ion interaction and its temperature dependence in a poly(propylene-oxide)-based- $\text{NaCF}_3\text{SO}_3$ -polymer electrolyte. *Journal of Chemistry Physics*, 92, pp. 6271-6276.

Kang, X., 2004. Nonaqueous Liquid Electrolytes for Lithium-Based Rechargeable Batteries. *Chemical Reviews*, 104, pp. 4303-4417.

Karan, N.K. et al., 2008. Solid polymer electrolytes based on polyethylene oxide and lithium trifluoro-methane sulfonate (PEO- $\text{LiCF}_3\text{SO}_3$ ): Ionic conductivity and dielectric relaxation. *Solid State Ionics*, 179, pp. 689-696.

Kim, H.S. et al., 2003. Electrochemical and physical properties of composite polyelectrolyte of poly(methyl methacrylate) and poly(ethylene glycoldiacrylate). *Journal of Power Sources*, 124, pp. 221-224.

Krawiec, W. et al., 1995. Polymer nanocomposites: a new strategy for synthesizing solid electrolytes for rechargeable lithium batteries. *Journal of Power Sources*, 54, pp. 310-315

Kyritsis, A., Pissis, P. and Grammatikakis, J., 1995. Dielectric relaxation spectroscopy in poly(hydroxyethyl acrylates)/water hydrogels. *Journal of Polymer Science Part B: Polymer Physics*, 33, pp. 1737-1750.

Linden, D. and Reddy, T., 2002. *Handbook of Batteries*. 3<sup>rd</sup> Edition. New York: McGrawHill.

Li, Q. et al., 2003. All solid lithium polymer batteries with a novel composite polymer electrolyte. *Solid State Ionics*, 159, pp. 97-109.

Li, T. and Balbuena, P.B., 1999. Theoretical studies of Lithium Perchlorate in Ethylene Carbonate, Propylene Carbonate, and their mixture. *Journal of The Electrochemical Society*, 146, pp. 3613-3622.

Liu, Y., Lee, J.Y., and Hong, L., 2002. Functionalized SiO<sub>2</sub> in poly(ethylene oxide)-based polymer electrolytes. *Journal of Power of Power Sources*, 109(2), pp. 507-514.

Low, S.P., Ahmad, A. and Rahman, M.Y.A., 2010. Effect of ethylene carbonate plasticizer and TiO<sub>2</sub> nanoparticles on 49% poly(methylmethacrylate) grafted natural rubber-based polymer electrolyte. *Ionics*, 16, pp. 821-826.

MacArthur, D., and Powers, R., 1996. The Challenges of Polymer Electrolytes for lithium Batteries. *Proceedings of the Eleventh Annual Battery Conference on Applications and Advances*, pp. 307-310.

MacCallum, J.R., Tomlin, A.S., and Vincent, C.A., 1986. An investigation of the conducting species in polymer electrolytes. *European Polymer Journal*, 22, pp. 787-791.

Mahendran, O, and Rajendran, S., 2003. Ionic conductivity studies in PMMA/PVDF polymer blend Electrolyte with lithium salts. *Ionics*, 9, pp. 282-288

Mahendran, O. et al., 2005. Investigation on PMMA-PVdF polymer blend electrolyte with ester of Dibenzoic Acids as plasticizer. *Ionics*, 11, pp. 251-258.

Michael, M.S. et al., 1997. Enhanced lithium ion transport in PEO-based solid polymerelectrolytes employing a novel class of plasticizers. *Solid State Ionics*, 98, pp. 167-174.

Miyamoto, T., and Shibayama, K., 1973. Free-volume model for ionic conductivity in polymers. *Journal of Applied Physics*, 44(12), pp. 5372-5376.

Nada, A.M.A., Dawy, M. and Salama, A.H., 2004. Dielectric properties and ac-conductivity of cellulose polyethylene glycol blends. *Materials Chemistry and Physics*, 84, pp. 205-215.

Ng, B.C. et al., 2011. Development and characterization of poly-ε-caprolatone-based polymer electrolyte for lithium rechargeable battery. *International Journal of Electrochemical Science*, 6, pp. 4355-4364.

Nithya, H. et al., 2011. Thermal and dielectric studies on polymer electrolyte based on P(ECH-EO). *Materials Chemistry and Physics*, 126, pp. 404-408.

Osaka, T. et al., 1997. Performances of lithium/ gel electrolyte/ polypyrrole secondary batteries. *Journal of Power Sources*, 68, pp. 392-396

Osinska, M. et al., 2009. Study of the role of ceramic filler in composite gel electrolytes based on microporous polymers membranes. *Journal of Membrane Science*, 326, pp. 582-588.

Osman, Z. et al., 2005. Infrared and conductivity studies on blend of PMMA/PEO based polymer electrolytes. *Ionics*, 11, pp. 431-435.

Othman, L., Chew, K.W. and Osman, Z., 2007. Impedance spectroscopy studies of poly(methyl methacrylate)-lithium salts polymer electrolyte systems. *Ionics*, 13, pp. 337-342

Ozer, N. et al., 1999. Optical properties of sol-gel deposited  $\text{Al}_2\text{O}_3$  films. *Solar Energy Materials and Solar Cells*, 59, pp. 355-366.

Pandey, K. et al., 2008. Structural, thermal and ion transport studies on nanocomposite polymer electrolyte- $\{(\text{PEO}+\text{SiO}_2):\text{NH}_4\text{SCN}\}$  system. *Ionics*, 14, pp. 515-523.

Pistoia, G., Antonini, A. and Wang, G., 1996. Impedance study on the reactivity of gel polymer electrolytes towards a lithium electrode. *Journal of Power Sources*, 58, pp. 139-144.

Pradhan, D.K., Choudhary, R.N.P. and Samantaray, B.K., 2008. Studies of dielectric relaxation and ac conductivity behavior of plasticized polymer nanocomposite electrolytes. *International Journal of Electrochemical Science*, 3, pp. 597-608.

Quartarone, E. et al., 1998. Long term structural stability of PMMA-based gel polymer electrolytes. *Electrochimica Acta*, 43(10-11), pp. 1435-1439.

Ragavendran, K. et al., 2004. Characterization of plasticized PEO based solid polymer electrolyte by XRD and AC impedance methods. *Portugaliae Electrochimica Acta*, 22, pp. 149-159.

Raghavan, P. et al., 2010. Electrochemical performance of electrospun poly (vinylidene fluoride-co-hexafluoropropylene) based nanocomposite polymer electrolytes incorporating ceramic fillers and room temperature ionic liquid. *Electrochimica Acta*, 55, pp. 1347-1354.

Rajendran, S. and Mahendran, O., 2001. Experimental investigation on plasticized PMMA/PVA polymer blend electrolyte. *Ionics*, 7, pp. 463-468.

Rajendran, S., Mahendran, O. and Kannan, R., 2002. Ionic conductivity studies in composite solid polymer electrolyte electrolytes based on methylmethacrylate. *Journal of Physics and Chemistry of Solids*, 63, pp. 303-307.

Rajendran, S., Sivakumar, M. and Subadevi, R., 2003. Effect of salt concentration in poly(vinyl alcohol)-based solid polymer electrolytes. *Journal of Power Sources*, 124, pp. 225-230.

Rajendran, S., Sivakumar, M. and Subadevi, R., 2004. Investigations on the effect of the various plasticizers in PVA-PMMA solid polymer blend electrolytes. *Materials Letter*, 58, pp. 641-649.

Rajendran, S. and Sivakumar, P., 2008. An investigation of PVdF/PVC-based blend electrolytes with EC/PC as plasticizers in lithium battery applications. *Physica B*, 403, pp. 509-516.

Rajendran, S., Babu, R.S. and Devi, K.R., 2009. Ionic conduction behavior in PVC-PEG blend polymer electrolytes upon the addition of TiO<sub>2</sub>. *Ionics*, 15, pp. 61-66.

Rajendran, S. and Prabhu, M.R., 2010. Effect of different plasticizer on structural and electrical properties of PEMA-based polymer electrolytes. *Journal of Applied Electrochemistry*, 40, pp. 327-332.

Rajendranm S., Bama, V.S. andPrabhu, M.R., 2010. Effect of lithium salt concentration in PVAc/PMMA-based gel polymer electrolytes. *Ionics*, 16, pp. 27-32.

Ramesh, S. andArof, A.K., 2001. Ionic conductivity studies of plasticized poly(vibyl chloride) polymer electrolytes. *Materials Science and Engineering B-Solid State Materials for Advanced Technology*, 85, pp. 11-15.

Ramesh, S. et al., 2007. FTIR studies of PVC/PMMA blend based polymer electrolytes. *SpectrochimicaActaPart A: Molecular and Biomolecular Spectroscopy*, 66, 465, pp. 1237-1242.

Ramesh, S. and Wen, L.C., 2010. Investigation on the effect of addition of SiO<sub>2</sub> nanoparticles on ionic conductivity, FTIR, and thermalproperties of nanocomposite PMMA-LiCF<sub>3</sub>SO<sub>3</sub>-SiO<sub>2</sub>. *Ionics*, 16, pp. 255-262.

Ramesh, S., Yahaya, A.H. andArof, A.K., 2002. Dielectric behaviour of PVC-based polymer electrolytes. *Solid State Ionics*, 152, pp. 291-294.

Ramya, C.S. et al., 2008. Investigation on dielectric relaxations of PVP-NH<sub>4</sub>SCN polymer electrolyte. *Journal of Non-Crystalline Solids*, 354, pp. 1494-1502.

Raveh, A., Tsameret, Z.K., and Grossman, E., 1997. Surface characterizationof thin layers of aluminium oxide. *Surface and Coating Technology*, 88, pp.103-111.

Reicha, F.M. et al., 1991. Conducting polymers. v. electrical conductivity of polymer complexes of bis-2,6-diaminopyridinesulphoxide-copper halides. *Journal of Physics D:Applied Physics*, 24, pp. 369-374.

Saikia, D. et al., 2008.Investigation of ionic conductivity of composite gel polymerelectrolyte membranes based on P(VDF-HFP), LiClO<sub>4</sub> and silicaaerogel for lithium ion battery. *Desalination*, 234, pp. 24-32.

Saikia, D. et al., 2009. LiNMR spectroscopy and ion conduction mechanism of composite gel polymer electrolyte: A comparative study with variation of salt and plasticizer with filler. *Electrochimica Acta*, 54, pp. 1218-1227.

Schmidt-Rohr, K. et al., 1994. Molecular Nature of the  $\beta$ -relaxation in poly(methacrylate) investigated by multidimensional NMR. *Macromolecules*, 27, pp. 4733-4745.

Scrosati, B., 2000. Recent advances in lithium ion battery materials. *Electrochimica Acta*, 45, pp. 2461-2466.

Scrosati, B., Croce, F. and Persi, L., 2000. Impedance spectroscopy study of PEG-based nanocomposite polymer electrolytes. *Journal of the Electrochemical Society*, 147, pp. 1718-1721.

Sekhon, S.S., Arora, M. and Chandra, S., 2003. Proton conducting polymer gel electrolytes with NO<sub>2</sub> substituted carboxylic acids. *European Polymer Journal*, 39, pp. 915-920.

Sekhon, S.S., Arora, M. and Sing, H.P., 2003. Effect of donor number of solvent on the conductivity behaviour of nonaqueous proton-conducting polymer gel electrolytes. *Solid State Ionics*, 160, pp. 301-307.

Sekhon, S.S. et al., 2006. Proton conducting membrane containing room temperature ionic liquid. *Electrochimica Acta*, 52, pp. 1639-1644.

Selvasekarapandian, S. et al., 2006. Laser Raman and FTIR studies on Li<sup>+</sup> interaction in PVAc- LiClO<sub>4</sub> polymer electrolytes. *Spectrochimica Acta A*, 65, pp. 1234-1240.

Sharma, J.P. and Sekhon, S.S., 2007. Nanodispersed polymer gel electrolytes: Conductivity modification with the addition of PMMA and fumed silica. *Solid State Ionics*, 178, pp. 439-445.

Shukla, N. and Thakur, A. K., 2009. Role of salt concentration on conductivity optimization and structural phase separation in a solid polymer electrolyte based on PMMA-LiClO<sub>4</sub>. *Ionics*, 15, pp. 357-367.

Singh, P. K., Kim, K. W. and Rhee, H. W., 2009. Development and characterization of ionic liquid doped solid polymer electrolyte membranes for better efficiency. *Synthetic Metals*, 159, pp. 1538-1541.

Smart, L. and Moore, E.A., 2005. Physical Methods for Characterizing Solids. *SolidState Chemistry: An introduction*. (pp. 175-238). New York:Taylor & Francis.

Song, H.J., Zhang, Z.Z. and Men, X.H., 2006. Effect of nano-Al<sub>2</sub>O<sub>3</sub> surface treatment on the tribological performance of phenolic compositecoating. *Surface & Coating Technology*, 201, pp. 3767-3774.

Song, J.Y., Wang, Y.Y. and Wan, C.C., 1999. Review of gel-type electrolytesfor lithium-ion batteries. *Journal of Power Sources*, 77, pp. 183-197

Stallworth, P.E. et al., 1995. Lithium-7 NMR and ionic conductivity studies of gelectrolytes based on poly(methylmethacrylate). *ElectrochimicaActa*, 40, pp. 2137-2141.

Stephan, A.M. et al., 2000. Ionic conductivity and FT-IR studies on plasticized PVC/PMMA blend polymer electrolytes. *Journal of Power Sources*, 89, pp. 80-87.

Stephan, A.M. et al., 1999. A study on polymer blend electrolyte based onPVC/PMMA with lithium salt. *Journal of Power Sources*, 81-82, pp.782-758.

Stephan, A.M. et al., 2002. Preparation and characterization of PVC/PMMA blend polymer electrolytes complexed with  $\text{LiN}(\text{CF}_3\text{SO}_2)_2$ . *Solid State Ionics*, 148, pp. 467-473.

Sung, H.Y., Wang, Y.Y. and Wan, C.C., 1998. Preparation and Characterization of Poly(vinyl chloride-co-vinyl acetate)-based gelectrolytes for Li-ion batteries. *Journal of The Electrochemical Society*, 145, pp. 1207-1211.

Tan, C.G. et al., 2007. The effects of ceramic filler on the PMMA-based polymer electrolyte systems. *Ionics*, 13, pp. 361-364.

Tobishima, S. and Yamaji, A., 1984. Ethylene carbonate-propylene carbonate mixed electrolyte for lithium batteries. *Electrochimica Acta* 29, pp. 267-271.

Tsuchida, E., Ohno, H. and Tsunemi, K., 1983. Conduction of lithium ions in polyvinylidene fluoride and its derivatives-1. *Electrochimica Acta*, 28, pp. 591-595.

Wang, Z. et al., 1996. Infrared spectroscopic study of the interaction between lithium salt  $\text{LiClO}_4$  and the plasticizer ethylene carbonate in the polyacrylonitrile-based electrolyte. *Solid State Ionics*, 85, pp. 143-148.

Wang, Z. et al., 1997. Competition between the plasticizer and polymer on associating with  $\text{Li}^+$  ions in polyacrylonitrile-based electrolyte. *Journal of The Electrochemical Society*, 144, pp. 778-786.

Weston, J.E. and Steele, B.C.H., 1982. Effect of inert filler on the mechanical and electrochemical properties of lithium salt-poly(ethylene oxide) polymer electrolytes. *Solid State Ionics*, 71, pp. 75-79.

Xiong, H.M., Chen, J.S. and Li, D.M., 2003. Controlled growth of  $\text{Sb}_2\text{O}_5$  nanoparticles and their use as polymer electrolyte fillers. *Journal of Material Chemistry*, 13, pp. 1994-1998.

Xu, W. et al., 1998. The influence of the compatibility of plasticizer with polymer ionic conductors on ionic conduction. *Journal of Solid State Electrochemistry*, 2, pp. 257-261.

Yen, Y.C. et al., 2008. Effect of  $\text{LiClO}_4$  on the thermal and morphological properties of organic/inorganic polymer hybrids. *Polymer*, 49, pp. 3625-3628.